



**Politecnico
di Torino**

Politecnico di Torino

Ingegneria Biomedica

A.A. 2021/2022

Sessione di Laurea Luglio 2022

Design, development and functionalization of 3D printed air filters with antibacterial properties

Design, sviluppo e funzionalizzazione di filtri per aria
stampati in 3D con proprietà antibatteriche

Relatori:

Dott.sa Francesca Frascella

Dott. Ignazio Roppolo

Candidati:

Maria D'Aloia

s275215

ABSTRACT

3D printing, or additive manufacturing, is becoming increasingly important in the biomedical field due to the possibility of developing affordable custom devices with high flexibility in terms of materials, personalization, complexity and high precision. However, surface treatments and modifications are often needed to enable the required bio-functionality characteristics, such as biocompatibility, wettability or bioactivity.

The aim of this work is to develop air filters 3D printed by Digital Light Processing (DLP) with antibacterial properties. DLP is based on the photopolymerization of liquid polymer resins and allows a rapid printing of objects with high resolution. In this thesis work, two strategies were followed: on the one hand, the design and fabrication of complex geometries which can reduce the microorganisms' flow; on the other hand, a study of surface functionalization to obtain the desired final properties.

Different printable formulations based on acrylic monomers were studied, optimizing printing parameters to obtain the designed geometries; subsequently, different surface functionalization methods (conventional heating, microwave heating, dip-coating and chlorination) were compared to impart bacterial adhesion characteristics to the filters. In this context, arginine, agmatine, dopamine and polyethylenimine were used as grafting agents. Here the goal was to exploit functional groups to promote microorganisms' adhesion and killing.

At last, biological studies were performed evaluating bacterial adhesion and proliferation. The effectiveness of the filters was studied with Gram-positive and Gram-negative bacteria, achieving promising results for the implementation of these devices.

This thesis work was performed in collaboration with "*Instituto de Ciencia y Tecnología de Polímeros (ICTP – CSIC)*" and "*Institute for Biofunctional Studies of the Universidad Complutense (UCM)*" in Madrid.

INDEX

CHAPTER 1: INTRODUCTION AND AIM OF THE WORK	7
CHAPTER 2: 3D PRINTING	11
2.1 3D POLYMERIC PRINTING	11
2.2 PHOTOPOLYMERIZATION-BASED TECHNIQUES	12
2.2.1. PHOTOPOLYMERIZATION MECHANISMS	12
2.2.2. PHOTOPOLYMERIZATION-BASED 3D PRINTING	13
2.2.3. SLA: MECHANISM AND CHARACTERISTICS	14
2.2.4. DLP: MECHANISM AND CHARACTERISTICS	14
2.3 3D PRINTING FORMULATIONS	17
CHAPTER 3: SURFACE MODIFICATION FOR ANTIBACTERIAL APPLICATIONS	19
3.1. 3D PRINTING AND SURFACE MODIFICATION	19
3.2. PROPERTIES FOR SURFACE ADHESION	21
3.3. BACTERICIDAL SURFACES	22
3.4. BACTERIAL CELL WALL	24
3.5. SURFACE-BACTERIA INTERACTIONS	25
3.6. STRATEGIES FOR SYNTHESIS	26
3.6.1. MICROWAVE AND CONVENTIONAL HEATING	28
3.6.2. DIP-COATING WITH POLY-DOPAMINE	29
3.6.3. CHLORINATION	31
CHAPTER 4: MATERIALS AND METHODS	33
4.1. DLP 3D PRINTER	33
4.2. MATERIALS FOR 3D PRINTING	33
4.3. PREPARATION OF 3D PRINTING FORMULATIONS AND PRINTING PROCEDURE	35
4.4. MATERIALS FOR FUNCTIONALIZATION	36
4.5. SURFACE MODIFICATION REACTIONS	38
4.6. FUNCTIONALIZATION METHODS	39
4.6.1. GRAFTING THROUGH CONVENTIONAL HEATING	39
4.6.2. GRAFTING THROUGH MICROWAVE HEATING	39
4.6.3. DIP-COATING	41
4.6.4. CHLORINATION	41
4.7. PROTOCOL FOR BIOLOGICAL TEST	42

4.8.	CHARACTERIZATION METHODS	44
4.8.1.	3D SCANNER	44
4.8.2.	SWELLING AND RECOVERY TEST	44
4.8.3.	FTIR-ATR SPECTROSCOPY	45
4.8.4.	CONTACT ANGLE	46
4.8.5.	EDX	47
4.8.6.	TGA	47
4.8.7.	OPTICAL DENSITY	47
4.8.8.	FLUORESCENCE MICROSCOPE	48
4.8.9.	IMAGE-PROCESSING WITH IMAGEJ	48

CHAPTER 5: PRINTING AND SURFACE TREATMENT: RESULTS AND DISCUSSION 51

5.1.	SOLIDWORKS DESIGN	51
5.2.	PRINTING PARAMETERS OPTIMIZATION	53
5.2.1.	PEGDA/AA MATRIX	53
5.2.2.	PEGDA/GMA MATRIX	54
5.2.3.	OTHER MATRICES: PEGDA, PEGDA/ABUT, PEGDA/AA/ABUT	56
5.3.	3D SCANNER	57
5.4.	PEGDA/AA-BASED MATRIX	58
5.4.1.	SWELLING TEST	58
5.4.2.	FTIR-ATR SPECTROSCOPY	59
5.4.2.1.	PEGDA/AA + Arginine	59
5.4.2.2.	PEGDA/AA + Agmatine	62
5.4.2.3.	PEGDA/AA + Dopamine	64
5.4.2.4.	PEGDA/AA + PEI600	65
5.4.3.	CONTACT ANGLE	67
5.4.3.1.	PEGDA/AA + Arginine	67
5.4.3.2.	PEGDA/AA + Agmatine	67
5.4.3.3.	PEGDA/AA + Dopamine	68
5.4.3.4.	PEGDA/AA + PEI600	68
5.4.4.	CHOICE OF THE BEST SAMPLES	69
5.4.5.	TGA	71
5.4.5.1.	PEGDA/AA + Arginine	71
5.4.5.2.	PEGDA/AA + Agmatine	72
5.4.6.	EDX	73
5.4.6.1.	PEGDA/AA + Arginine	73
5.4.6.2.	PEGDA/AA + Agmatine	74
5.4.7.	FINAL COMMENTS	75
5.5.	PEGDA/GMA-BASED MATRIX	76
5.5.1.	SWELLING TEST	76
5.5.2.	FTIR-ATR SPECTROSCOPY	77

5.5.2.1.	PEGDA/GMA + Arginine	77
5.5.2.2.	PEGDA/GMA + Agmatine	79
5.5.2.3.	PEGDA/GMA + Dopamine	81
5.5.2.4.	PEGDA/GMA + PEI	82
5.5.3.	CONTACT ANGLE	84
5.5.3.1.	PEGDA/GMA + Arginine	84
5.5.3.2.	PEGDA/GMA + Agmatine	84
5.5.3.3.	PEGDA/GMA + Dopamine	85
5.5.3.4.	PEGDA/GMA + PEI	85
5.5.4.	CHOICE OF THE BEST SAMPLES	86
5.5.5.	TGA	87
5.5.5.1.	PEGDA/GMA + Arginine	87
5.5.5.2.	PEGDA/GMA + Agmatine	88
5.5.6.	EDX	89
5.5.6.1.	PEGDA/GMA + Arginine	89
5.5.6.2.	PEGDA/GMA + Agmatine	90
5.5.7.	FINAL COMMENTS	91
5.6.	OTHER MATRICES: PEGDA, PEGDA/ABut, PEGDA/AA/ABuT	92
5.6.1.	SWELLING TEST	92
5.6.2.	FTIR-ATR SPECTROSCOPY	92
4.6.2.1.	PEGDA ₂₅₀ + Dopamine	93
4.6.2.2.	PEGDA/ABut + Dopamine	94
4.6.2.3.	PEGDA/AA/ABut + Dopamine	95
5.6.3.	CONTACT ANGLE	96
5.6.4.	FINAL COMMENTS	96
CHAPTER 6: BIOLOGICAL TESTS: RESULTS AND DISCUSSION		97
6.1.	PEGDA/AA-BASED SAMPLES	97
6.2.	PEGDA/GMA-BASED SAMPLES	99
6.3.	OTHER MATRICES	101
6.4.	BIOLOGICAL TESTS ON FILTERS	103
CHAPTER 7: CONCLUSION		106
REFERENCES		110

CHAPTER 1: INTRODUCTION AND AIM OF THE WORK

Air filtration is a topic of strong interest, both from an environmental and human health perspective. Complex pollutants, in the form of solid particulate matter and gaseous substances, are present in the air, posing a threat to human health and contributing to environmental pollution [1]. In addition, various biological particles, including viruses, bacteria, spores and fungi, are present in aerosol form, which can cause health problems [2]; the recent COVID-19 pandemic has made the need to ensure appropriate air filtration even more evident, not only for personal protective equipment, such as face masks, but also for ventilation and air conditioning systems in enclosed spaces [3]. Thus, effective control of airborne pollutants, harmful biological agents, allergens, and aerosol particles is of great importance [4].

Filtration can take place through several mechanisms: sieving, gravity settling, inertial impaction, interception, diffusion, and electrostatic attraction [1] [5].

Sieving is the main mechanism of air filters and occurs when particles are too large to enter the pores of the filters. Larger particles, which undergo a net downward movement, can be filtered by gravity, although this method is of little relevance to air filters: these particles, in fact, tend to settle before they reach the surface of the filter [1]. In contrast, smaller particles are subject to strong inertia and can break away from the air flow line and collide with the filter material; this mechanism is called inertial impaction. If the inertia is not such that the particles are pulled away from the gas flow line, they can still be separated by interception in the event of collision with the filter medium. Another mechanism is diffusion, and it is based on Brownian motion and the displacement of small particles (less than $0.5\ \mu\text{m}$) toward regions of low concentration, that is, toward the filter surface. Finally, the electrostatic attraction mechanism promotes filtration due to the interaction between the surface electric charge of the filter and the particles. Not all of these mechanisms come into play simultaneously in air filtration, and they are dependent on the physicochemical properties of the particles and the filter, as well as the size of the particles [1].

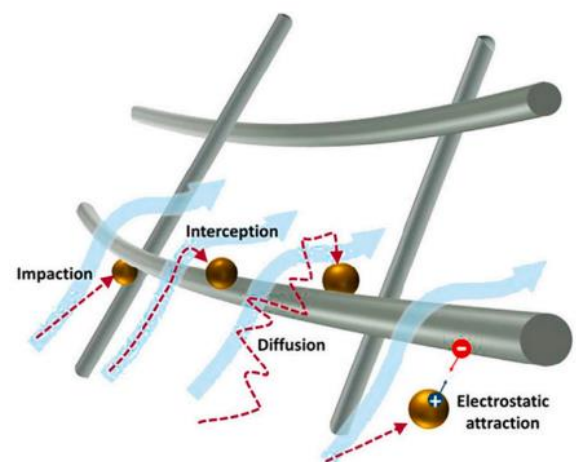


Figure 1 – Four types of filtration mechanisms: impaction, interception, diffusion and electrostatic attraction [5]

It is therefore necessary to carefully adjust the structural and chemical properties of filters to achieve effective filtration. Some of the most important properties are pore size, surface charge, hydrophilicity, specific surface area, and mechanical stability [1].

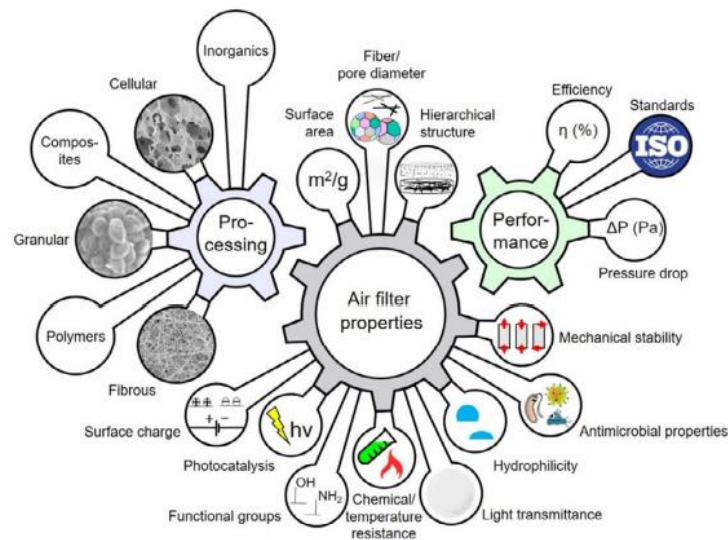


Figure 2 - Schematic illustration showing the dependence of air filter performance on the properties, which are governed by the choice of material and processing technique [1]

Most air filters are made of polymeric materials [1], usually processed into nanofibrous structures or porous membranes [3]. The most commonly used materials for this purpose are polyacrylonitrile (PAN), polyurethane, polylactide, nylon-6, and others [3]. The most widely used technique for producing this type of filter is electrospinning [1] [2] [3], which allows for structures with high specific surface area and small pore size [2]. Many studies have reported the effectiveness of filters obtained by electrospinning [2] [3] [4]. Despite this, electrospinning is a technique with low throughput, and often the use of a substrate is required to make up for the weak mechanical stability of electrospun fibers, e.g., fabric, plastic or metal mesh [2] [3].

Recently, additive manufacturing (AM) techniques, or 3D printing, have been used in combination or as an alternative to electrospinning [2]. These techniques enable the design and fabrication of structures with fine features and complex internal and external geometries [6]. They also offer the advantages of speed, sustainability, flexibility and accessibility, at relatively low cost. On the other hand, they do not allow the fabrication of large objects and allow limited material selection (3).

Another goal of great interest is to make the filter material have antimicrobial characteristics. One of the most common methods involves the incorporation of metal nanoparticles, such as silver, copper, and nickel [1]. The NPs interact electrostatically with the microorganisms, releasing metal ions; this causes disruption of the cell membrane and interruption of metabolic processes. Other methods involve surface modification of the filter using common antibiotics, antimicrobial polymers, carbon nanoparticles and nanostructures.

The purpose of this work is the realization of 3D printed air filters with antibacterial properties. The antibacterial properties come both from the geometric complexity of the filter, which reduces the flow of microorganisms, and from an appropriate surface modification of the printed filter.

Thus, the first step was the design of the filter geometry using CAD software to ensure not only the desired antibacterial properties, but also good printability and mechanical properties. The designed filters were 3D printed by Digital Light Processing (DLP), using polymeric resins based on acrylic monomers. Different formulations were tested, and printing parameters were optimized in order to minimize production time. Print fidelity was evaluated using 3D scanner techniques to compare the printed object with the CAD model.

Next, different combinations of functionalization molecules and surface modification techniques were studied. The molecules were chosen so as to promote microorganisms' adhesion and killing on the filter surface. The success of these treatments was evaluated by various characterization techniques, including FTIR-ATR spectroscopy, contact angle measurement, EDX and TGA. The goal was to obtain the binding between the functionalization molecule and the functional groups exposed on the filter surface, in the shortest time and at the lowest possible temperature. Maintaining the geometry of the filter and its mechanical properties was another goal.

Finally, the last step was preliminary biological testing with bacteria to assess their ability to adhere to the modified material. Both Gram-positive and Gram-negative bacteria were tested. After the live/dead experiment, a confocal microscope and ImageJ software were used for bacterial quantification.

CHAPTER 2: 3D PRINTING

2.1 3D POLYMERIC PRINTING

3D printing, also known as additive manufacturing (AM) or rapid prototyping, refers to a set of bottom-up technologies based on layer-by-layer deposition of a material to build a three-dimensional geometry. The geometric information is contained in an STL file created with computer-aided design (CAD) software; the file is used to perform slicing of the object, which is divided into thin horizontal sections [7]. Layers are deposited on the X-Y plane in defined positions, one on top of the other. The process is repeated on the Z axis, following the slicing of the object.

These techniques allow the fabrication of objects with complex geometries and high resolution, in a relatively quick and economical way, since there is no need for molds or other tools. In addition, 3D printing offers the advantage of being able to modulate the mechanical, physical and chemical characteristics of the final object through the study of the starting materials and printing methods.

3D printing techniques can be divided into three main categories [8]:

- Extrusion-based methods: these techniques are based on the phase transition from a solid to a liquid state of thermoplastic filaments [8]. The filaments pass through a heated nozzle, which causes them to melt and guide their deposition at the desired location. Then, the material cools and solidifies in a very short time. The most widely used of these techniques is Fused Deposition Modeling (FDM).
- Powder-based methods: these techniques involve the deposition of a thin layer of powders, which are pressed and compacted. Then, a binder or a laser radiation is used to melt the powders at the desired locations. One technique that falls into this category is Selective Laser Sintering (SLS).
- Photopolymerization-based methods: these techniques involve the use of monomers and oligomers that react when exposed to UV light, changing from a liquid to a solid state through photopolymerization. These methods are fairly fast, easy, and do not involve high temperatures [7]. Stereolithographic techniques, including Digital Light Processing (DLP), fall into this category.

In the next section, photopolymerization and stereolithographic techniques will be described, focusing in particular in the DLP technique, which is the one used in this work.

2.2 PHOTOPOLYMERIZATION-BASED TECHNIQUES

2.2.1. PHOTOPOLYMERIZATION MECHANISMS

Photoinitiated polymerization is a process that uses light as an energy source to induce the conversion of small unsaturated molecules in the liquid state into solid macromolecules, as a result of polymerization reactions [9]. The basic components of the starting liquid are monomers, oligomers, or prepolymers that can solidify in two ways: polymerization or cross-linking. Polymerization proceeds via chain reactions, so the quantum yield is very high. In cross-linking, on the other hand, the addition of each monomer unit requires the absorption of one photon, leading to a quantum yield of 1 or less [9].

Photopolymerization can be induced by different types of radiation (IR, X-rays, γ -rays, microwaves, electron or ion beams...) but more commonly is activated by radiation in the UV-visible spectrum (250-450 nm). This radiation is absorbed by a photoinitiator present in the mixture, a molecule that converts light energy into chemical energy in the form of reactive intermediates, such as free radicals or cations. It is necessary that the emission spectrum of the light source and the absorption spectrum of the photoinitiator overlap [10].

A more detailed description of the characteristics of monomers/oligomers and photoinitiators can be found in Section 2.3.

Depending on whether the reactive species is a radical or an ion, we call it a radical, cationic, or anionic photopolymerization mechanism.

- Radical mechanism: the reactive species is a free radical that induces a propagation of the reaction. Three main phases can be distinguished: initiation, propagation, and termination. In the initiation step, light activates the photoinitiator and a reactive species, a radical, is generated. In the propagation phase, the photoproducted radicals react with monomers to form monomeric radicals, which react with other monomers, resulting in a chain reaction. In the termination phase, the reaction stops. In the radical mechanism, this usually occurs by combination: two growing chains meet, and the radicals inactivate. If impurities are present, termination can occur by another mechanism, called disproportionation: an impurity reacts with active groups and terminates the chain growth [9].
- Ionic mechanism: the reactive species, in this case, is an ion (typically a cation). Cationic photopolymerization is less common than the radical one, mainly because it proceeds at a slower rate and sometimes additional heat treatment is required to increase monomer conversion. [9] Ionic polymerization termination cannot occur through direct combination (as in the radical mechanism) as reaction between similar ions is not achievable. The chain reacts with impurities or other specifically added reagents through the disproportionation process.

2.2.2. PHOTOPOLYMERIZATION-BASED 3D PRINTING

Photopolymerization-based printing techniques can also be called vat curing methods, since the liquid precursor is located in a vat. The precursor layers are sequentially exposed to light radiation (usually UV) and then selectively solidify. A printing platform moves vertically so that only one layer of resin is exposed to light. A photoinitiator is required to activate the polymerization reaction only in the exposed regions. After developing a layer, a new liquid resin film is deposited and undergoes the same process [11].

Vat polymerization techniques can be classified according to the direction of incident light or according to the method of irradiation.

According to the classification based on the direction of light, there are two categories:

- Free-surface approach: light comes from above the vat;
- Constrained surface approach: light comes from below.

According to the irradiation method, there are three categories:

- Point-by-point irradiation by a laser;
- Area irradiation;
- Illumination through a liquid crystal display (LCD) photomask [11].

Among these techniques, SLA and DLP are the most versatile, as they combine high resolution with affordable prices for materials and equipment. They are both based on the spatially controlled solidification of photosensitive liquid resins [12] by a programmable light source controlled by software; the light emission can be controlled in terms of intensity, field distribution, and wavelength [13]. A more detailed description of these techniques can be found in the following sections.

If we compare photopolymerization with other 3D printing techniques, we see that it is characterized by the best resolution and the smallest characteristic size (down to 25 μm) [8]. In addition, these techniques offer the greatest flexibility on the object's final properties due to the ability to modify the chemistry of the starting resin [14]. Another important advantage of these techniques is that the resin does not need to have any particular surface tension, viscosity or volatility characteristics, properties that must be carefully modulated for other techniques, e.g. FDM. Finally, a significant advantage is that the printing of complex structures does not require any backing material, as the uncured material itself acts as a support [8].

Although photopolymerization is now widely used in many 3D printing techniques, it has disadvantages [14], such as:

1. UV photons only penetrate at shallow depths, so the single polymerizable layer has very low thickness; this leads to an increase in the time required for printing, which can be a problem especially for large objects.
2. Prolonged exposure to UV light could lead to degradation of reagents or products

3. In bio-printing, whose purpose is to insert cells into polymer resin, the use of UV light could lead to cellular photodamage.

Another disadvantage of using these methods is that only one material can be used, since the object is printed within a solution in the bath [8].

2.2.3. SLA: MECHANISM AND CHARACTERISTICS

Classical stereolithography (SLA) is a free-surface technique that uses a punctual laser as the light source.

The printing platform on which the object grows is located in a tank filled with resin, so that only a layer of liquid resin can cover it. The light irradiation typically comes from above and causes the resin to solidify. After that, the platform translates downward so that a layer of liquid resin covers the newly cured one. This sets the stage for the subsequent layer. Each layer is then cured by a UV laser moving in the x-y plane. The movement of the laser is guided by an optical system in combination with two galvanometers. [11]

Several factors contribute to the resolution of this technique, which can be as low as 5-10 μm . Not only the composition of the resin, but also the diameter of the laser spot and its speed must be carefully optimized. [11]

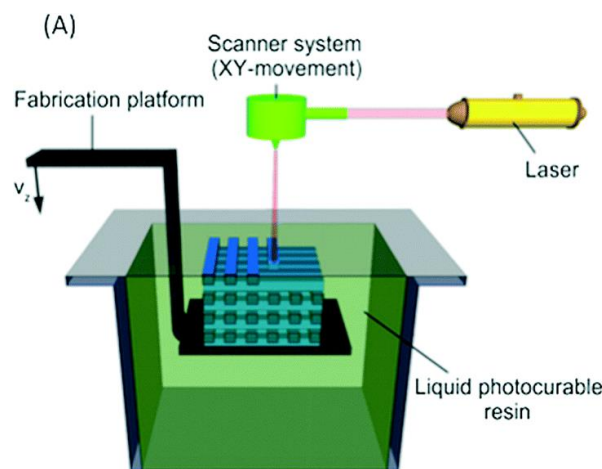


Figure 3 - SLA printing configuration [15]

2.2.4. DLP: MECHANISM AND CHARACTERISTICS

DLP technique follows a constrained surface approach, in which the light source is placed below the vat and the printing platform is suspended above the resin bath. The main difference with the SLA technique is that an entire layer of resin is illuminated simultaneously, allowing solidification of an area instead of one spot at a time. This is achieved by inserting a digital micro-mirror device

(DMD) into the optical path of the laser [16]. The DMD is the key component of a DLP printer. It consists of an array of thousands of movable micro-mirrors, each of which can be individually set to an "on" or "off" state depending on whether it reflects light emitted from the source or not. Each mirror represents a single pixel: individual tilting of every mirror enables fast and reliable switching of pixels [11]. The DMD then allows to project the entire image of the layer at once, thanks to the possibility of having bright regions and dark regions. The object is then printed layer by layer with multiple exposures [13].

A DLP printer uses a light source with a typical wavelength of 365 or 405 nm [7], and can achieve a resolution of 25 μm [11]. The light source is located below the vat, which has a transparent bottom. The light illuminates the DMD, which is oriented to project the all-in-one design onto the light-curing resin contained in the vat, causing the layer to solidify and adhere to the printing platform. The platform is then raised a distance equal to the thickness of the layer. The object then grows upward from the bottom and remains suspended on the platform [11].

Once the printing process is complete, the printed object must be removed from the platform, and the support structures that were needed for the printing process must be removed. In photopolymerization-based techniques, it is the resin itself that forms the support, as we saw in Section 2.2.2.

Appropriate solvents must be used to remove excess resin. Usually, the object undergoes a post-polymerization treatment in a UV chamber to complete the conversion and achieve better mechanical properties.

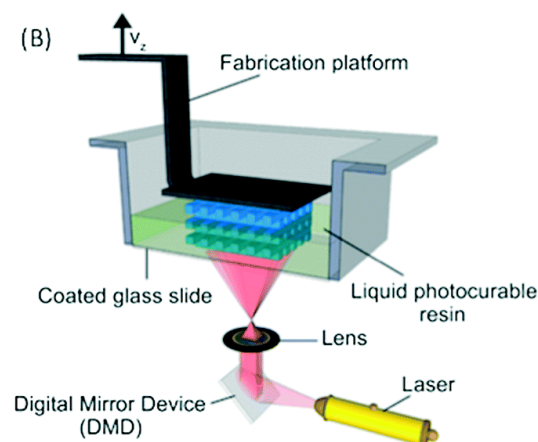


Figure 4 - DLP printing configuration [15]

There are several advantages when compared to SLA: first of all, illuminating an entire layer at a time greatly reduces printing time. In addition, there is a cost reduction due to the fact that a reduced amount of resin is required, since the sample does not have to be fully immersed in the vat. DLP printers are therefore faster and more efficient, and allow the use of light sources with a

wide range of wavelengths [16]. The precision in platform movement along the z-axis allows smooth surfaces to be obtained with accuracy down to 0.1-1 μm [11].

However, this technique also has disadvantages. The main disadvantage is related to the attractive forces between the molded part and the vat floor, which must be overcome so that the newly solidified layer adheres to the previous ones. Several methods are used to reduce the intensity of these forces, including the application of hydrophobic coatings to the bottom of the tank [11]. Since the exposure mechanism is pixel-based, this technique can cause roughness on curved surfaces. Therefore, if good resolution is required, the pixel size must be reduced with appropriate optical systems. Since the DMD has a fixed number of mirrors, this leads to image shrinkage and reduces the maximum size of the geometry. The large parts are therefore often printed at lower resolutions than the small parts. [11]

In conclusion, although SLA has better resolutions, DLP has lower costs and higher printing speed [16].

2.3 3D PRINTING FORMULATIONS

The main elements in a 3D printing photocurable resin are photoreactive precursors (monomers or oligomers) and at least a photoinitiator (radical or cationic).

Other elements can be added, such as additives (inhibitors, diluents, dyes...), absorbers (UV, visible) and fillers (ceramic, metallic, composite).

Precursors

Precursors are monomers, oligomers, or prepolymers that solidify after exposure to light. These elements constitute the matrix and establish the final physical and mechanical characteristics. Oligomers generally contain at least two reactive groups, from which both cross-linking and polymerization can occur. Monomers have one or more reactive groups and a much smaller molecular weight. Monomers are sometimes used to dilute resins so that they are less viscous [9]. Depending on the application and desired characteristics, different precursors can be used. For 3D printing processes, monomers/oligomers with low viscosity, low shrinkage rate, fast reaction time and high polymerization efficiency are chosen.

Some of the most common resins are those based on acrylic precursors, which are compatible with several types of commercially available 3D printers. [14] Their mechanism of polymerization is a radical one. Their main advantage is their high reactivity. As a disadvantage, they often experience shrinkage during printing; stress associated with shrinkage could result in deformation and printing defects [11]. Depending on the molecular structure of the monomer/oligomer, the amount of shrinkage changes. However, there are several strategies to reduce these kinds of problems, including the use of high molecular weight oligomeric acrylates (with a lower concentration of reactive groups), which can reduce the shrinkage rate, but on the other hand, give higher viscosity, so heating may be required to make the resin more fluid during printing [14]. In addition, these types of resins are sensitive to oxygen, which can inhibit polymerization by reacting with free radicals. One possible solution is the use of additives (such as tertiary amines) to reduce oxygen inhibition in open vat 3D systems [14]. Some of the most common methacrylate monomers/oligomers used in 3D printing are polyethylene glycol diacrylate (PEGDA), triethylene glycol dimethacrylate (TEGDMA), bisphenol A-glycidyl methacrylate (Bis-GMA) [14].

Other common resins are those based on epoxy systems, which cure by a cationic mechanism. Reaction times are longer and the mechanism can be inhibited by high ambient humidity, but they are stable in the presence of oxygen. In addition, shrinkage is significantly less. [11]

It is possible to combine the advantages of the two resins by using acrylate and epoxy-based resins.

Photoinitiators

The resin must contain at least one photoinitiator (PI), which is the component that reacts with light, initiates the solidification reaction and establishes the reactivity of the resin. The type of PI and its amount have a major influence on the reaction kinetics, conversion and mechanical properties of the final object. Depending on the precursors used, an appropriate PI must be chosen. A good photoinitiator must provide radicals or cations active enough to react with monomers or oligomers. In addition, it must be readily reduced to an initiator species upon light irradiation. It is crucial that photoinitiator window of absorption/reactivity well match the wavelength employed by the 3D printer.

In some cases, the energy collection and triggering chain polymerization are cooperatively accomplished by multi-type molecules [9], such as photosensitizers or photocatalysts. The photosensitizer is a molecule that absorbs light and transfers the energy to a photoinitiator; the photocatalyst does not absorb light, but is still involved in the production of radical species.

Additives

Additives can be added to improve the quality of the resin and the printing process. For example, dyes or inhibitors can be added to control light penetration and ensure high resolution. [8] In addition, diluents can be used to reduce the viscosity of the resin, as well as the use of higher temperatures. Rheological additives and stabilizers can extend the durability of the resin and its stability during longer printings [11].

Absorbers

If complex geometries need to be printed, the depth of light penetration must be precisely defined to avoid over-polymerization in the vertical direction. In order to reduce the depth of penetration into the resin, a light absorber can be used. These chemical species absorb the radiation, competing with the photoinitiator, thus decreasing rate of polymerization and penetration of the radiation. The most commonly used UV absorbers are benzotriazole derivatives [11].

Fillers

Metal or ceramic powders can be added to polymer resin to obtain 3D printable composite materials. The addition of these particles allows further modification of the physical, mechanical, electrical, and optical properties of the final object [11].

CHAPTER 3: SURFACE MODIFICATION FOR ANTIBACTERIAL APPLICATIONS

3.1. 3D PRINTING AND SURFACE MODIFICATION

Often, especially in biomedical applications, polymer resins printed by additive manufacturing techniques do not have the required biofunctionality characteristics, like biocompatibility or transparency. However, it is possible to improve these characteristics through modifications after printing [17]. These modifications may have two main effects: modifying the geometry (physical modification) and/or functionalizing the surface of 3D printed components (chemical modification).

The processes to which a construct can be subjected after 3D printing can be top-down or bottom-up: top-down modifications, such as polishing, sandblasting, and physical etching, do not lead to evident changes in chemical composition but modify the morphology of the components; on the contrary, bottom-up processes, including physical/chemical deposition, coating, and grafting, lead to chemical functionalization of the surface [18].

In the case of functionalized 3D printed objects, it should be emphasized that surface modification strategies must be compatible with the printed structures, i.e. to be effective on complex shapes. The most common modification techniques used in this field can be divided into four categories [18]:

1. Etching treatments, such as plasma etching, laser etching, electrochemical etching.
This top-down technique is widely used to effectively endow the surface with features based on the intrinsic material used in 3D printing, rather than introducing external materials to the surface. Among etching techniques, plasma treatments using various gaseous mediums (oxygen, nitrogen etc.) are widely used to endow the surface with biocompatibility, hydrophilicity, reactivity and adhesion characteristics. Laser and electron beam etching are also often used to obtain surfaces with oriented micro/nano structures, or to reduce surface roughness [18].
2. Deposition processes, e.g. electrochemical deposition, spray-coating or dip-coating.
These bottom-up processes involve the direct deposition of external organic or inorganic compounds to build up the functional surface. Deposition methods commonly encompass both surface chemistry (i.e., functional chemical compositions) and topological micro-nanostructures (i.e., nanoparticles, nanotubes, nano-arrays, nanosheets, etc.). These methods can improve the characteristics of electrical conductivity (e.g., through electrodeposition of a gold layer), hydrophobicity/hydrophilicity (through dip-coating or spin-coating), and in general physicochemical, mechanical and biological properties. However, through the deposition process, it is difficult to impart surface functions to inert materials [18].

3. Graft-polymerization using dopamine.

These techniques have been widely used to achieve chemical functionalization of the surface. A simple and widely used strategy involves the exploitation of certain adhesive proteins in mussels that show strong adhesion to both organic and inorganic surfaces. In particular, dopamine contains catechol and amine groups that are spontaneously deposited on surfaces under appropriate pH conditions [18].

4. Surface functionalization, such as polymer brushes or hydrogel coating.

Grafting techniques have been widely used to impart superwetting, antibacterial, and biocompatibility characteristics to surfaces. Among these techniques, one of the most widely used is polymer brushes, due mainly to their chemical controllability [18].

In the design of antibacterial air filters, the first purpose is not necessarily to kill microorganisms, but to block their passage. Thus, in this context the aim is to modify the surface so that bacteria remain attached. Killing adhering bacteria is thus a secondary purpose for air filters.

In the following sections, the characteristics of an adhesive surface for bacteria, and those of a bactericidal surface, will be described.

3.2. PROPERTIES FOR SURFACE ADHESION

The mechanism of bacterial adhesion to surfaces is very complex and is influenced by several factors [19]. Although this mechanism is not completely understood, it has been reported that interactions between surfaces and bacteria include nonspecific and specific interactions such as charge interactions, hydrophobic interaction, van der Waals forces and specific receptor-adhesion interactions [20]. Therefore, bacterial adhesion depends on the surface chemistry of both the surface and the bacterium itself, as well as the environment and the surrounding conditions.

In designing a surface for bacterial adhesion, several factors must be considered, including surface energy, wettability, surface charges, and material topography [21].

Surface energy is one of the most important physicochemical properties of a solid surface. When a surface is dipped in an aqueous solution, atoms on the surface tend to interact with molecules in the solution, and the type of interaction depends on the chemistry of the surface and the solution [19]. Surface free energy provides a direct measure of interfacial interaction forces. Many studies have shown that bacterial adhesion increases with increasing substrate surface energy [19]. In general, materials can be divided into two macro-categories: high surface energy materials, which are generally hydrophilic, negatively charged, (e.g., inorganic materials such as glass or metals) and low surface energy materials, which are relatively hydrophobic and low electrostatically charged (e.g., organic polymers) [22].

Another property that significantly affects bacterial adhesion is the wettability of the surface. Hydrophobic and ionic interactions between the polymer surface and bacterial cell membranes play a key role in bacterial adhesion [20]. Bacteria, in general, show good adhesion to surfaces with moderate wettability, preferring hydrophobic surfaces over hydrophilic ones [21]. However, it has also been reported that extremely hydrophobic surfaces reduce bacterial adhesion [23], as well as superhydrophilic substrates, which show limited bacterial binding due to reduced hydrophobic interaction and possible repulsive interaction between the bacteria and the surface [21].

Regarding surface topography, a rough surface can promote bacterial adhesion, even topographic patterns favorable to adhesion cannot be generalized, as the shape and size of bacteria also play a role in interactions with surfaces [21].

3.3. BACTERICIDAL SURFACES

Depending on their effect on bacteria, antibacterial surfaces can be divided into two categories: antibiofouling surfaces and bactericidal surfaces.

Biofouling is the growth of microbes on the material's surface, initiated by protein adsorption or microorganisms on the surface of substrate [24]. Antifouling surfaces have a passive effect, drastically reducing the adhesion of bacteria to the surface; they achieve their purpose by having a surface topography or chemistry unfavorable to the adhesion of microorganisms. Examples of this type of material include poly(ethylene glycol) (PEG) coatings and their derivatives [25] [26].

Bactericidal surfaces, on the other hand, have an active effect: they interact directly with bacteria, breaking their membranes or inhibiting their vital processes [27] [28]. Various antimicrobial materials or drugs are exploited for this purpose including, for example, cationic polymers, antimicrobial peptides, antibiotics, and silver ions [26]. Some surfaces can exhibit both effects, reversibly switching between antibiofouling and bactericidal effects [26].

Only surfaces with bactericidal characteristics will be described here, since those with antifouling properties are not inherent to our purpose.

A bactericidal surface is modified or functionalized for the purpose of rapidly killing bacteria that come into contact or approach, inhibiting their proliferation and biofilm formation. These surfaces can act by two mechanisms, depending on whether their effect is based on surface-bacteria contact, or on the release of bactericidal agents [29].

Contact-based bactericidal surfaces contain antibacterial agents that kill bacteria as a consequence of adhesion by covalent bonding or physical adsorption. Most of these antibacterial molecules use their positive charges to disrupt the bacterial membrane or to inhibit the normal metabolic activities of bacterial cells [29].

Release-based bactericidal surfaces, on the other hand, are based on adding antibacterial substances into the existing material by physical and chemical methods or using coatings containing an antibacterial agent. Antibacterial agents released from the material or coating can kill bacteria found near the surfaces of biomaterials, reducing the growth and adhesion of bacteria on the surface. Release-based bactericidal surfaces require bactericides to be loaded or incorporated so that release is gradual over time [29].

There are several categories of materials with antimicrobial properties that can be used for surface modification: common antibiotics, metal ions and oxides, antimicrobial polymers, nanoparticles, and others [30].

Some antimicrobial agents, such as common antibiotics or metal oxides, have long been used for this purpose. Recently, attention has also been paid to new techniques involving the use of antimicrobial polymers or peptides [28] [31].

Antimicrobial polymers can inhibit or inactivate the adhesion or development of microorganisms due to the presence of specific functional groups in its backbone or side chains. Because their

mechanism of action is nonspecific, they do not develop microbial resistance against these polymers.

The biocidal action of most of these polymers depends on contact with bacteria, which are absorbed from the surface through electrostatic interaction. These polymers can be synthetic, such as Poly(ethyleneimine) (PEI), or natural, such as chitosan, which is often used as an antimicrobial coating for biomedical devices, drugs, and others [30].

It is becoming increasingly common to use antimicrobial peptides (AMPs) for the design of antibacterial surfaces [31]. Since AMPs are positively charged, the initial interaction with the bacterial membrane is electrostatic. These peptides destroy the bacterial membrane bilayer through several mechanisms, including pore formation, membrane disintegration, and attack on metabolic functions [32]. In general, two characteristics are common to AMPs: positive charge and a large number of hydrophobic residues. The former property promotes selectivity for negatively charged microbial cytoplasmic membranes, while the latter facilitates interactions with fatty acyl chains [32].

By tuning some critical characteristics such as positive charge, molecular weight, amphipathicity, chain length and functional groups, synthetic mimics of antimicrobial peptides (SMAPs) can be obtained [31]. SMAPs generally have a broad spectrum of activity against bacteria, pathogenic fungi, viruses, and sometimes even to cancer cells. These synthetic polymers are inexpensive and easy to prepare, enabling industrial-scale production of antimicrobial materials [31].

3.4. BACTERIAL CELL WALL

Interactions of bacteria with substrates are closely related to the composition and structure of their membrane, and its behavior depending on the external environment [33].

Bacteria can be divided into two categories according to the structure of their cell wall: Gram-positive and Gram-negative bacteria. The efficacy of the printed devices will be tested toward both Gram-positive (in particular, *Staphylococcus Aureus*) and Gram-negative (*Escherichia Coli*) bacteria.

Gram-positive bacteria have a thin cell wall consisting mainly of murein (or peptidoglycan), which is responsible for the rigidity of the structure. Murein is made up of a polysaccharide backbone consisting of alternating N-Acetylmuramic acid (NAM) and N-acetylglucosamine (NAG) residues in equal amounts. NAM and NAG only differ in the presence, in muramic acid, of a lactic residue; this residue is very important because it provides a docking site for peptide chains. Peptide chains consisting of 4 amino acids, called tetrapeptides, are bound to the carboxyl group of the lactyl residue. The glycan chains are linked together by the bonds between the respective tetrapeptides. In addition to murein, two other important constituents of Gram-positive cell walls are teichoic acid, a polymer of glycopyranosyl glycerol phosphate, and teichuronic acid, which is similar to teichoic acid, but replaces the phosphate functional groups with carboxyls [33].

The cell walls of Gram-negative bacteria are more complex and thicker, with murein making up only 15-20% of the total wall, and the quantitatively largest component being the outer membrane. The outer membrane is a phospholipid bilayer membrane; it confers no particular structural rigidity, which is the task of murein also in gram-negative bacteria. The outer membrane contains phospholipids, lipoproteins, lipopolysaccharides, and proteins [33].

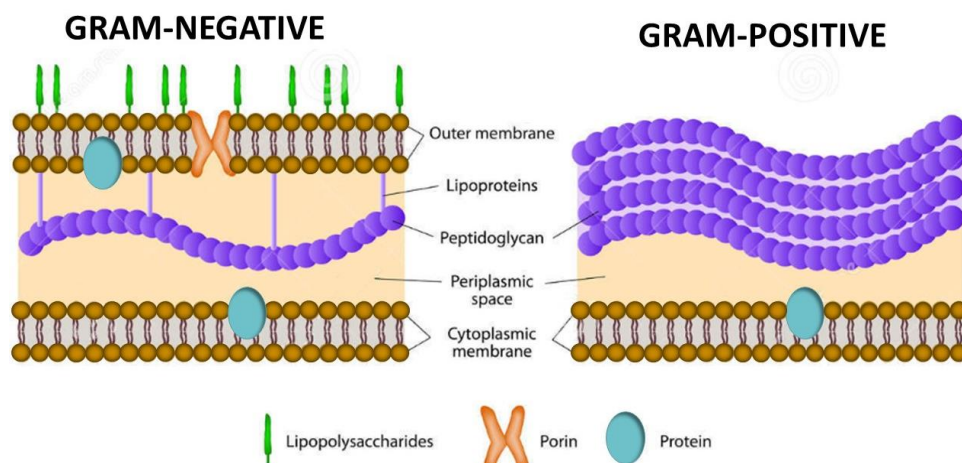


Figure 5 – Differences in Gram-negative and Gram-positive bacteria cell wall

Thus, bacterial cell walls are composed of different polymers and macromolecules that possess carboxyl, hydroxyl, amide and phosphate functional groups.

Despite the fact that the cell walls of Gram-positive bacteria have significant differences from those of Gram-negative bacteria in both structure and chemical composition, the chemistry of surface functional groups is identical. It is possible, however, that differences exist between the minor components and their structure, which may lead to variations in reactivity [33].

3.5. SURFACE-BACTERIA INTERACTIONS

Bacterial adhesion to a surface is a very complex process that depends not only on the properties of the bacterium and the characteristics of the surface, but also on environmental conditions, associated flow conditions, and the presence of proteins or antimicrobial agents [34].

This process can be divided into two phases: an initial phase, which is rapid (in the order of minutes) and reversible; and then a second phase, which is irreversible and occurs on a time scale of several hours [34] [35].

During phase one, the adhesive force between bacteria and surfaces increases rapidly. Initial attachment occurs through the effects of physical forces, such as Brownian motion, van der Waals forces of attraction, gravitational forces, electrostatic and hydrophobic interactions. Thus, phase one is related to long-range physical interactions (nonspecific interactions, with distances >50 nm between bacteria and surfaces) and short-range physical interactions (distances <5 nm, involving hydrogen bonds, ionic interactions, dipoles, and hydrophobic interactions) [34]. It has been shown that electrostatic interactions are the main forces of interaction between bacteria and surfaces, and do not cause significant adverse effects toward pathogens [36]. Hydrophobic interactions also play an important role; although it has not been clearly defined, studies have shown that this type of interaction can lead to bacterial cell wall damage and thus bacterial death [36].

At this stage, surface characteristics (roughness, chemical composition) and bacterial properties (surface charge, bacterial hydrophobicity) play an important role.

The second phase, on the other hand, is related to specific reactions between the bacterial surface structures and the surface [34].

Therefore, the binding between the 3D printed filter surface and the bacterial wall can be of various types, taking advantage of electrostatic charges, hydrogen bonds, interactions with specific functional groups or hydrophobic interactions.

3.6. STRATEGIES FOR SYNTHESIS

Molecules containing amine groups will be used for surface modification of 3D printed samples. The amine groups of the functional molecules will be exploited to bind to the pendant groups of the polymer matrix. Depending on the matrix, different functional groups will be present on the surface.

A more detailed description of the polymer matrices and functionalization molecules used will be given in Chapter 4.

The reactions that will take place are as follows:

1. MICHAEL ADDITION BETWEEN AN ACRYLIC DOUBLE BOND + AMINE GROUP

This reaction consists in the addition of a nucleophile (the amine group) to the double bond of the acrylic group, as shown in the figure below:

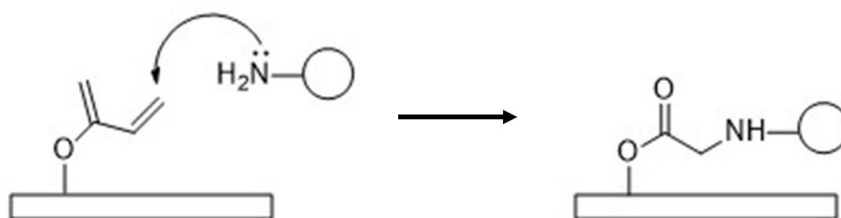


Figure 6 - Michael's addition of the amine group to the acrylic group.

2. NUCLEOPHILIC ADDITION TO AN EPOXY RING

In this reaction, the nucleophilic amine group attacks the electron-deficient carbon atom from the epoxy ring, followed by the transference of a hydrogen atom from the amine group to the oxygen, and the formation of the bond between carbon and nitrogen.

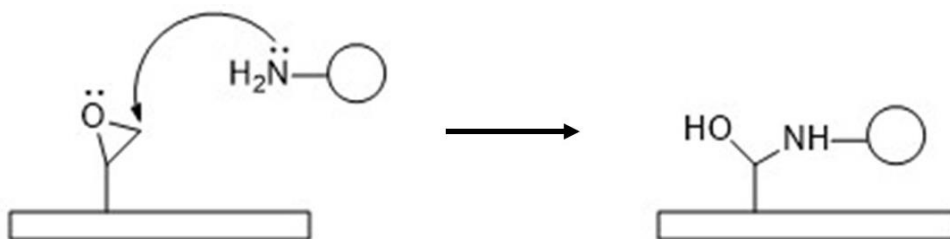


Figure 7 -Reaction between epoxy ring and amine group

3. AMIDATION OF CARBOXYL GROUP

The formation of an amide group can take place through the reaction between the carboxylic group and the amine group. This reaction usually needs to be promoted by the presence of

molecules which enhance the reactivity of the carboxyl group, such as EDC/NHS (1-ethyl-3-(3-dimethylaminopropyl) carbodiimide/*N*-hydroxysuccinimide), activators of carbodiimide chemistry.

The reaction between the carboxylic group and EDC produces an unstable product that, in the absence of NHS, undergoes hydrolysis by reforming the free carboxylic group. Otherwise, the NHS promotes the production of a stable amide bond. This type of reaction is described by the diagram below:

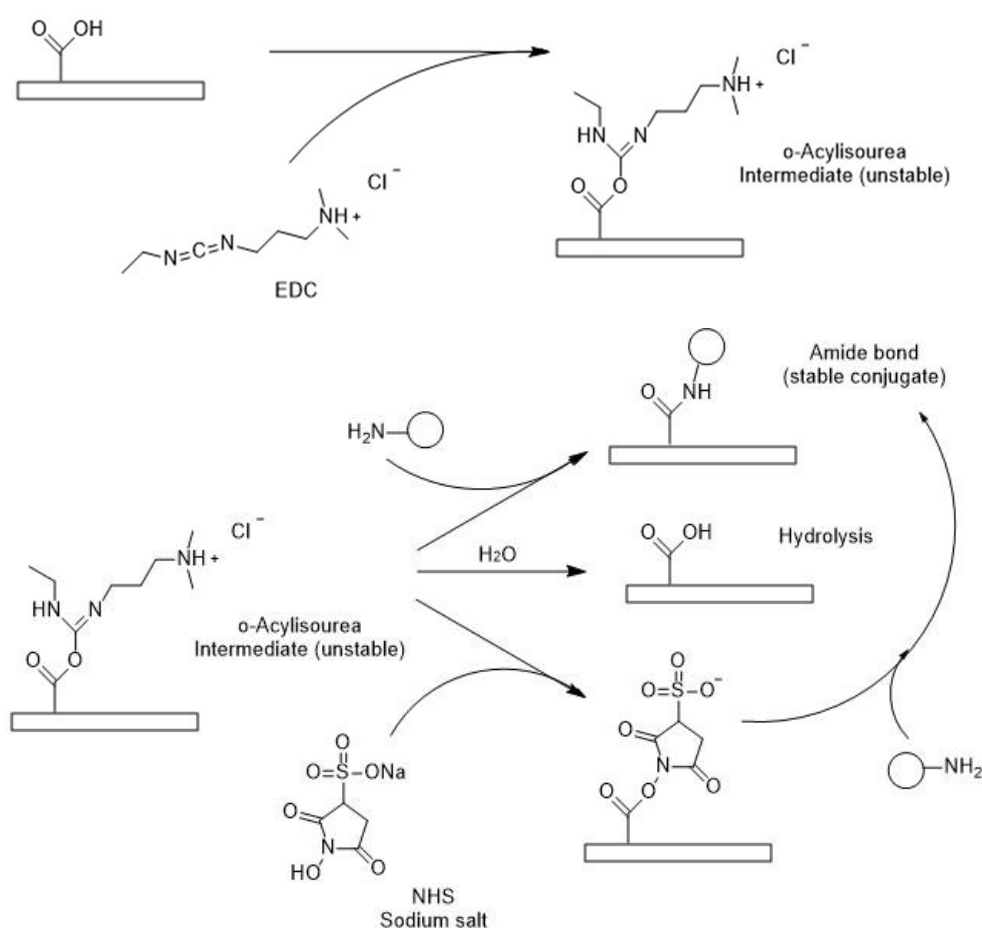


Figure 8 - Activation of carbodiimide chemistry through EDC/NHS for the bonding between carboxyl and amine group

Different techniques will be used for functionalization: conventional and microwave heating, dopamine dip-coating and chlorination to obtain N-halamines. These techniques are described in the next sections.

3.6.1. MICROWAVE AND CONVENTIONAL HEATING

The strategy followed here to give the material adhesion and bactericidal properties is to include functional groups in the surface of 3D printed samples. The grafting reaction is thermally activated when a certain temperature is reached.

Conventionally, this type of reaction is carried out by conductive heating with an external heat source of a liquid medium that contains the sample and the grafting agents, raising the temperature by convection. Although this method is quite effective, it is slow method and presents several critical aspects. First, it depends on convection currents and the thermal conductivity of the materials/fluids used. Also, because the reaction takes place in a vessel heated by an external heat source, the temperature of the vessel is higher than that of the mixture inside. Finally, a thermal gradient often develops, and local overheating can lead to poor reaction control and/or sample degradation. The heating rate must be slow to reduce the strong thermal gradient that leads to process-induced stresses [37]. Therefore, a large amount of energy is consumed [38].

As an alternative to conventional heating, microwave heating has been shown to be faster and more efficient [39]. This method is not based on heat transfer, but on the conversion of electromagnetic energy into thermal energy [37].

Microwaves are electromagnetic waves with wavelengths between 1 mm and 1 m and corresponding frequencies between 300 MHz and 300 GHz [40] [37]. The most commonly used frequencies are 0.915 GHz and 2.45 GHz, as they maximize penetration depth [37].

Microwave energy easily penetrates inside the material and it can be heated all at once resulting in volumetric heating [39], whereas in the conventionally heated vessel, the reaction mixture in contact with the vessel wall is heated first [38].

This is accomplished by rotational and vibrational effects, thus reducing heat transfer problems. Thus, the thermal gradient in microwave-treated material is inverse to that of material treated by conventional heating [37].

However, microwave irradiation could affect the chemical and morphological structure of the sample, including some physical properties [39]. In addition, using a microwave reactor has other disadvantages, mainly related to the fact that the microwave reactor is a closed environment. This makes almost impossible to add reagents during the reaction, and to perform online monitoring of the reaction. In addition, the equipment is very expensive [38].

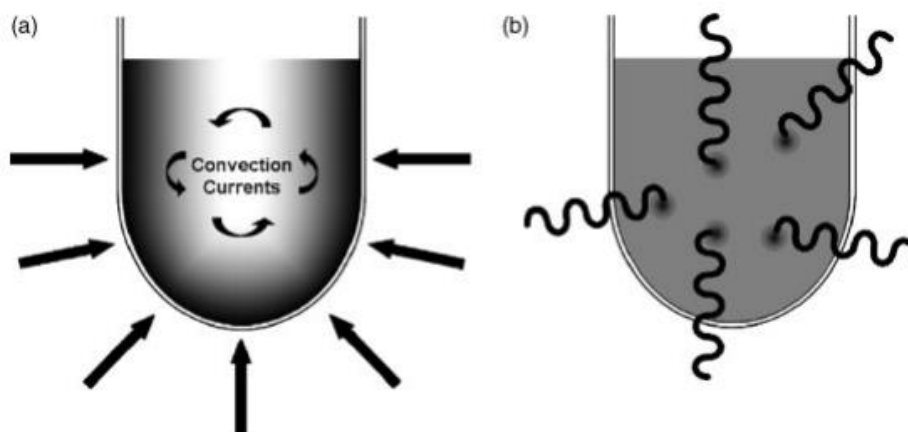


Figure 9 - Comparison of (A) conventional and (B) microwave heating [38]

3.6.2. DIP-COATING WITH POLY-DOPAMINE

Dopamine is a mussel-derived bio-adhesive molecule with unique adhesion properties to various substrates, even in aqueous solutions [41]. DOPA is a catechol: the pendant catechol group is directly responsible for moisture-resistant adhesion [42].

When exposed to an aerobic environment, dopamine undergoes oxidation; the oxidation product, dopamine quinone, undergoes an intramolecular nucleophilic cyclization reaction that also leads to the formation of 5,6-dihydroxyindole (DHI) [43]. Although this process has not yet been fully elucidated, it is most likely that polydopamine is formed through two different and simultaneous processes: the polymerization of these two molecules to form a heteropolymer [43] and a noncovalent "self-assembly" of dopamine, dopamine quinone, and DHI [43].

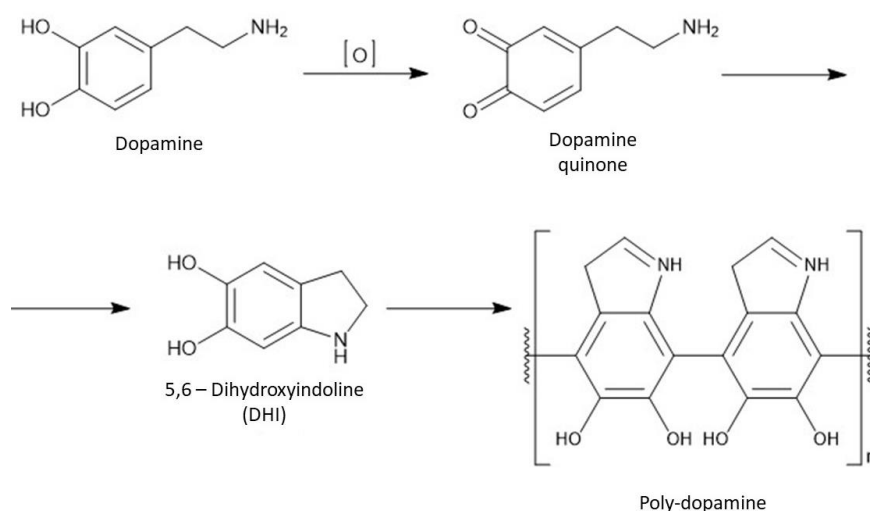


Figure 10 – Mechanism of dopamine polymerization

DOPA and its polymeric form, polydopamine (PDA), are widely used for surface functionalization through simple and highly adaptable methods [43].

The use of polydopamine (PDA) increases adhesion to organic surfaces by forming high-strength irreversible covalent bonds but tends to drastically reduce the strength of interactions with inorganic surfaces [44].

However, the adhesion mechanism is mainly due to catechol groups, which generate strong noncovalent bonding interactions [42], depending on the surface chemistry of the substrate: for example, they may interact with amine groups in biological tissues through a combination of hydrogen bonds, cation- π interactions and Michael addition [44]. In the following figure we can see some examples of the DOPA-surface interaction, which include hydrophobic interactions, hydrogen bonds, π - π and cation- π interactions [41] [44].

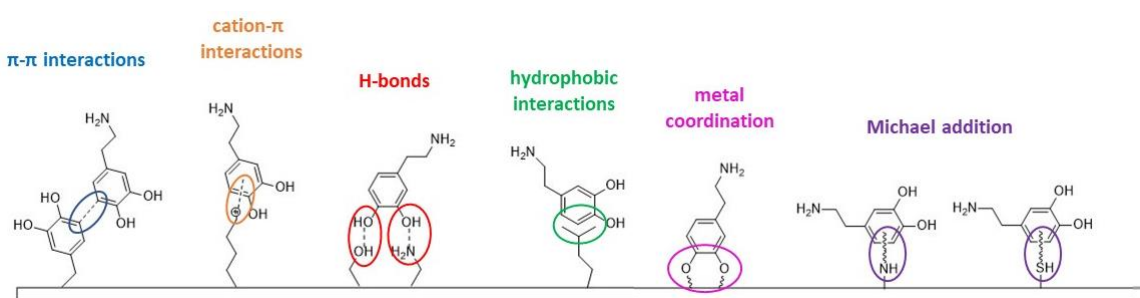


Figure 11 – Schematic representation of the types of bonds dopamine can make

Due to the ability of catechol groups to form different types of bonds, the method of coating with DOPA or PDA involves simply immersing it in an aqueous alkaline dopamine solution for an adjustable period of time. During the incubation period, DOPA or PDA is spontaneously deposited as a uniform thin film on organic and inorganic surfaces, regardless of geometry and size. The coating can be used as a "primer" for further coatings or without further modification [43].

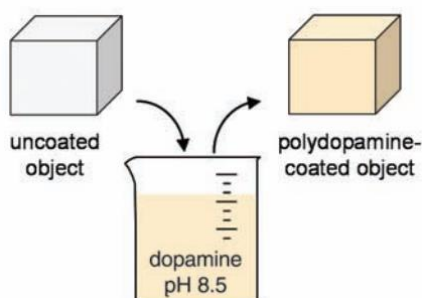


Figure 12 – Dip-coating mechanism

3.6.3. CHLORINATION

An N-halamine is an organic or inorganic compound containing one or more nitrogen-halogen covalent bonds [45] [46], which is formed by halogenation of an amine, amide, or imide compound; we speak of amine N-halamines, amide N-halamines, and imide N-halamines, respectively [45]. The halogen can be chlorine, bromine or iodine, but the most common is chlorine [45].

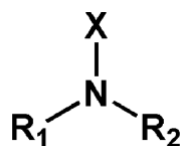


Figure 13 - Structural illustration of N-halamine compound.
 $\text{R}_1, \text{R}_2 = \text{H}, \text{X}$, inorganic group and/or organic group. $\text{X} = \text{Cl}, \text{Br}$, or I .

Halogen-based antibacterial agents have been adopted because of their cost-effectiveness and ability to kill most microorganisms quickly [45]. The use of N-halamines has some advantages over free halogens, such as long-term stability in aqueous solution, high durability, good safety for humans and the environment, less corrosion than free halogens, and low cost [45] [46].

Because halogen atoms are in a strong oxidative state, N-halamines have been reported to exhibit potent antibacterial activity against pathogens without causing bacterial resistance [45]. When microorganisms come into contact with N-halamines, a halogen exchange reaction occurs, resulting in cell expulsion [46].

The chlorination reaction is carried out by immersing the samples, bearing amine groups on the surface, in a 2% HClO aqueous solution.

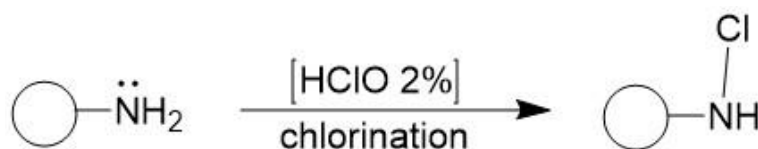


Figure 14 – Chlorination reaction

CHAPTER 4: MATERIALS AND METHODS

4.1. DLP 3D PRINTER

As 3D printing equipment, a Pico 2 HD DLP-3D printer (Asiga, Australia) was used. This 3D printer has a LED light source with a wavelength of 405 nm, build area of $64 \times 40 \times 76 \text{ mm}^3$ with nominal XY resolution of 50 μm , and minimum Z-axis control of 1 μm . All CAD designs were produced with the FreeCAD program and exported in STL format.

The structures were produced by fixing a printing slicing of 200 μm . Other printing parameters, such as light intensity and exposure time, are different depending on the geometry and formulation.

4.2. MATERIALS FOR 3D PRINTING

The functional monomer chosen as the structural ingredient for the polymer matrix is poly(ethylene glycol)diacrylate (PEGDA), which is known for its dimensional stability and good printability. PEGDA is a light-curable compound that can cross-link due to the presence of two double bonds in its structure. The presence of the acrylate groups promotes a radical-type polymerization. That is why PEGDA-based material combinations are widely used in 3D printing techniques employing photopolymerization. [47]

In addition to PEGDA, several functional monomers were investigated. Two strategies were investigated:

- one strategy involves the choice of monomers that can provide functional groups useful for subsequent chemical modification, such as acrylic acid (AA) and glycidyl methacrylate (GMA);
- the second strategy involves using a monomer for its chemical-physical characteristics, such as butyl acrylate (ABut), which we choose for its hydrophobicity.

Photopolymerization reaction also requires a photoinitiator: phenylbis (2,4,6-trimethylbenzoyl) phosphine oxide (BAPO) was used in all the formulations, since it adequately absorbs the 3D printer emission wavelength at 405 nm.

The chemical structures of the components used are shown in Figure 15.

In some of the formulations, a dye is added to better control 3D printing, avoiding uncontrolled polymerization. The chosen dye is brilliant green (BG), a type of triphenylmethane dye since its antiseptic properties have been extensively studied and its bactericidal activity against gram-

positive organisms has been demonstrated [48]. The chemical structure of the dye is shown in Figure 16.

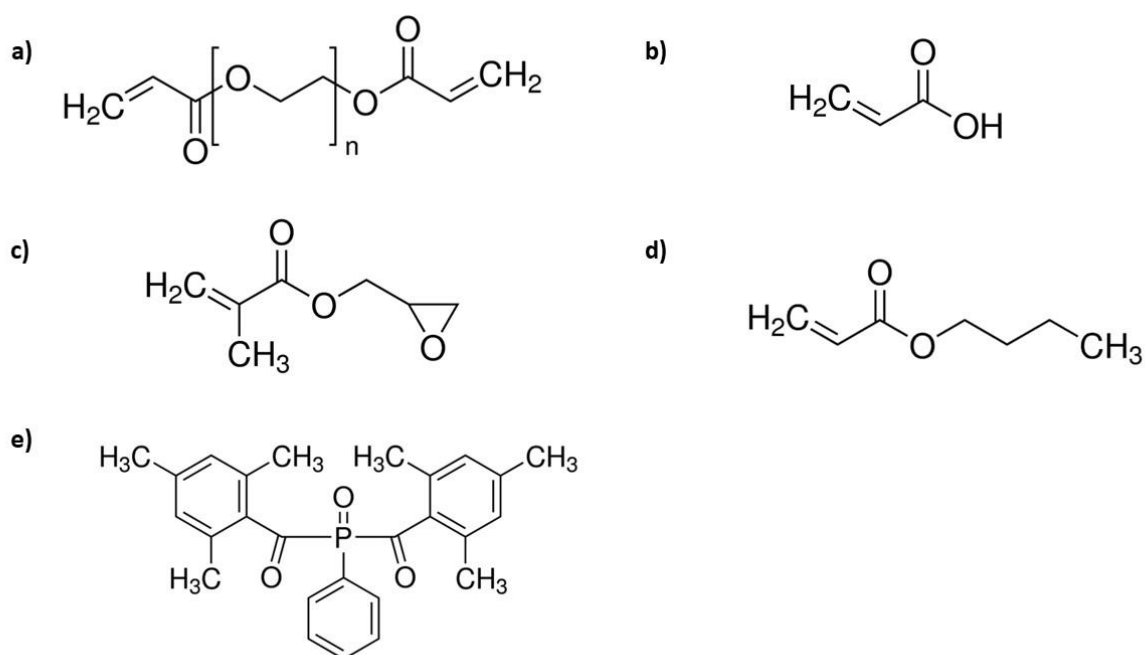


Figure 15 - Chemical structures of (a) polyethylene glycol diacrylate (PEGDA₂₅₀), (b) acrylic acid (AA), (c) glycidyl methacrylate (GMA), (d) butyl acrylate (ABut) and (e) phenyl bis(2,4,6-trimethylbenzoyl)phosphine oxide (BAPO) [49]

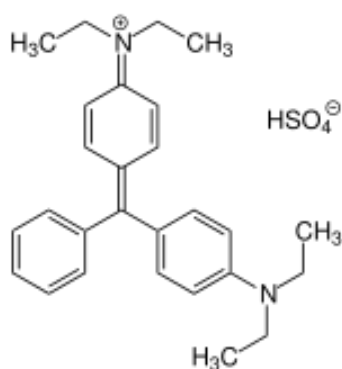


Figure 16 - Chemical structure of brilliant green (BG) [49]

PEGDA₂₅₀ (Mn = 250 g/mol), AA (99%, Mn = 72.063 g/mol), GMA (97%, Mn = 142.15 g/mol), ABut (99%, Mn = 128,171 g/mol), BAPO (97 %) and brilliant green (BG, dye content ~90 %) [49] were purchased from Sigma-Aldrich (Merck Company, Darmstadt, Germany) and used as received. Ethanol (EtOH, 99.8 %) was also used for the washing/sonication steps.

4.3. PREPARATION OF 3D PRINTING FORMULATIONS AND PRINTING PROCEDURE

Five photocurable formulations were prepared with different weight ratios between monomers:

1. PEGDA₂₅₀
2. PEGDA₂₅₀/ABut (80:20)
3. PEGDA₂₅₀/AA/ABut (80:15:5)
4. PEGDA₂₅₀/AA (80:20)
5. PEGDA₂₅₀/GMA (80:20)

Each formulation was prepared by adding 2 phr (per hundred resins) of BAPO.

Formulation 2 requires the use of brilliant green, which was added in an amount of 0.1 phr. In this case, after adding the dye, the solution was stirred mechanically at 40°C until complete dissolution.

Each solution is prepared in a black falcon to avoid polymerization due to visible light. The solution is then sonicated for a few minutes to make it homogeneous.

During the printing procedure, small amounts of resin should be added at a time: this serves both to avoid waste and to prevent unwanted polymerization.

After printing, the object is peeled off the printing plate with the help of a blade. It is placed in a beaker containing ethanol and sonicated for 10-30s to remove residual resin. Finally, the object is post-cured for 1-3 minutes using an UV chamber (Broad-band from Asiga, light intensity of 10mW/cm²).

4.4. MATERIALS FOR FUNCTIONALIZATION

Four molecules were selected for functionalization. In details:

1 Arginine (L-arginine, 98%):

Arginine is a natural amino acid whose side chain is composed of a hydrophobic propyl moiety and a large polar guanidinium cationic group, capable of creating up to 6 hydrogen bonds [50]. The guanidinium group has a pKa greater than 12, so arginine is protonated and positively charged in all biological environments. Because of its polar and positively charged nature, arginine is often considered the most hydrophilic of the 20 natural amino acids [50].

2 Agmatine (agmatine sulfate, 97%):

Agmatine is a primary amine formed by the decarboxylation of L-arginine by the enzyme arginine decarboxylase (ADC) [51]. Thus, it has the same structure as arginine but lacks the carboxyl group

3 Polyethylenimine, branched (PEI600, Mw=800, Mn=600):

Polyethylenimine (PEI) is a polymer with repeating units composed of the amine group and two aliphatic carbon $\text{CH}_2\text{-CH}_2$ spacers. Branched polyethylenimines contain primary, secondary and tertiary amine groups, unlike linear polyethylenimines that contain only secondary amines [52].

4 Dopamine hydrochloride (DOPA):

As seen in Chapter 3, dopamine is a catechol with strong adhesion properties to various substrates, even in aqueous solutions.

The chemical structures of these molecules are shown in Figure 17.

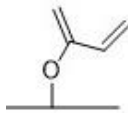
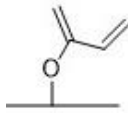
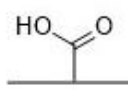
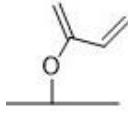
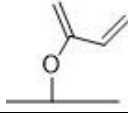
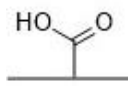
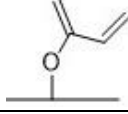

In some of the reactions, EDC/NHS were used as coupling agents.

Agmatine was purchased from Alfa Aesar (Thermo Fisher Scientific, USA); arginine, dopamine, polyethylenimine, EDC and NHS were purchased from Sigma-Aldrich (Merck Company, Darmstadt, Germany). All the products were used as received.

4.5. SURFACE MODIFICATION REACTIONS

In all formulations, acrylic double bonds are present because they are remaining unreacted groups on surface. The following table provides a summary of the functional groups associated with the respective matrices.

Table 1 - Functional groups associated with each matrix

Matrix	Pendant functional groups	
PEGDA ₂₅₀	Acrylic group	
PEGDA ₂₅₀ /AA	Acrylic group	
	Carboxyl group	
PEGDA ₂₅₀ /ABut	Acrylic group	
PEGDA ₂₅₀ /AA/ABut	Acrylic group	
	Carboxyl group	
PEGDA ₂₅₀ /GMA	Acrylic group	
	Epoxy ring	

As we saw in Chapter 3, several reactions take place, depending on the matrix and functionalization molecule:

1. Michael addition to double bonds → it involves Arginine, Agmatine and PEI, and occurs in all matrices, as they all have surface acrylic groups;
2. Epoxide group ring opening → it involves Arginine, Agmatine and PEI, and occurs only in the matrix containing GMA;
3. Amidation of the carboxylic group → it involves Arginine and Agmatine, and occurs only in matrices containing acrylic acid (PEGDA/AA and PEGDA/AA/ABut);
4. Synthesis of pDOPA coating the surface.

4.6. FUNCTIONALIZATION METHODS

4.6.1. GRAFTING THROUGH CONVENTIONAL HEATING

The general procedure for surface modification through conventional reaction is the following: in a round-bottom flask provided with a magnetic stirrer and a refrigerator the solid reactants are placed and sufficient volume of the specific buffer solution is added. When the solution is clear, the 3D printed specimen is added, and the reaction is maintained at the desired temperature for the selected time with the aid of a sand bath (see all conditions in Table 2). At the end of the reaction the sample is removed, exhaustively washed with water and dried with absorbent paper. Finally, the sample is placed in a vacuum dessicator at -70 cmHg, for at least 6 hours at room temperature, to remove any excess of water.

Table 2 - Experimental conditions for reactions obtained by conventional heating

MATRIX	REACTANT	TYPE OF REACTION	COUPLING AGENT	BUFFER	pH	REACTION TIME	TEMPERATURE
PEGDA/AA	Arg (15.2 mg/mL)	- Michael addition - Amidation	EDC (5,4 mg/mL) NHS (3,9 mg/mL)	Phosphate	5.8	24h	100°C
	Agm (19.7 mg/mL)	- Michael addition	-----	Tris HCl	8.6	24h	100°C
PEGDA/GMA	Arg (15.2 mg/mL)	- Michael addition - Epoxy opening	-----	Tris HCl	8.6	24, 72h	100°C
	Agm (19.7 mg/mL)	- Michael addition - Epoxy opening	-----	Tris HCl	8.6	24, 48, 72h	100°C

4.6.2. GRAFTING THROUGH MICROWAVE HEATING

Microwave reactions are performed in an Anton-Paar Monowave 300 reactor, with maximum operating temperature of 300°C and maximum attainable pressure of 30 bar. A 10 mL vial, sealed with silicon septum and made of borosilicate glass, with operation volume of 2-6 mL (G10 vial), is used. [53].

The reactor requires setting the reaction parameters: heating temperature, irradiation time, stirring speed and cooling temperature. The reaction proceeds following 3 steps:

1. First, the sample is heated from room temperature to the selected temperature.

2. According to the treatment process, the system is then subjected to an isothermal MW irradiation phase for a specific time and temperature (irradiation time and temp).
 3. Finally, the sample is cooled down to room temperature.
- A different value of stirring speed can be set for each phase.

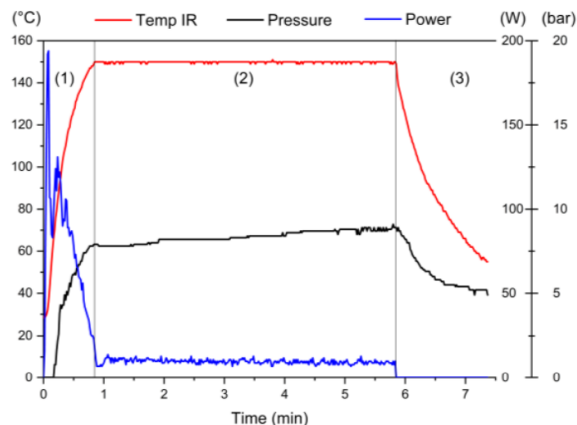


Figure 18 - Example of a microwave treatment; The graph shows the power (W) and pressure (bar) given to the system to reach the desired temperature (°C) during a specific time (t).

The procedure for surface modification through microwave reaction is the following:

Solvent, reactants and the 3D printed sample are placed into the vial, and the desired reaction parameters are set: heating temperature, irradiation time, stirring speed and cooling temperature. At the end of the reaction the sample is removed, exhaustively washed with water and dried with absorbent paper. The sample is placed in vacuum dessicator at -70 cmHg, for at least 6 hours at room temperature, to remove any excess of water. All experimental parameters are summarized in table 3.

Table 3 - Experimental conditions for reactions obtained by microwave heating

MATRIX	REACTANT	TYPE OF REACTION	COUPLING AGENT	BUFFER	pH	REACTION TIME	TEMPERATURE
PEGDA/AA	Arg (15.2 mg/mL)	- Michael addition - Amidation	EDC (5,4 mg/mL) NHS (3,9 mg/mL)	Phosphate	5.8	3, 5min	150°C
	Agm (19.7 mg/mL)	- Michael addition	-----	Tris HCl	8.6	3, 5, 7min	150°C
	PEI600 (33.3 mg/mL)	- Michael addition	-----	Acetonitrile		1 min	150°C
PEGDA/GMA	Arg (15.2 mg/mL)	- Michael addition - Epoxy opening	-----	Tris HCl	8.6	3, 5, 7, 10min	150°C
	Agm (19.7 mg/mL)	- Michael addition - Epoxy opening	-----	Tris HCl	8.6	3, 5, 7, 10min	150°C
	PEI600 (33.3 mg/mL)	- Michael addition		Acetonitrile		1min	150°C

4.6.3. DIP-COATING

Modification with poly-dopamine is done by following the same technique used by Lee and coauthors [54].

The reaction occurs by simply immersing the substrate in a dilute aqueous solution of dopamine, buffered to pH=8.5, a pH typical of marine environments. Dopamine concentration is 3mg/mL.

The reaction proceeds in an open flask, under gentle agitation (80 rpm) for 24h at room temperature; thus oxygen oxidizes dopamine and polymerization to give poly-DOPA occurs. A thin p-DOPA coating onto the surface is formed, which could be detected by a colour change.

At the end of the reaction the sample is exhaustively washed with water, dried with absorbent paper and placed in a vacuum dessicator at -70 cmHg, for at least 6 hours at room temperature.



Figure 19 - Dip-coating treatment: gentle agitation of open flasks (on the left); oxidized dopamine (on the right)

4.6.4. CHLORINATION

The chlorination reaction is carried out by immersing the samples, bearing amine groups on the surface, in a 2 percent HClO aqueous solution. The solution must completely fill the vessel, which must be closed so as to limit the formation and minimize escape of the gases. The reaction is carried on under stirring (160 rpm) for 2h at room temperature.

At the end of the reaction, the sample is dried with blotting paper and immersed in plenty of water, under magnetic stirring, for 2h. Then is placed in a vacuum pump at -70 cmHg, at room temperature, overnight.

4.7. PROTOCOL FOR BIOLOGICAL TEST

Biological tests are conducted following the protocol designed by Institute for Biofunctional Studies of the Universidad Complutense de Madrid (UCM). The procedure is the following:

- DAY 1

1. STERILIZATION OF SURFACES

- In a multiwell plate, perform 3 washes with a 70% ethanol solution. The solution should completely cover the sample. Each wash will last 10 minutes.
- Perform 1 wash with PBS for 10 minutes.
- Remove the previous PBS and pour new PBS.
- Place the samples under an ultraviolet lamp for sterilization for 20 minutes for both sides of the sample.
- Under a fume hood, remove the PBS and cover the samples with new PBS.

2. PROTOCOL INOCULUM PREPARATION AND BACTERIAL AMPLIFICATION

- In a falcon, under a fume hood, prepare a 1:10 dilution of bacteria (from a previous bacterial culture) in bacterial medium.
- Incubate the falcon in a dynamic incubator at 37 °C and 125 rpm for 24 hours. Make sure that the falcon stopper is half open. This allows air to enter and flow into the falcon so that the bacteria can carry out gas exchange.

- DAY 2

1. OPTICAL DENSITY PROTOCOL

The optical density protocol is used to check the amount of bacteria being grown. The higher the optical density, the more bacteria there will be in the medium and therefore the less time it will take to grow once the surfaces are seeded. We use a spectrophotometer that gives us information about absorbance at 600 nm. The ideal optical density corresponds to a coefficient of 0.8-1.0. If a lower value is obtained, an additional dynamic incubation period is required. If a higher value is obtained, bacterial medium can be added to dilute and decrease the density.

The absorbance of 1ml of medium is measured as a reference.

2. SEEDING PROTOCOL

PBS is used as medium for the experiment because, in this environment, bacteria has an adequate rate of growth to be analyzed.

- Remove the PBS and add the bacterial culture solution to each specimen until completely covered.
- Incubate at 37 °C for 1 hour.
- Remove the solution from the wells.
- Add new PBS until the surfaces are completely covered.
- Leave the samples incubating at 37 °C for 48 hours.

- DAY 4

1. LIVE/DEAD PROTOCOL

The live/dead bacteria protocol uses two different reagents, in a 1:1 ratio:

- SYTO: enters by endocytosis into all cells (alive and dead) and binds to bacterial DNA.
- Propidium iodide: enters in dead cells through pores. As it has more charge than SYTO, in dead cells replaces this last one by binding to bacterial DNA.
- Prepare a dye solution at 3 µl per ml with distilled water or PBS (1.5 µl of each reagent per ml of solution).
- Mix and incubate for 15 minutes. The dyes are sensitive to light, so they should not be exposed to light sources.
- Pour the dye solution onto the specimens until they are completely covered.
- Incubate for 15 minutes, away from light sources.
- Remove the solution and add PBS until the surfaces are completely covered.
- Use fluorescence microscopy to view the bacteria, with the 10x and 20x objectives. Use the green light filter to see the live bacteria and the red filter for the dead ones.

4.8. CHARACTERIZATION METHODS

4.8.1. 3D SCANNER



Figure 20 - 3Shape E4 scanner

A 3D scanner was used to compare the printed geometry with the one drawn on CAD software, and thus be able to evaluate the printing fidelity. The scanner used is the 3Shape E4 (3Shape A/S, Copenhagen, Denmark), equipped with four 5 MP cameras and with a measurement accuracy of 4 μm . Scan analysis was performed with Convince software from 3Shape.

The sample is covered with a thin layer of talc and placed on the scanner platform. The resulting image is compared with the original CAD file to obtain a colorimetric map.

4.8.2. SWELLING AND RECOVERY TEST

The samples were immersed in 25 mL of water for 24 hours at room temperature. Swelling percentage (ws%) in water was determined by measuring the weight difference between the swelled sample (W_w) and the initial one (W_i).

$$ws\% = \left(\frac{W_w - W_i}{W_i} \right) * 100$$

After the swelling test, a recovery test was performed to evaluate the effectiveness of the drying procedure. Samples were weighed after a period of 24 h immersed in water; afterwards, they were placed in a vacuum pump for 6 h and weighted again (W_f); the difference between these two values gives the percentage of recovery (wr%).

$$wr\% = 100 - \left[\left(\frac{W_f - W_i}{W_i} \right) * 100 \right]$$

4.8.3. FTIR-ATR SPECTROSCOPY

The FTIR spectroscopy measures the absorption of a sample in the mid-infrared range of the electromagnetic spectrum ($4000\text{--}500\text{cm}^{-1}$). All functional groups present a specific absorption in a given wavelength, so the analysis of the bands in the spectrum gives information about its chemical composition. When working in absorbance mode, the measurement of the intensity of the bands is a quantitative measurement. By Fourier transform operations, the raw data is converted into the final spectrum, composed of multiple peaks where the absorption intensity is associated with the change of a molecule's dipole moment. An attenuated total reflectance (ATR) accessory is used to measure samples' properties at a surface level rather than the entire bulk of the material. In this case, the IR signal slightly penetrates inside the sample's surface, of around 1-2 micrometers.

Here, FTIR spectroscopy is used to characterize the samples by following the change of the peaks related to functional groups.

The IR spectra were recorded with a PerkinElmer Spectrum Two spectrometer in transmission mode, with a resolution of 4 cm^{-1} , averaging 4 scans for each spectrum, in a wavenumbers range of $400 - 4000\text{ cm}^{-1}$.

The obtained spectra were referenced at $\text{Abs}_{4000}=0$. In this way, all the spectra have the same baseline. As the amount of ester groups ($-\text{COOR}$) is constant for all samples, the spectra were normalized with respect to the 1720 cm^{-1} peak, corresponding to this group.



Figure 21 - PerkinElmer Spectrum Two spectrometer

4.8.4. CONTACT ANGLE

Contact angle measurement is a very simple approach to determine the surface energy, wettability and hydrophilicity of a solid sample and can also provide a good understanding of surface properties. [55].

Quantitative evaluation of the hydrophilicity and surface energy of a solid is done measuring the contact angle θ of a drop of water deposited onto the surface. Figure 22 shows a schematic diagram for the contact angle and interfacial stresses at the boundary of the three phases.

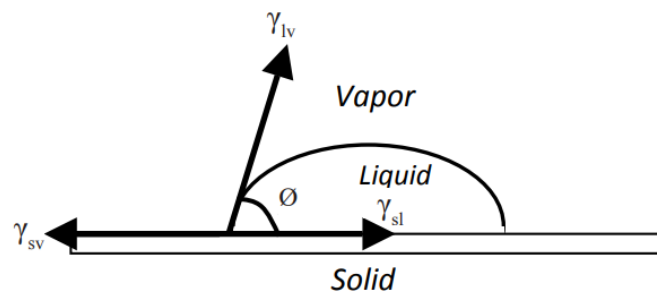


Figure 22 - Schematic diagram of contact angle [55]

The most important relationship concerning the contact angle is Young's equation, which relates the contact angle θ , the liquid surface tension γ_l , the solid surface energy γ_s , and the solid-liquid surface tension γ_{sl} as expressed in the following equation:

$$\gamma_s = \gamma_{sl} + \gamma_l \cos \theta$$

Contact angle measurement were determined using an CAM200 goniometer (KSV instruments), equipped with a video camera and an image analyzer. The tests were performed at room temperature using the sessile drop technique. A 3 μL droplet of water (72,8 mN/m) was placed onto the sample surface, and the static angle was measured. The test was repeated ten times for each sample.

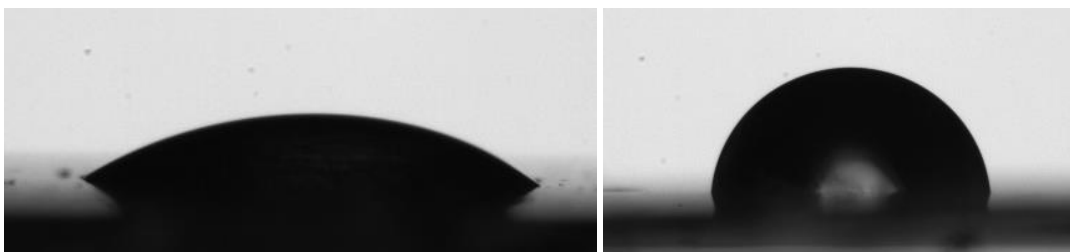


Figure 23 - Comparison between a hydrophilic (on the left) and a hydrophobic (on the right) substrate

The contact angle measurement can be a very useful indication: a change in this parameter indicates that a surface modification has occurred. In our case, we expect a decrease in contact angle (and thus an increase in surface hydrophilicity) after the chemical modifications. In the conditions of our measurements, the variation of the contact angle gives an empirical indication of the success of the modification reactions.

4.8.5. EDX

The distribution of nitrogen on surface of modified materials are evaluated by Scanning Electron Microscopy (SEM) with Energy Dispersive X-Ray Analysis (EDX). A Bruker Nano equipment with XFlash Detector 5030 was used to investigate the relative concentration of nitrogen retained on the unreacted and modified coating surface after the different reaction processes. A probe current of 2.0×10^{-9} A and an accelerating voltage of 15 kV were used. The spot size irradiated was approximately 0.5 mm² for all specimens. To determine the relative nitrogen concentrations on the membrane surface, X-ray net counts were obtained at three random locations for each specimen with a collection time of 30 s. Three specimens were used for each condition. Samples were metalized with Cr prior to be analyzed. From all samples, an X-ray map was obtained showing an homogeneous distribution of nitrogen along the entire surface.

4.8.6. TGA

TGA Q500 thermal analyzer (TA instruments, New Castle, DE, USA) was used to perform thermogravimetric measurements under dynamic mode using air atmosphere. Samples were heated from room temperature to 800°C at a heating rate of 10°C/min. The initial degradation temperature (T_0) were obtained at 5% of mass loss and temperature at the maximum degradation rate (T_{MAX}) were obtained from the first derivative of the TGA curves (DTG).

4.8.7. OPTICAL DENSITY

The optical density of the bacterial culture was measured using a Specord 250 spectrophotometer (Analytic Jena) in combination with WinASPECT software.

4.8.8. FLUORESCENCE MICROSCOPE

An inverted fluorescence microscope IX51 from Olympus Co. (Tokyo, Japan) was used to evaluate bacteria viability over the samples.



Figure 24 - IX51 fluorescence microscope

4.8.9. IMAGE-PROCESSING WITH IMAGEJ

The processing of the images taken with fluorescence microscope is done with ImageJ software, which allows us to know the number of bacteria present and the percentage of area they cover. Three steps were carried out for the bacteria quantification:

1. transforming the images to 16 bits;
2. applying a manual threshold;
3. analyzing particles to obtain the number of bacteria and the percentage of live or dead bacteria on the surface.

An example of image processing is shown in Figure 25.

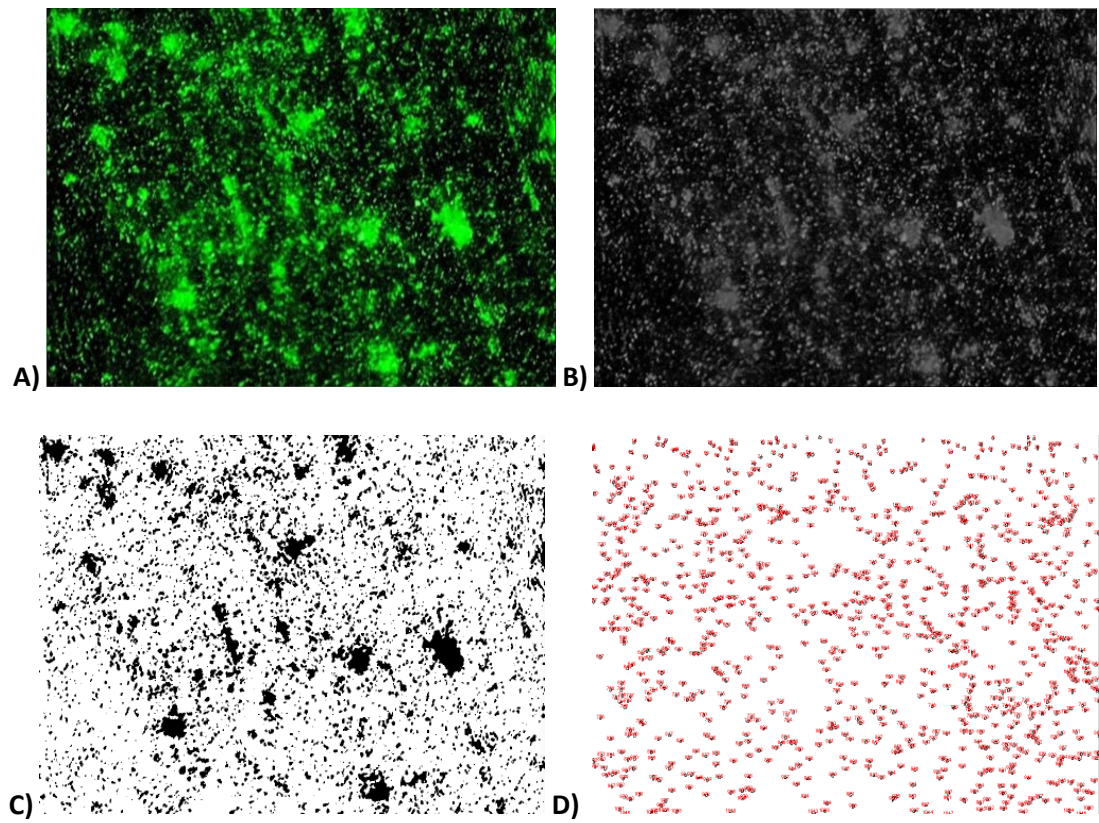


*Figure 25 - Image processing: A) original image B) image at 16-bits
C) image with the applied threshold D) count of particles*

CHAPTER 5: PRINTING AND SURFACE TREATMENT: RESULTS AND DISCUSSION

5.1. SOLIDWORKS DESIGN

Before the printing process, a CAD file representing the desired geometry must be created. Different geometries were drawn and then printed with different resins. The two geometries found to be the best from the point of view of printing performance will be reported in detail.

The first geometry involves the superposition of several layers that are equal to each other but rotated; this type of geometry works in the predominantly axial direction and is not effective with radial or circumferential air flows.

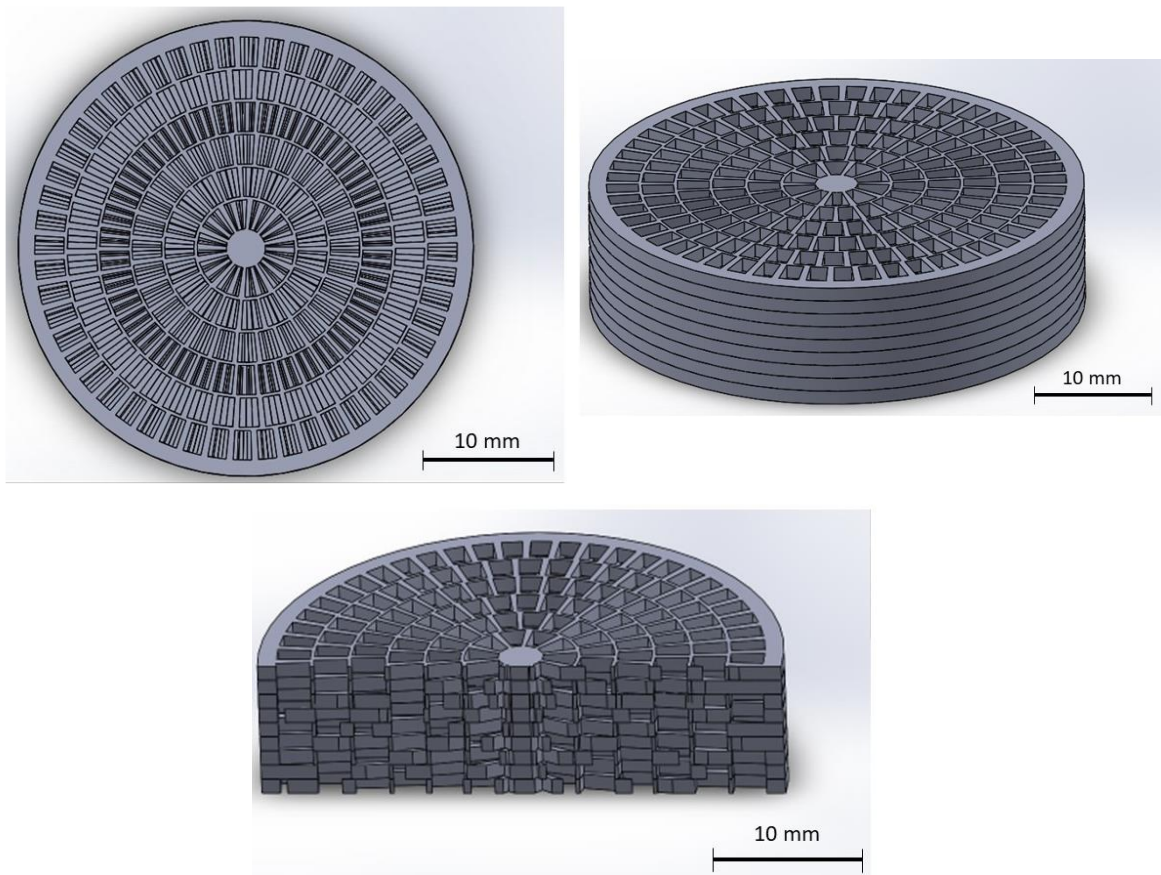


Figure 26 - Geometry 1, consisting in nine identical layers overlapped.

The second approach is to create a filter that is accessible in all directions; in order to filter in the radial direction, a series of concentric perforated walls are used; in the axial direction, the same

principle as above is used, i.e. a series of layers of equal geometry offset from each other. These layers also have the function of holding the walls together.

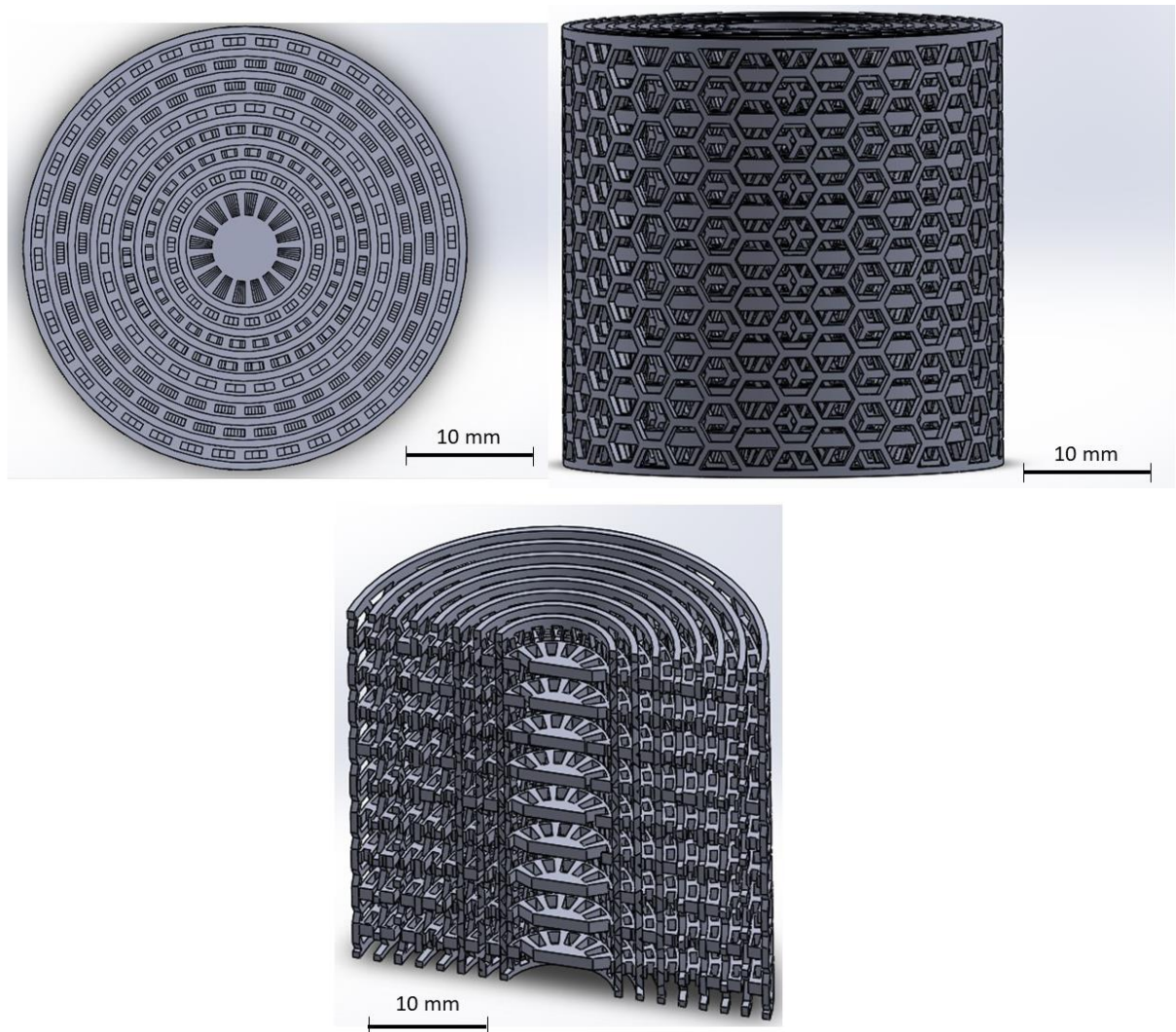


Figure 27 - Geometry 2, consisting of 8 concentric cylindrical walls, perforated with a honeycomb geometry, held together by a series of equal layers staggered from each other.

5.2. PRINTING PARAMETERS OPTIMIZATION

For each geometry and resin, appropriate printing parameters were defined to have a fast process and suitable mechanical properties. In particular, the most significant parameters are slice thickness, temperature, light intensity, and exposure time.

Preliminary, 3D printing parameters were optimized before trying to print the actual filters. Thus, for each formulation, rectangular specimens with a thickness of 0.6mm were 3D printed.

In the following, optimized parameters were reported for each formulation. Images of the printed samples are also shown.

5.2.1. PEGDA/AA MATRIX

Printing parameters:

Table 4 - Printing parameters for PEGDA/AA matrix

Formulation name	Slice thickness	Burn-In	Heater temperature	Light intensity	Exposure time	Initial exposure time
P/AA	0,2 nm	0,2 nm	25°C	25 mW/cm ²	1 s/layer	2 s/layer

The samples are printed with excellent geometric quality and have good physical-mechanical properties even with low exposure time and light intensity. Washing is easy because the resin is not very viscous; this allows to fabricate filters with very small holes.

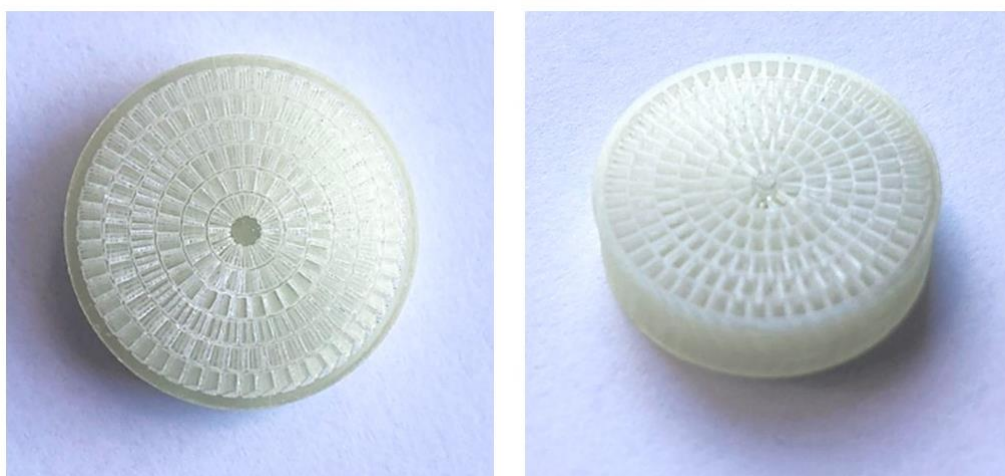


Figure 28 - Geometry 1 printed with PEGDA/AA-based resin

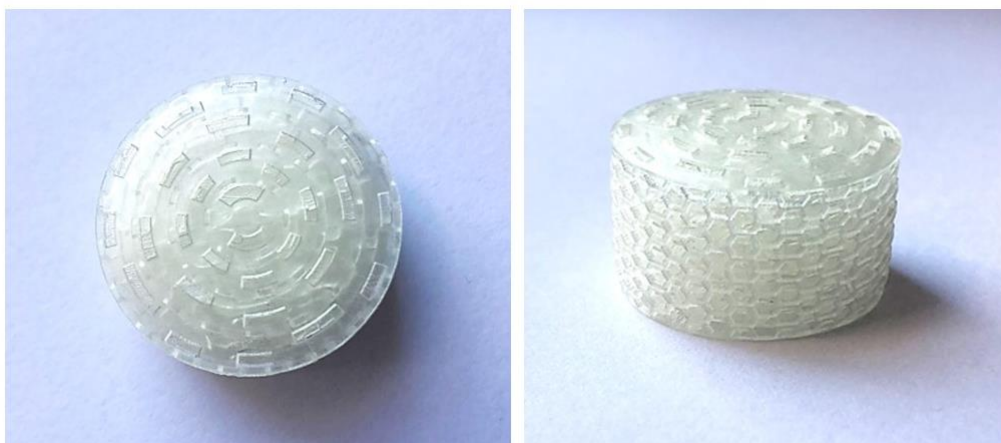


Figure 29 - Geometry 2 printed with PEGDA/AA-based resin

5.2.2. PEGDA/GMA MATRIX

Printing parameters:

Table 5 - Printing parameters for PEGDA/GMA matrix

Formulation name	Slice thickness	Burn-In	Heater temperature	Light intensity	Exposure time	Initial exposure time
P/GMA	0,2 nm	0,2 nm	30°C	35 mW/cm ²	5 s/layer	7 s/layer

Here, it is necessary to increase the intensity of light radiation and exposure time in order to cure the resin and give sufficient structural stability. Also, washing step is very difficult because the resin is viscous and tends to remain in the holes. For this reason, it was also necessary to increase the temperature during printing, to facilitate removal of resins.



*Figure 30 - Geometry 1 printed with PEGDA/GMA-based resin, without the aid of brilliant green.
Edges are not well defined and residual un-cured resin is present.*

However, this was not sufficient to allow the resin to flow out in samples thicker than 1 or 2mm. Thus, a dye is added to prevent the liquid resin from cross-linking, even partially, into the holes.

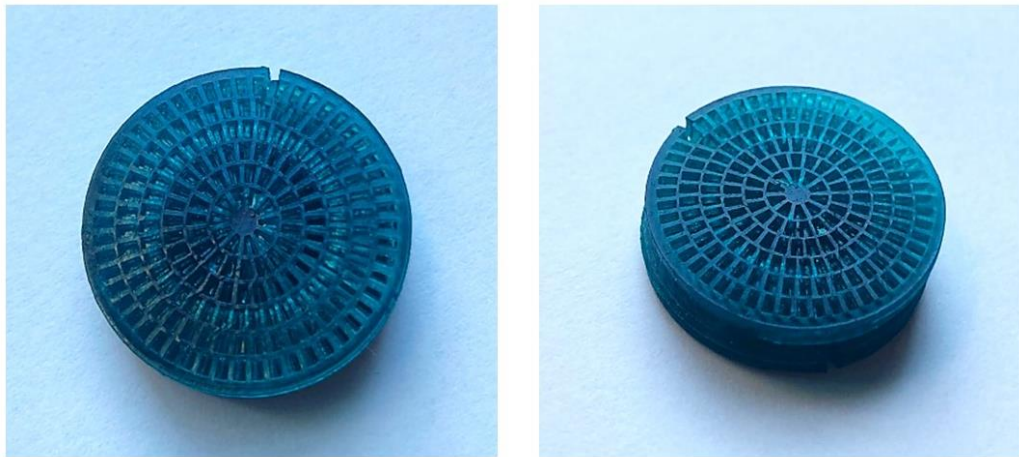


Figure 31 - Geometry 1 printed with the addition of brilliant green

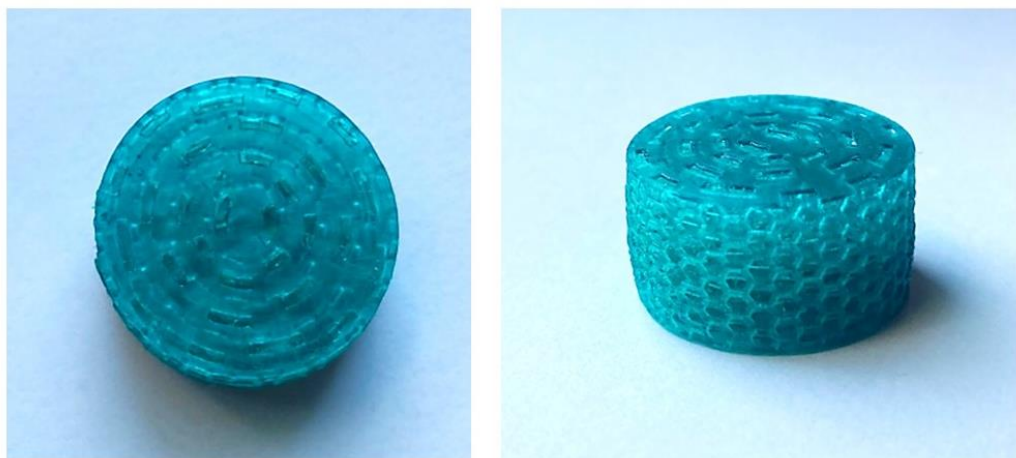


Figure 32 - Geometry 2 printed with the addition of brilliant green

5.2.3. OTHER MATRICES: PEGDA, PEGDA/ABUT, PEGDA/AA/ABUT

Filters based on PEGDA₂₅₀, PEGDA/ABut and PEGDA/AA/ABut were not produced by 3D printing. A preliminary analysis of the surface modification on these matrices was done using rectangular-shaped samples of size 1.5 cm x 8 cm and thickness of 140-150µm. These samples were made by placing liquid resin in a mold of the desired size; photopolymerization took place in a UV curing chamber at 365 nm. The samples were irradiated for 10 minutes per side.

Obviously, the printing output with this technique is not comparable to 3D printing. But for now we are only interested in evaluating whether these matrices react positively to surface modification and biological testing with bacteria. If the results are promising, we might consider 3D printing filters with these formulations as well.

5.3. 3D SCANNER

The use of the 3D scanner allowed us to evaluate the print fidelity between the printed object and the CAD model. A colorimetric map was created in which green represents a zero difference between the CAD model and the printed object, while red and blue represent a positive or negative difference, respectively.

From the following figures we can appreciate the high printing fidelity, especially for geometry 1. Geometry 2 has more defects, but this could also be due to the difficulty in properly scanning holes and cavities.

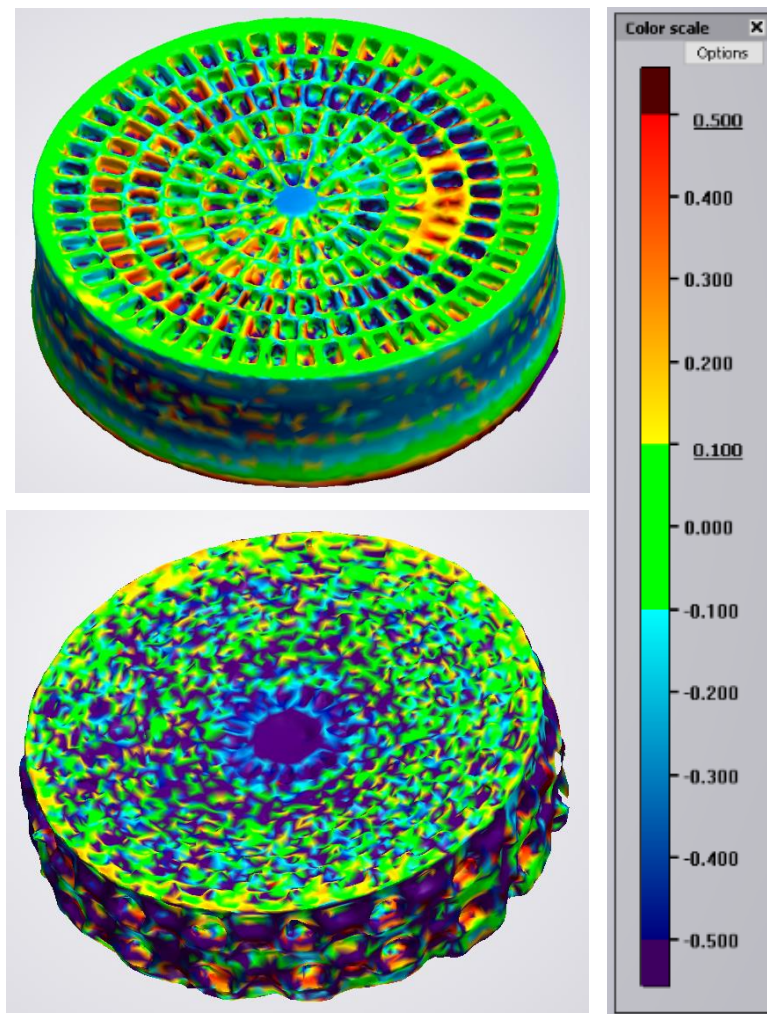


Figure 33 - 3D scan of geometry 1 (above) and geometry 2 (below)

5.4. PEGDA/AA-BASED MATRIX

The tests were initially performed on rectangular samples of size 1x5x0.6 cm. Subsequently, some filters of smaller size (diameter of 1.5 cm, thickness of 0.6 cm) were also tested.

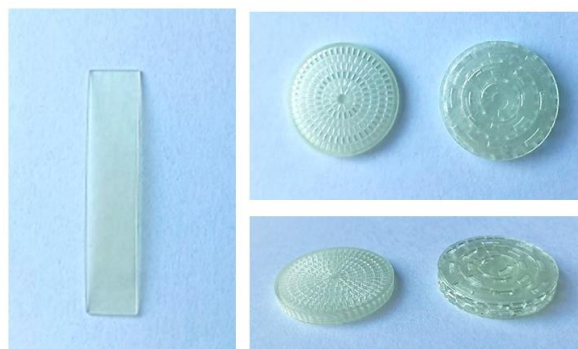


Figure 34 - Rectangular surface and smaller filters

5.4.1. SWELLING TEST

The percentage of swelling in water (ws%) was evaluated by measuring the weight difference between the swollen sample and the initial sample. The weight recovery percentage (wr%) after the sample was left 6 hours in a vacuum pump was also calculated.

For the PEGDA/AA-based samples, these are the results of the swelling and recovery tests, calculated as the average of 5 different measurements:

$$ws\% = 10.03\%$$

$$wr\% = 95.83\%$$

The same tests were also performed on the modified samples; the results are shown in the following table:

Table 6 - Results of swelling and recovery tests on PEGDA/AA-based samples after surface treatment

Molecule	Method	ws%	wr%
Arginine	Conventional heating	11.42	96.97
Arginine	Microwave heating	11.86	96.96
Agmatine	Conventional heating	11.24	96.01
Agmatine	Microwave heating	10.47	96.00
Dopamine	Dip-coating	7.91	94.77
PEI600	Microwave heating	n.a.	n.a.
PEI600 + Cl	Microwave heating + chlorination	n.a.	n.a.

5.4.2. FTIR-ATR SPECTROSCOPY

5.4.2.1. PEGDA/AA + ARGININE

Modifications of PEGDA/AA-based matrix samples with Arginine were conducted either by following the conventional method or by microwave heating. Different buffers with different pH were tested, with the best being phosphate buffer (pH=5.8). Activators of carbodiimide chemistry, EDC/NHS, were also used. In this way, both acrylic and carboxyl surface groups should react.

In the following figures we can see the result of IR spectroscopy. The evolution of the modification reaction was followed by the variation of the bands corresponding to the functional groups involved:

- 810 cm^{-1} → this peak is related to the C-H out of plane deformation vibration of the acrylate double bond [56] [57]; following the reaction of the acrylic group with the amine group, this peak should decrease;
- 1633 and 1672 cm^{-1} → these are the distinctive peaks of the guanidine group [58], and a peak in this band should appear as a consequence of the treatment;
- 2870 and 2920 cm^{-1} → these peaks are related to C-H symmetric stretching of $-\text{CH}_3$ [59], and these should also undergo an increase in intensity related to the increase in surface methyl groups;
- 3350 and 3450 cm^{-1} → finally, these peaks are related to the N-H stretching vibration of secondary amines [60], and therefore they should increase. However, we must be careful with these peaks because they may also be related to the O-H groups of water [61].

PEGDA/AA + Arginine
Arg, EDC/NHS, PBS buffer (pH=5,8)
Conventional heating – 100°C, 24h

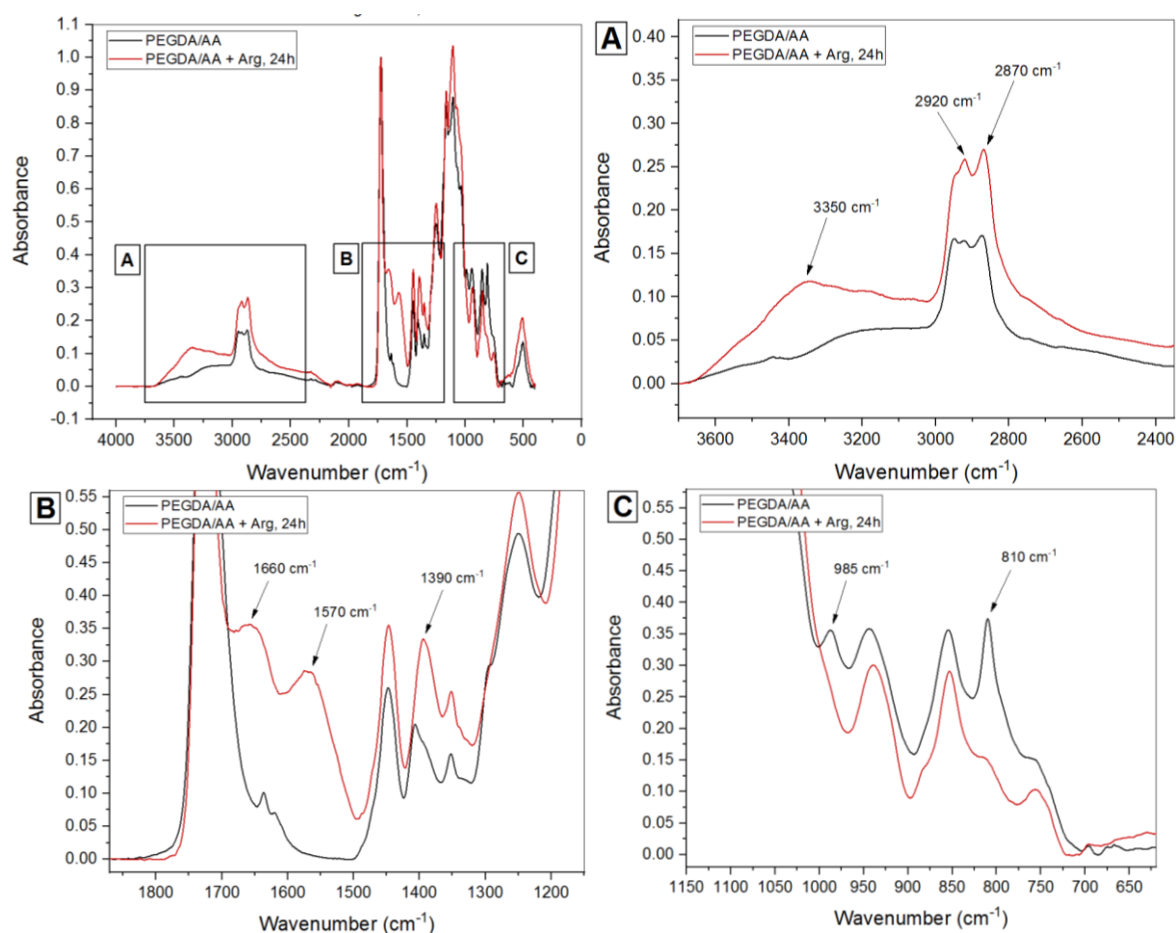


Figure 35 -IR spectrum of **PEGDA/AA**-based matrix (8:2) modified with **arginine** by conventional heating at **100°C** for **24h**. **(A)** Wavelengths between 3800 and 2400 cm^{-1} ; **(B)** wavelengths between 1850 and 1150 cm^{-1} ; **(C)** wavelengths between 1150 and 600 cm^{-1} .

PEGDA/AA + Arginine
Arg, EDC/NHS, PBS buffer (pH=5,8)
Microwave heating – 150°C, 3-5 min

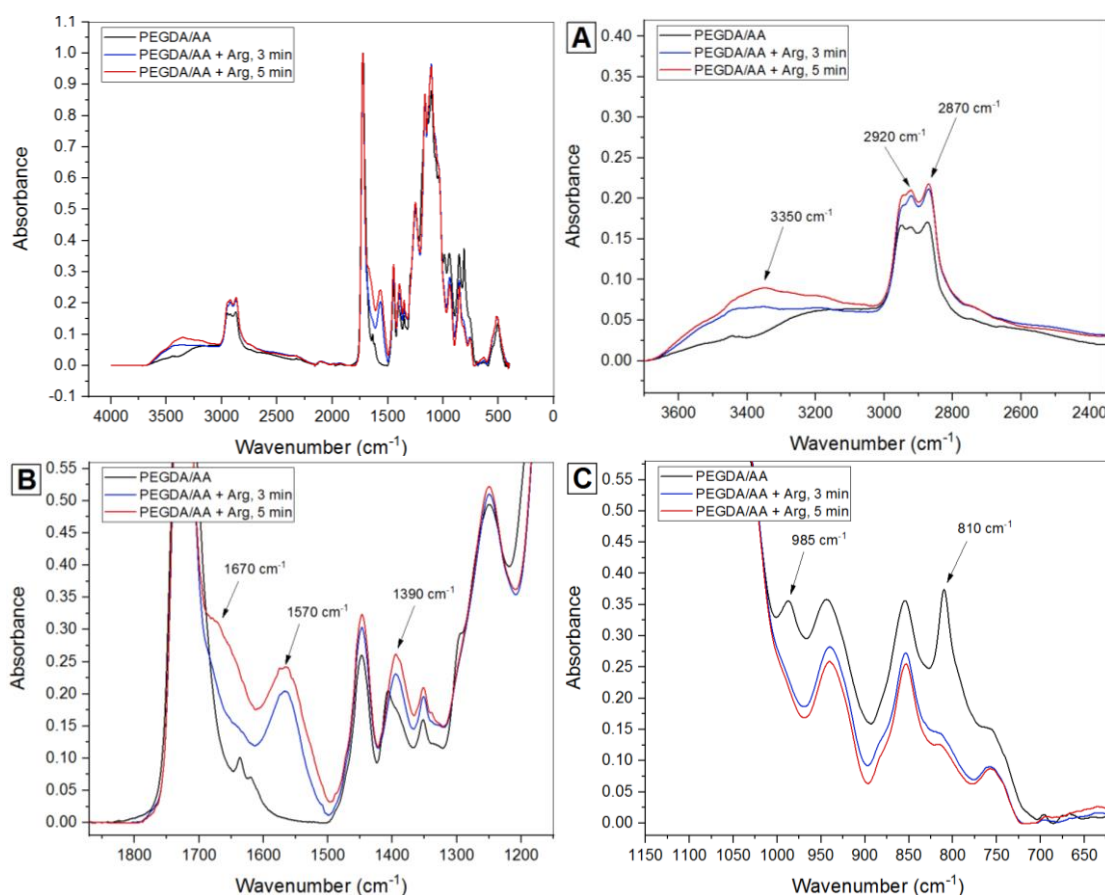


Figure 36 - IR spectrum of **PEGDA/AA**-based matrix (8:2) modified with **arginine** by microwave heating at **150°C** for **3 and 5 minutes**. (A) Wavelengths between **3800 and 2400 cm⁻¹**; (B) wavelengths between **1850 and 1150 cm⁻¹**; (C) wavelengths between **1150 and 600 cm⁻¹**.

To follow the kinetics of the modification reaction, the absorbance of the above described bands was measured as a function of the corresponding reaction times (Figure 32):

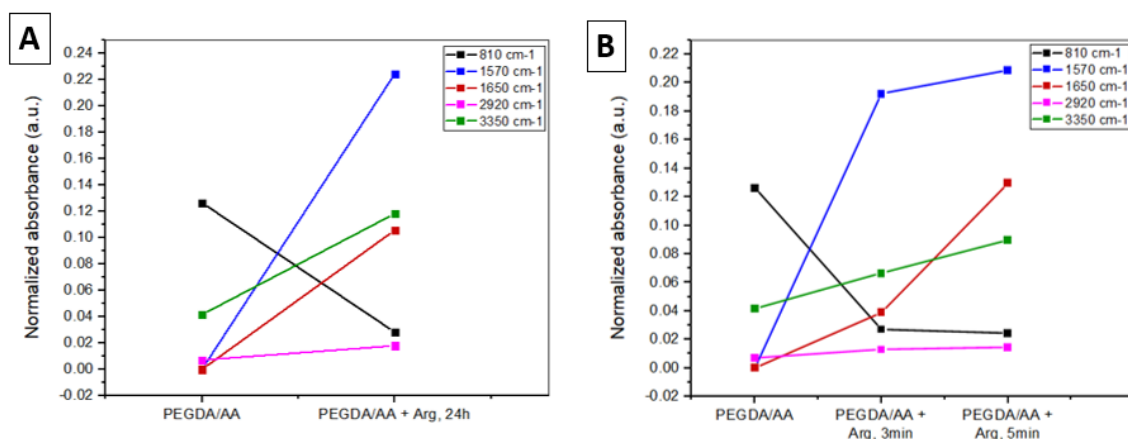


Figure 37 - Trend of peaks of interest (810, 1570, 1650, 2920 and 3350 cm⁻¹) in the samples subjected to treatment of (A) conventional heating and (B) microwave heating with arginine.

5.4.2.2. PEGDA/AA + AGMATINE

Treatment of PEGDA/AA-based matrix samples with agmatine were conducted following both conventional method and microwave heating. Several solutions have been tested, and the best one involves the use of an alkaline Tris-HCl buffer (pH=8.6). Due to the similarity between arginine and agmatine (they differ only in the presence, in arginine, of a carboxyl group in arginine structure), the peaks of interest are the same as those described in the previous paragraph. In the following figures we can see the result of IR spectroscopy.

PEGDA/AA + Agmatine Agm, Tris-HCl buffer (pH=8,6) Conventional heating – 100°C, 24h

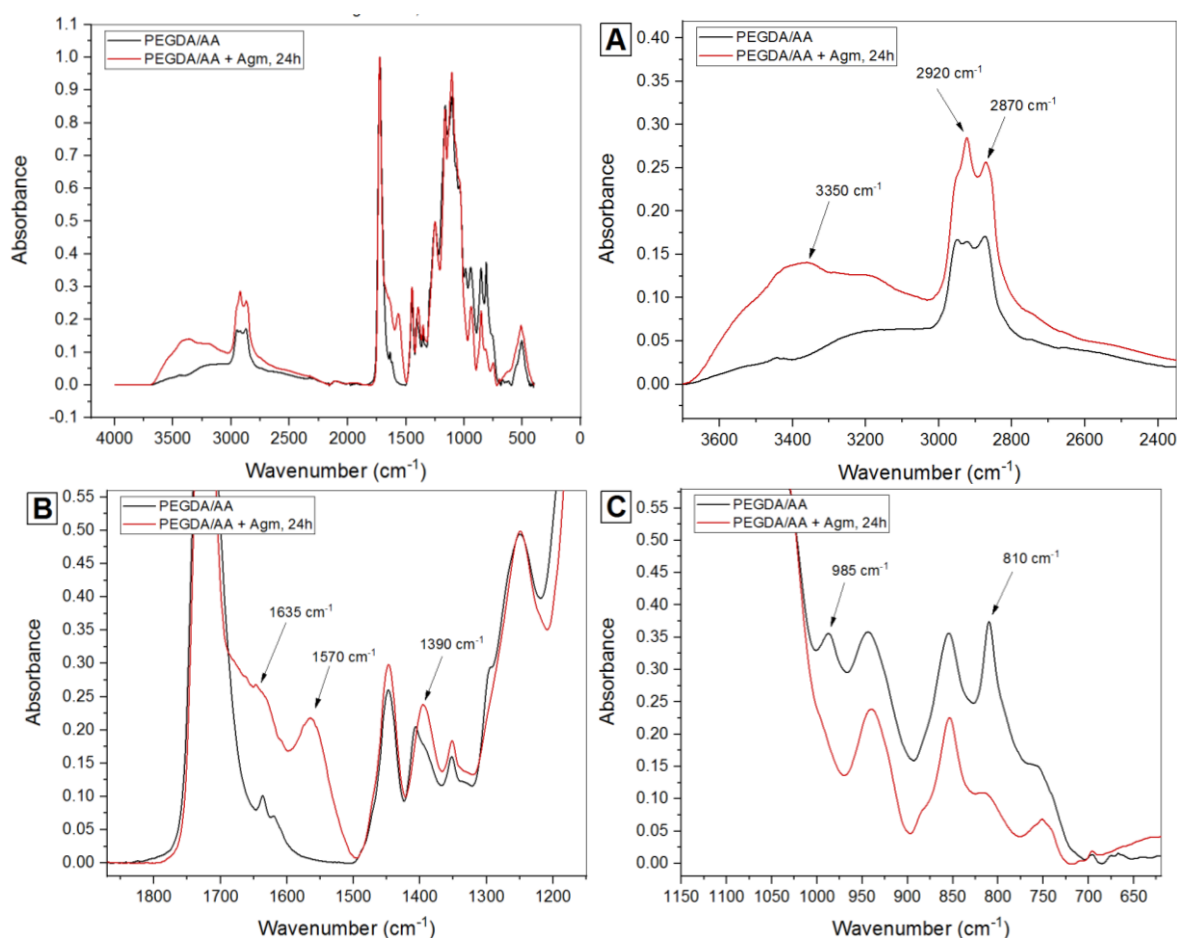


Figure 38 - IR spectrum of *PEGDA/AA*-based matrix (8:2) modified with *agmatine* by conventional heating at **100°C** for **24h**. (A) Wavelengths between 3800 and 2400 cm^{-1} ; (B) wavelengths between 1850 and 1150 cm^{-1} ; (C) wavelengths between 1150 and 600 cm^{-1} .

PEGDA/AA + Agmatine
 Agm, Tris-HCl buffer (pH=8,6)
 Microwave heating – 150°C, 3-5-7 min

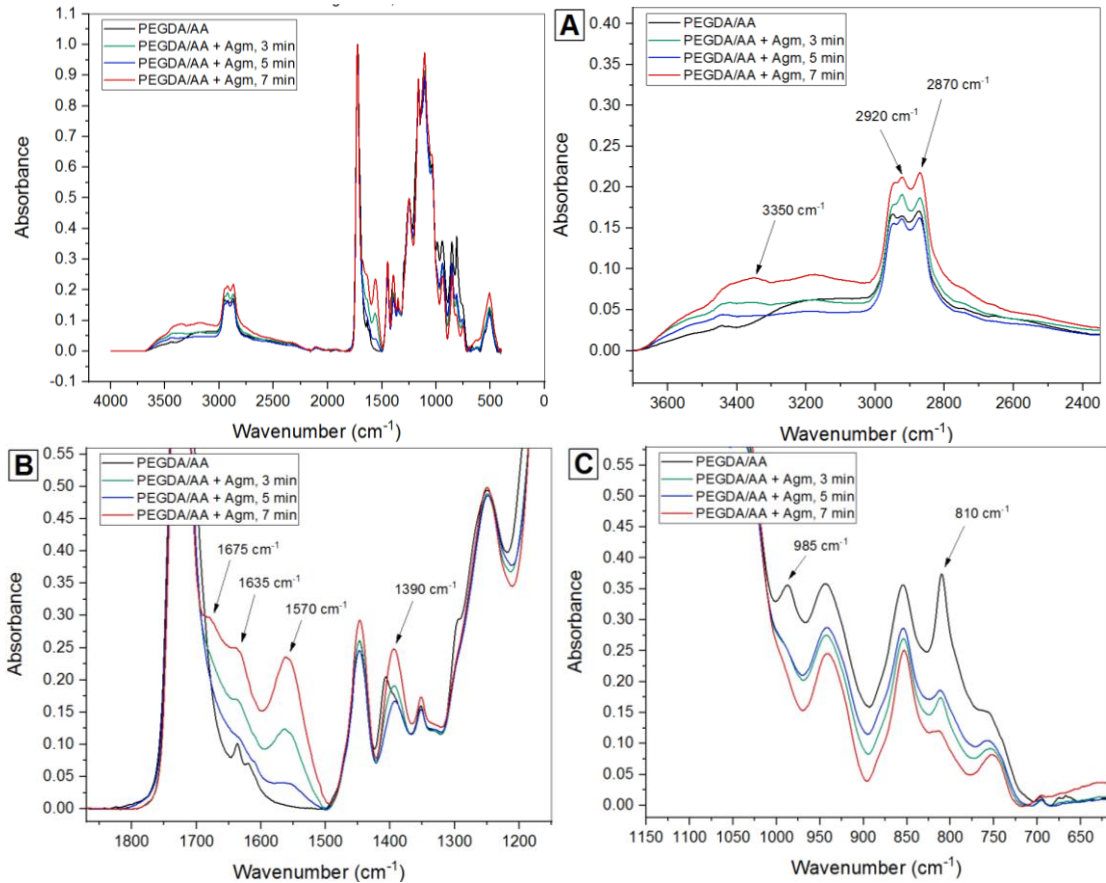


Figure 39 - IR spectrum **PEGDA/AA**-based matrix (8:2) modified with **agmatine** by microwave heating at 150°C for 3, 5 and 7 minutes. (A) Wavelengths between 3800 and 2400 cm^{-1} ; (B) wavelengths between 1850 and 1150 cm^{-1} ; (C) wavelengths between 1150 and 600 cm^{-1} .

In the following figures we can see the trend of the peak of interest depending on type and duration of the treatment.

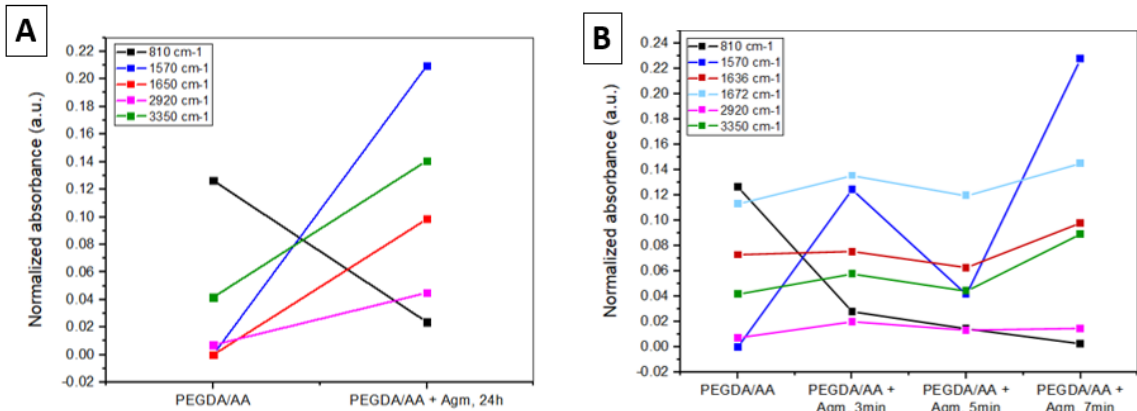


Figure 40 - Trend of peaks of interest in the samples subjected to treatment of (A) conventional heating and (B) microwave heating

5.4.2.3. PEGDA/AA + DOPAMINE

Dopamine treatment involves dipping the samples in an alkaline buffer at pH=8.5. The reaction proceeds for 24h at room temperature in an aerobic environment so that dopamine polymerizes and deposits on the substrate.

PEGDA/AA + Dopamine DOPA, Tris-HCl buffer (pH=8,5) Dip coating – 24h

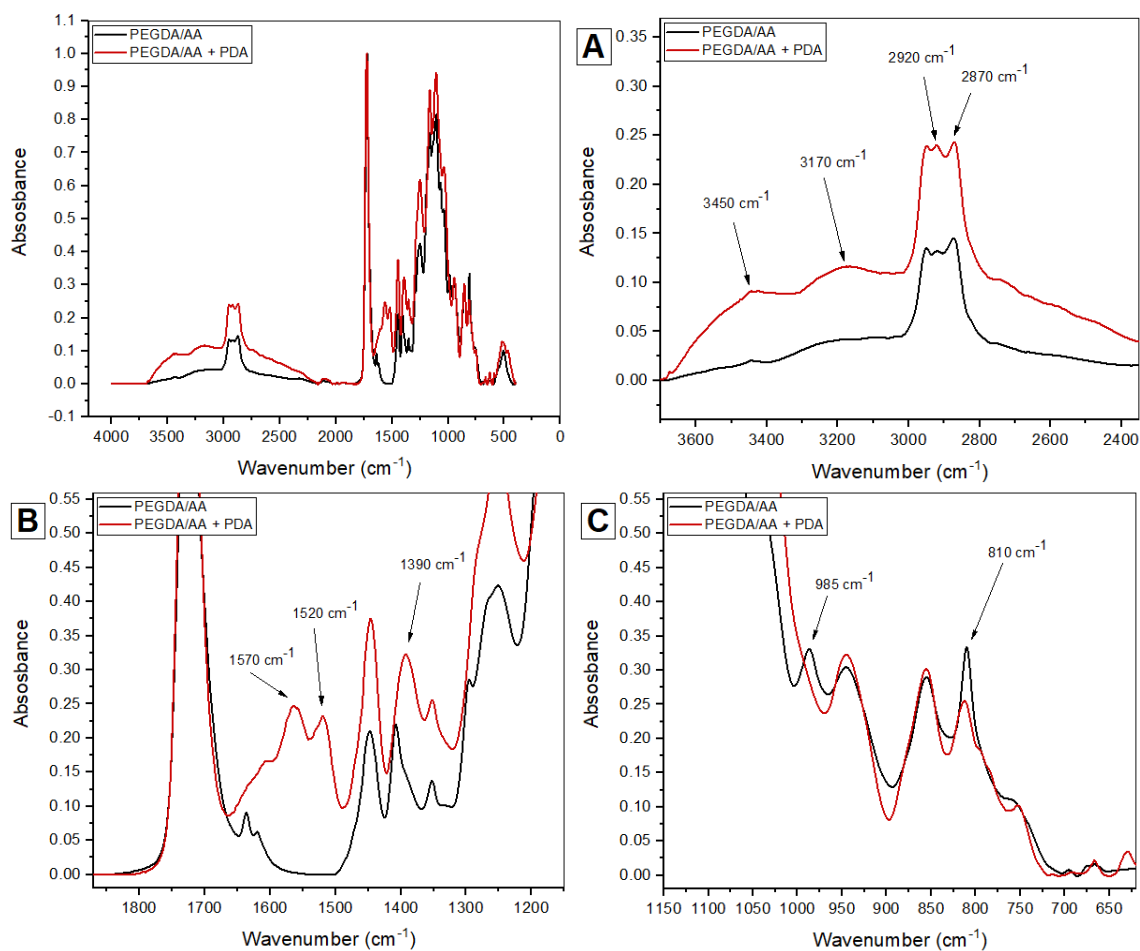


Figure 41 - IR spectrum **PEGDA/AA**-based matrix (8:2) modified with **DOPAMINE** by dip-coating at room temperature for **24h**. **(A)** Wavelengths between 3800 and 2400 cm^{-1} ; **(B)** wavelengths between 1850 and 1150 cm^{-1} ; **(C)** wavelengths between 1150 and 600 cm^{-1}

5.4.2.4. PEGDA/AA + PEI600

The reaction with PEI takes place in acetonitrile (Solution 5, section 4.7); this molecule reacts much faster than the others, so conventional heating would not make sense. Therefore, only microwave treatment is used.

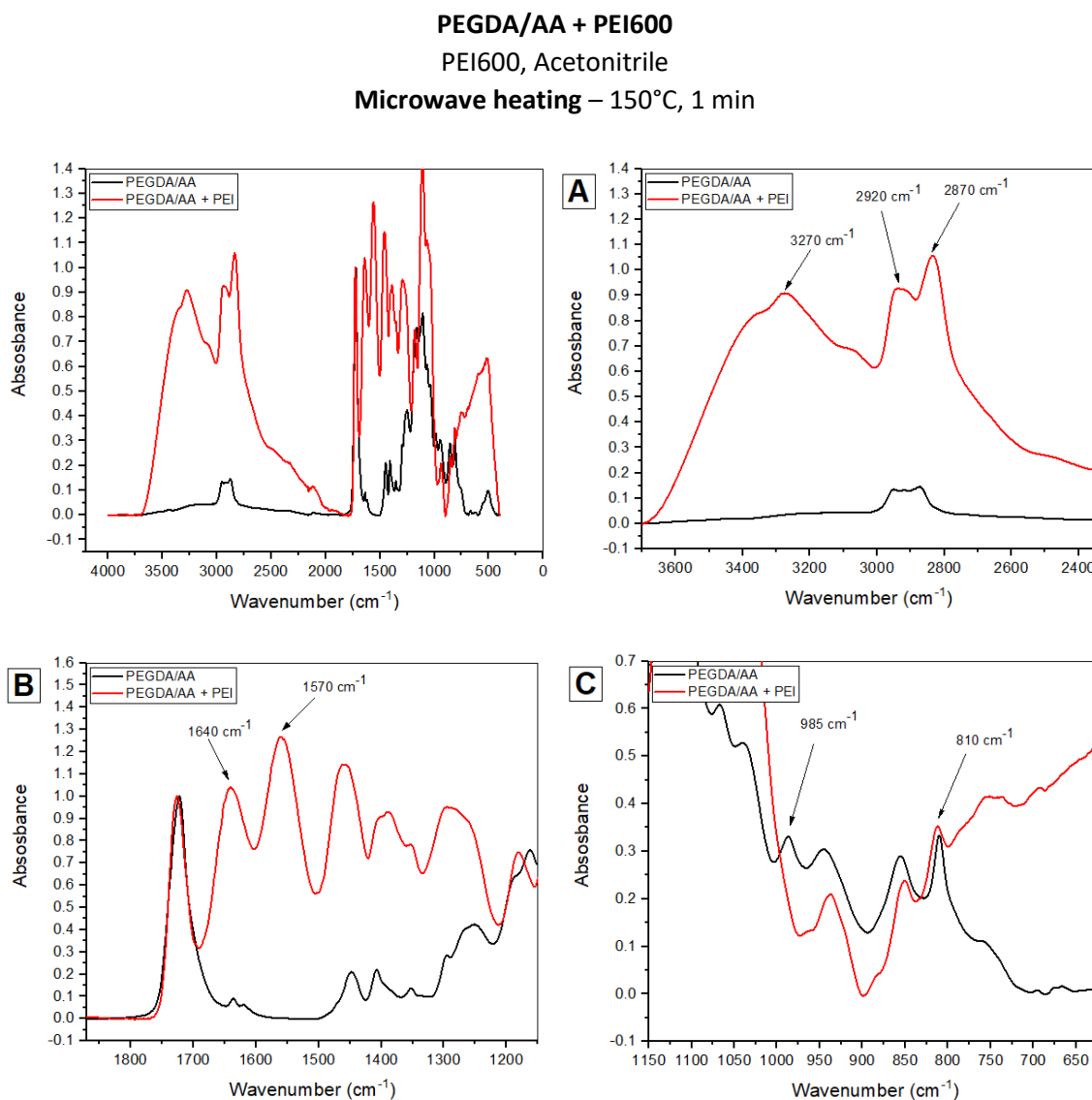


Figure 42 - IR spectrum of PEGDA/AA-based matrix (8:2) modified with PEI600 by microwave heating at 150°C for 1 minute. (A) Wavelengths between 3800 and 2400 cm⁻¹; (B) wavelengths between 1850 and 1150 cm⁻¹; (C) wavelengths between 1150 and 600 cm⁻¹.

A chlorination post-treatment was performed on some samples, following the protocol described in Section 4.7.4. After the modification with PEI, the samples were exposed to UV light (wavelength of 365 nm) for 7 minutes to try to polymerize any unreacted monomers or oligomers. After that, the samples were immersed in a 2% HClO solution (Solution 6) for 1h.

PEGDA/AA-PEI600 + Cl

1) PEI600 + Acetonitrile

Microwave heating – 150°C, 1min

2) HClO 2%

Chlorination - Room temperature, 1h, 160 rpm

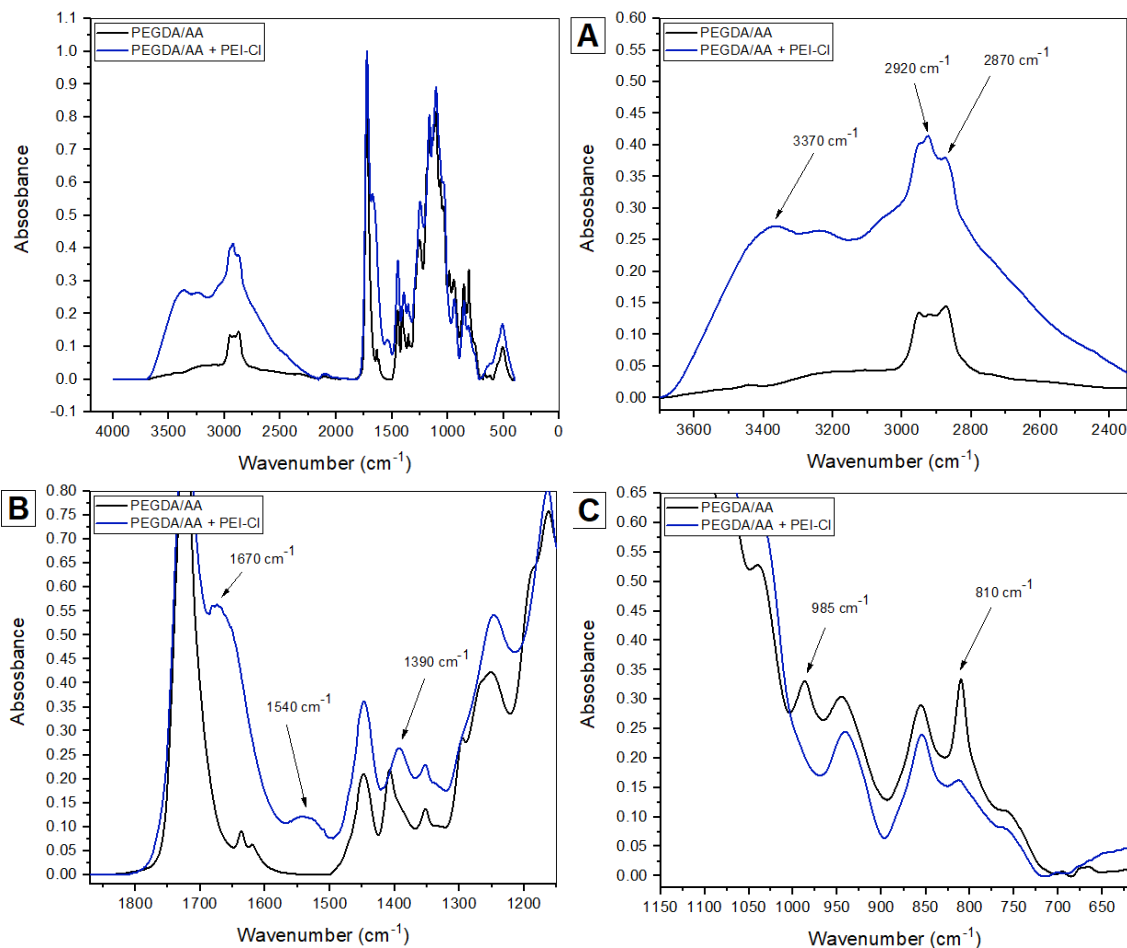


Figure 43 - IR spectrum of *PEGDA/AA*-based matrix (8:2) modified with *PEI600* by microwave heating at 150°C for 1 minute and then chlorinated in HClO solution for 1h. (A) Wavelengths between 3800 and 2400 cm⁻¹; (B) wavelengths between 1850 and 1150 cm⁻¹; (C) wavelengths between 1150 and 600 cm⁻¹

5.4.3. CONTACT ANGLE

Measuring the contact angle can be a good indicator of a successful surface modification. The decrease in contact angle, and thus the increase in hydrophilicity, occurs in all the treated samples, with different rates of decrease.

5.4.3.1. PEGDA/AA + ARGININE

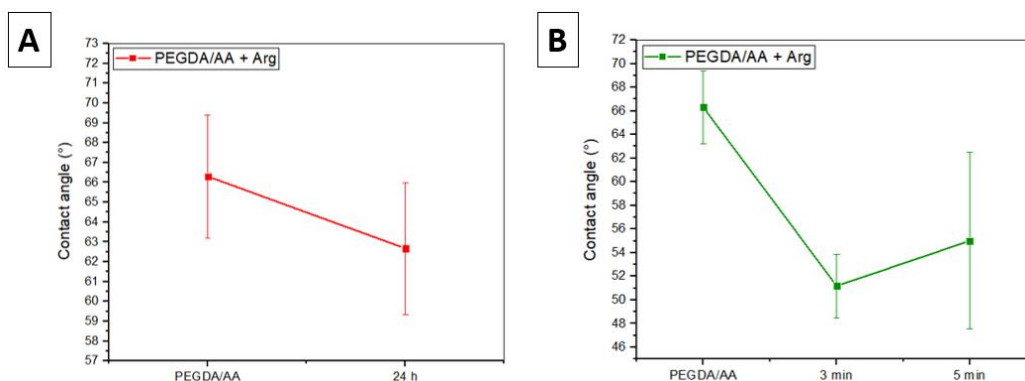


Figure 44 - Contact angle of **PEGDA/AA**-based sample modified with **arginine** under **(A)** conventional heating (24h) and **(B)** microwave heating (3 and 5 minutes), compared to the non-treated sample

5.4.3.2. PEGDA/AA + AGMATINE

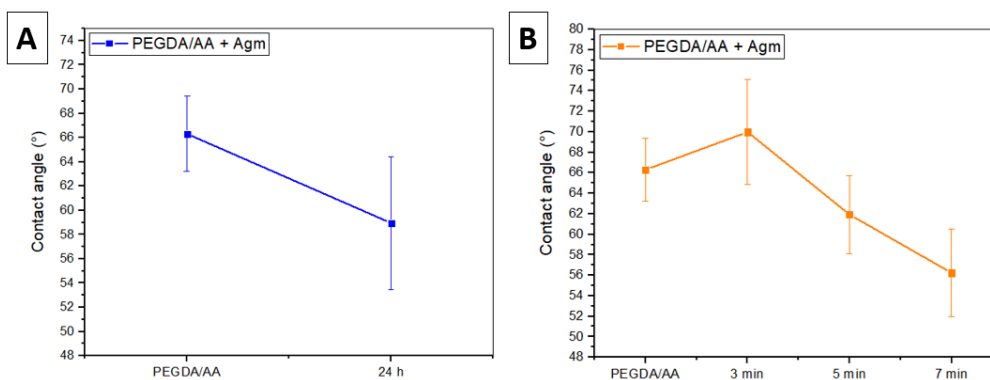


Figure 45 - Contact angle of **PEGDA/AA**-based sample modified with **agmatine** under **(A)** conventional heating (24h) and **(B)** microwave heating (3, 5 and 7 minutes), compared to the non-treated sample

5.4.3.3. PEGDA/AA + DOPAMINE

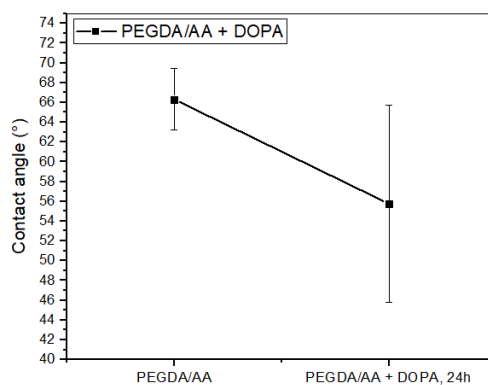


Figure 46 - Contact angle of **PEGDA/AA**-based sample modified with **dopamine** through dip-coating (24h)

5.4.3.4. PEGDA/AA + PEI600

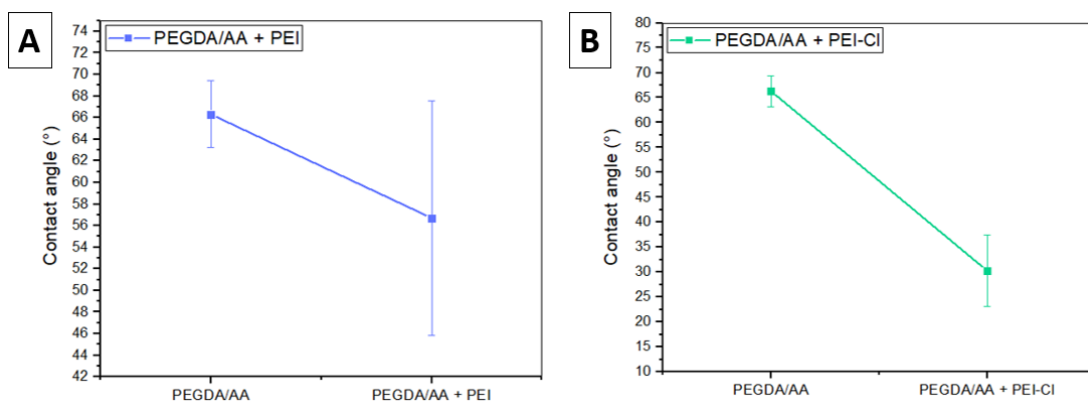


Figure 47 - Contact angle of **PEGDA/AA**-based sample modified with **PEI600** through microwave heating (150°C, 1 min), without (A) and with (B) chlorination

5.4.4. CHOICE OF THE BEST SAMPLES

Having analyzed the graphs of FTIR spectroscopy and contact angle, we are able to choose the process parameters that give the best surface modification. In choosing the best samples, we want the highest degree of functionalization (basically observed by the peak trend in FTIR-ATR spectroscopy and the contact angle) with the least physical damage and time/energy consumption. If the degree of functionalization and damage is similar for both types of energy, heating by microwave is better because it is more convenient in terms of energy/time savings.

The sample modified with Arginine by conventional treatment shows a significant increase in the intensity of the peaks related to guanidium group and nitrogen, while the peak related to acrylic groups practically disappears. These results are obtained with only 24 hours of treatment and were judged to be satisfactory. Therefore, there is no need to increase the reaction time. The increase in hydrophilicity also suggests that the treatment was successful.

In microwave treatment, we must choose the length of time for which we have satisfactory results. The results obtained after 3 minutes of treatment are already acceptable, but a 5-minute duration provides better results in terms of increase/decrease in peaks of interest.

For agmatine-treated samples we can make a similar reasoning: 24 hours of treatment is enough to have a satisfactory change in the case of conventional heating; in microwave treatment, 5 minutes is not enough to have acceptable results, which, instead, can be obtained after 7 minutes of treatment. The decrease in contact angle also suggests that 7 minutes leads to a better result. Nevertheless, further tests will be conducted on these samples to be sure of the success of the treatment.

Finally, samples modified with dopamine and PEI600 also show satisfactory results and will be used for biological tests with bacteria.

To sum up, the chosen samples are shown in the following table.

Table 7 - Chosen treatment conditions for PEGDA/AA-based samples

Name	Functionalizing molecule	Treatment	Treatment conditions
PAA-AR-F	Arginine	Conventional heating	100°C, 70rpm, 24h
PAA-AR-M	Arginine	Microwave heating	150°C, 5min
PAA-AG-F	Agmatine	Conventional heating	100°C, 70rpm, 24h
PAA-AG-M	Agmatine	Microwave heating	150°C, 7min
PAA-D	Dopamine	Dip-coating	80rpm, 24h
PAA-PEI	PEI600	Microwave heating	150°C, 1min
PAA-PEI-Cl	PEI600 + Cl	Microwave heating + chlorination	150°C, 1min + 160rpm, 1h

5.4.5. TGA

In the following graphs we can see, in green, the percentage reduction in weight (wt%) as a result of increased temperature. The blue line shows the rate of weight decrease as a function of temperature (wt%/°C) and is useful to clearly visualize the different events that occur during degradation.

5.4.5.1. PEGDA/AA + ARGININE

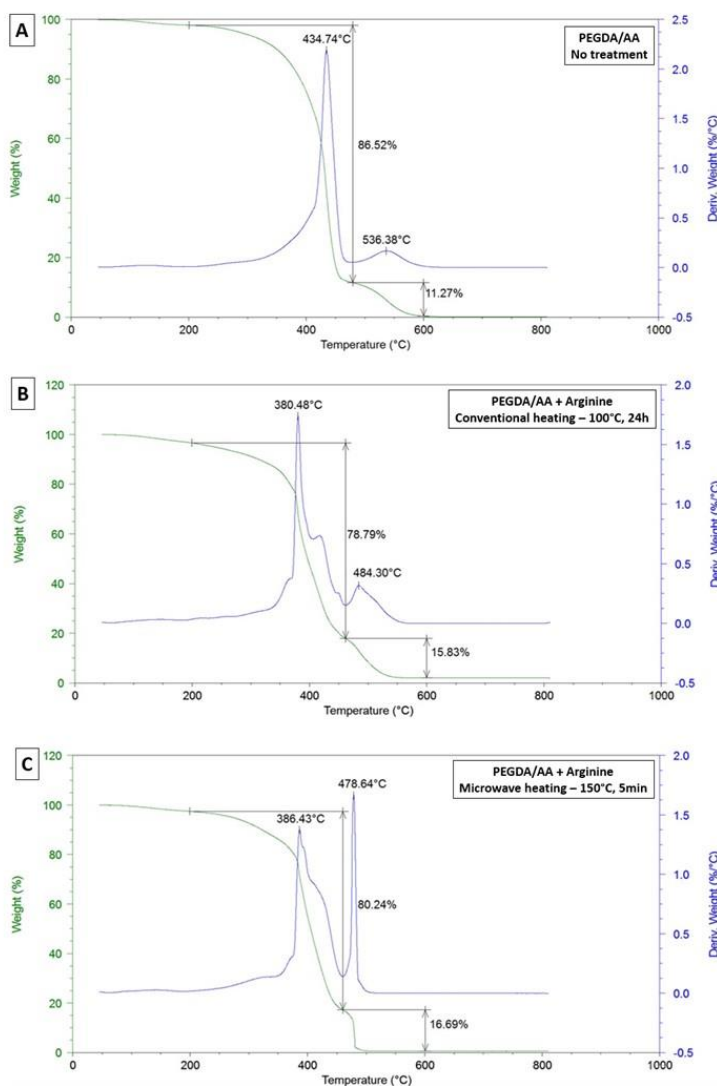


Figure 48 - Percent weight reduction as a function of temperature in samples (A) subjected to no treatment, (B) modified with **arginine** by conventional heating, and (C) modified with **arginine** by microwave heating.

PEGDA/AA sample undergoes two degradation events (Fig. 48 A). The main degradation occurs between 200 and 470°C; in this range the sample loses 86.52% of its weight. The highest degradation rate occurs at 434.74°C (corresponding to the peak of the blue line).

Residual degradation causes the sample to lose 11.27% of its weight between 470 and 600°C, with the highest degradation rate reached, in this event, at 536.30°C.

In arginine-modified samples (Fig. 48 B and C), the peak corresponding to the main event occurs at a lower temperature than in the unmodified sample, around 380°C. This behavior is compatible with the treatment, which may cause a loss of cross-links not only at the surface, but also in bulk. We also note that there are a number of secondary events consistent with surface amine degradation (before the main event) and bulk degradation (after the main event).

5.4.5.2. PEGDA/AA + AGMATINE

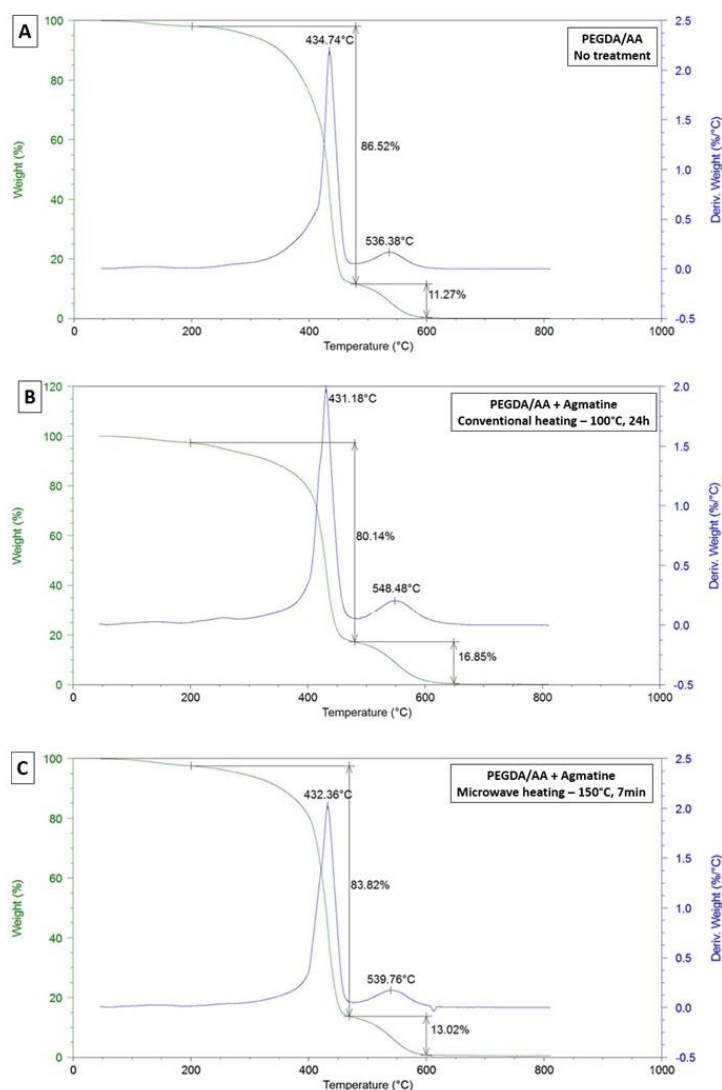


Figure 49 - percent weight reduction as a function of temperature in samples (A) subjected to no treatment, (B) modified with agmatine by conventional heating, and (C) modified with arginine by microwave heating

In the case of agmatine-modified samples, we do not notice any particular differences between the modified samples and the original sample. Both the temperature at which the maximum degradation rate occurs and the percentage of degradation relative to the main event are similar, as we can see in Figure 49.

5.4.6. EDX

Energy dispersive X-ray spectroscopy (EDX) allows us to chemically characterize the surface of a sample; in our case, we are interested in knowing the weight percentage of nitrogen present on the surface as a result of treatment with arginine or agmatine. In addition, we are interested in knowing whether the nitrogen on the surface is uniformly distributed or not.

5.4.6.1. PEGDA/AA + ARGININE

Table 8 - Results of EDX experiment on PEGDA/AA-based samples modified with arginine

	PEGDA/AA No treatment	PEGDA/AA + Arg Conventional	PEGDA/AA + Arg Microwave
ELEMENT	wt%	wt%	wt%
C	52.46	53.10	52.74
O	44.87	43.06	43.49
N	0.44	1.29	3.06
Na	0.63	0.93	0.18
Cl	0.61	0.61	0
Others	0.99	1.00	0.53
Total	100	100	100

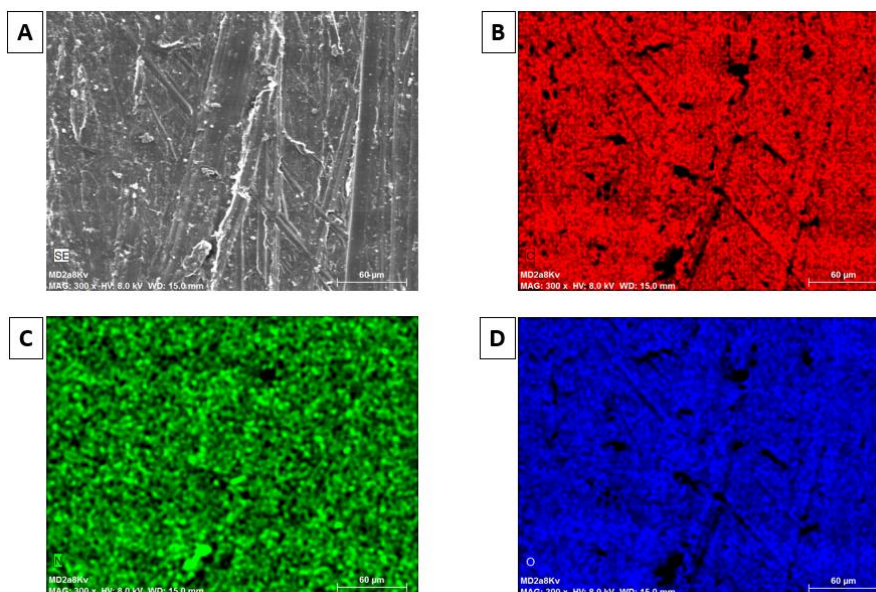


Figure 50 - Microscopic image of the surface of the agmatine-modified sample (A); distribution of carbon (B), nitrogen (C) and oxygen (D) atoms on the surface.

Table 8 show us that as a result of the treatments, the percentage of nitrogen on the surface increases: it goes from 0.44% in the unmodified sample to 1.29 and 3.06% in the samples modified by conventional heating and microwave heating, respectively.

Figure 50, moreover, shows us that nitrogen is distributed fairly evenly over the surface, although the distribution of carbon and oxygen is more homogeneous.

5.4.6.2. PEGDA/AA + AGMATINE

Table 9 - Results of EDX experiment on PEGDA/AA-based samples modified with agmatine

	PEGDA/AA No treatment	PEGDA/AA + Agm Conventional	PEGDA/AA + Agm Microwave
ELEMENT	wt%	wt%	wt%
C	52.46	52.60	52.79
O	44.87	41.38	41.56
N	0.44	3.25	3.66
Na	0.63	0.86	0.55
Cl	0.61	0.95	0.57
Others	0.99	0.96	0.87
Total	100	100	100

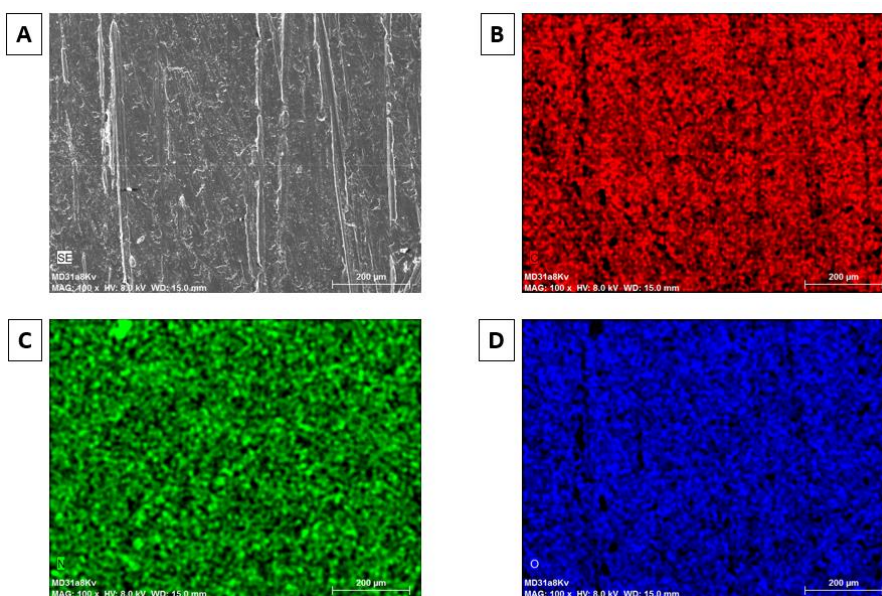


Figure 51 - Microscopic image of the surface of the agmatine-modified sample (A); distribution of carbon (B), nitrogen (C) and oxygen (D) atoms on the surface

Agmatine modification also provides good results: the percentage of nitrogen increases from 0.44% to 3.25 and 3.66% in the case of modification by conventional or microwave heating, respectively.

The distribution of nitrogen on the surface is also quite homogeneous.

5.4.7. FINAL COMMENTS

Thanks to the tests performed, it is possible to state that all samples were successfully modified, even if at different extents.

This is witnessed analyzing both FTIR spectra and contact angles. In fact, compared to the sample without treatment, all of the modified samples underwent an increase in hydrophilicity. It should be noted, however, that as seen in Chapter 3.2, excessive hydrophilicity (as well as excessive hydrophobicity) can be counterproductive in view of increasing bacterial adhesion to the surface.

In addition, we should point out that immediately after treatments there is a deterioration of the surface and a worsening of the mechanical properties: surfaces are sometimes rougher, and specimens are often more brittle and less robust. This may be largely due to swelling: in fact, there is at least a partial recovery of mechanical properties after drying.

In some cases, there is also change in color, as witnessed by Figure 53.

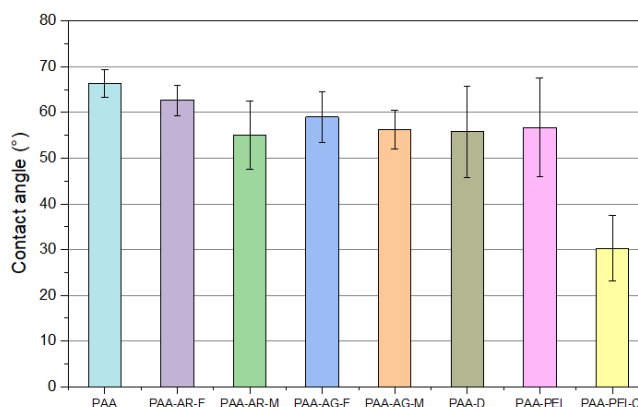


Figure 52 – Comparison of the contact angle of all the PEGDA/AA-based samples

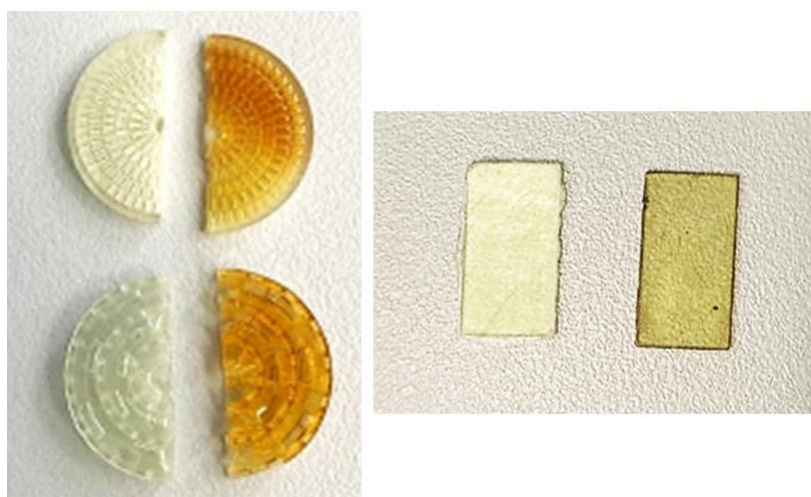


Figure 53 - Comparison between unmodified samples (on the right) and modified samples (on the left) to show the difference in color.

5.5. PEGDA/GMA-BASED MATRIX



Figure 54 - Rectangular surface and smaller filters

The tests were initially performed on rectangular samples of size 1x5x0.6 cm. Subsequently, some filters of smaller size (diameter of 1.5 cm, thickness of 0.6 cm) were also tested.

5.5.1. SWELLING TEST

For the PEGDA/GMA-based samples without any treatment, these are the results of the swelling and recovery tests, calculated as the average of 5 different measurements:

$$ws\% = 3.58\%$$

$$wr\% = 99.98\%$$

The same tests were also performed on the modified samples; the results are shown in the following table:

Table 10 - Results of swelling and recovery tests on PEGDA/GMA-based samples after surface treatment

Molecule	Method	ws%	wr%
Arginine	Conventional heating	4.31	99.48
Arginine	Microwave heating	4.77	99.11
Agmatine	Conventional heating	5.27	99.01
Agmatine	Microwave heating	5.50	99.20
Dopamine	Dip-coating	9.06	94.17
PEI600	Microwave heating	n.a.	n.a.
PEI600 + Cl	Microwave heating + chlorination	n.a.	n.a.

5.5.2. FTIR-ATR SPECTROSCOPY

5.5.2.1. PEGDA/GMA + ARGININE

Modifications of PEGDA/GMA-based matrix samples with arginine were conducted by both conventional and microwave heating. We found that acidic pH conditions give better results in terms of functionalization; a Tris-HCl buffer at pH=8.5 is used.

In the IR spectroscopy results, we have to pay attention to some peaks: in addition to those seen for PEGDA/AA-based samples (peak at 810 cm^{-1} related to the acrylic group, peaks at 1633 and 1672 cm^{-1} related to the guanidium group, peaks at 2870 and 2920 cm^{-1} related to the C-H bonds, peak between 3350 and 3450 cm^{-1} related to the N-H groups and O-H groups of water), there is a peak at 905 cm^{-1} related to the epoxy ring of glycidyl methacrylate [62]. Upon reaction with secondary amines of the functionalization molecules, this peak should decrease or disappear.

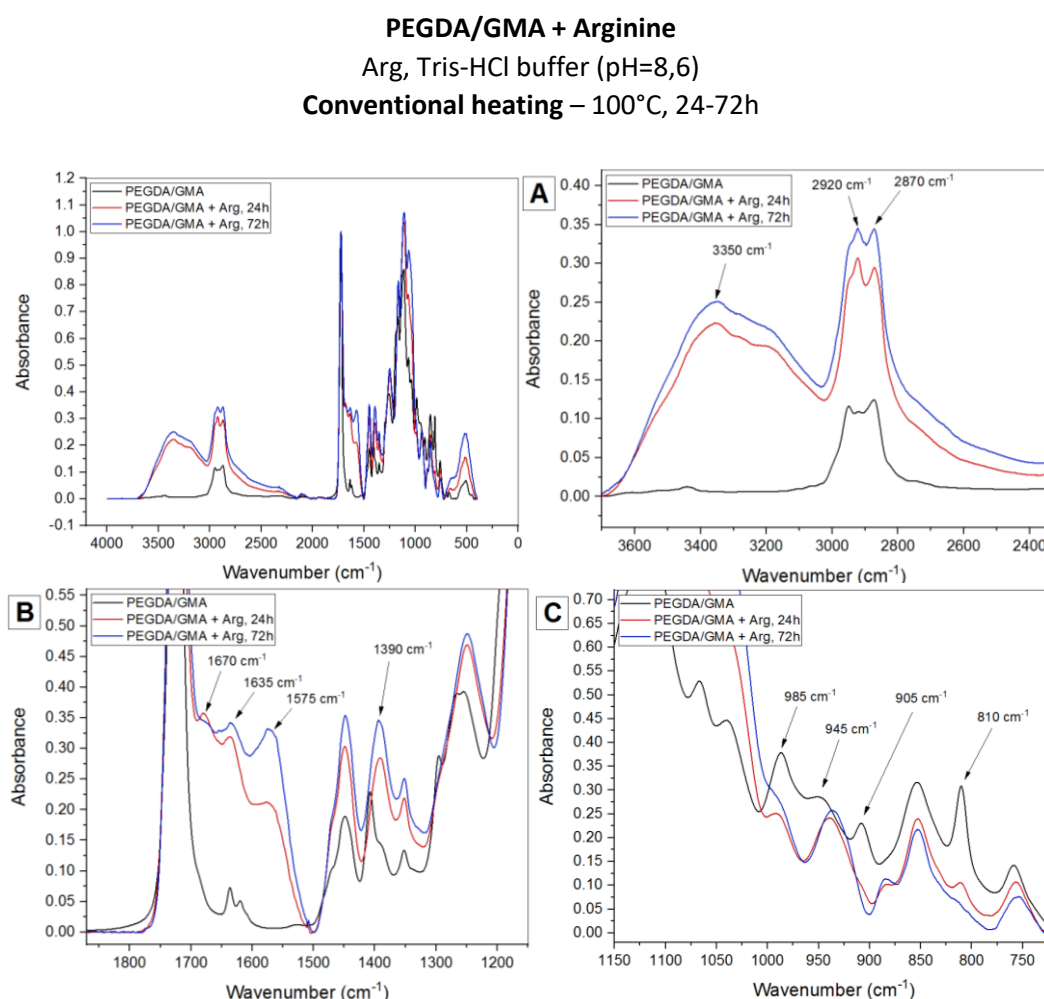


Figure 55 - IR spectrum of PEGDA/GMA-based matrix (8:2) modified with arginine by conventional heating at 100°C for 24h. (A) Wavelengths between 3800 and 2400 cm^{-1} ; (B) wavelengths between 1850 and 1150 cm^{-1} ; (C) wavelengths between 1150 and 600 cm^{-1} .

PEGDA/GMA + Arginine
Arg, Tris-HCl buffer (pH=8,6)
Microwave heating – 150°C, 3-5-7-10 min

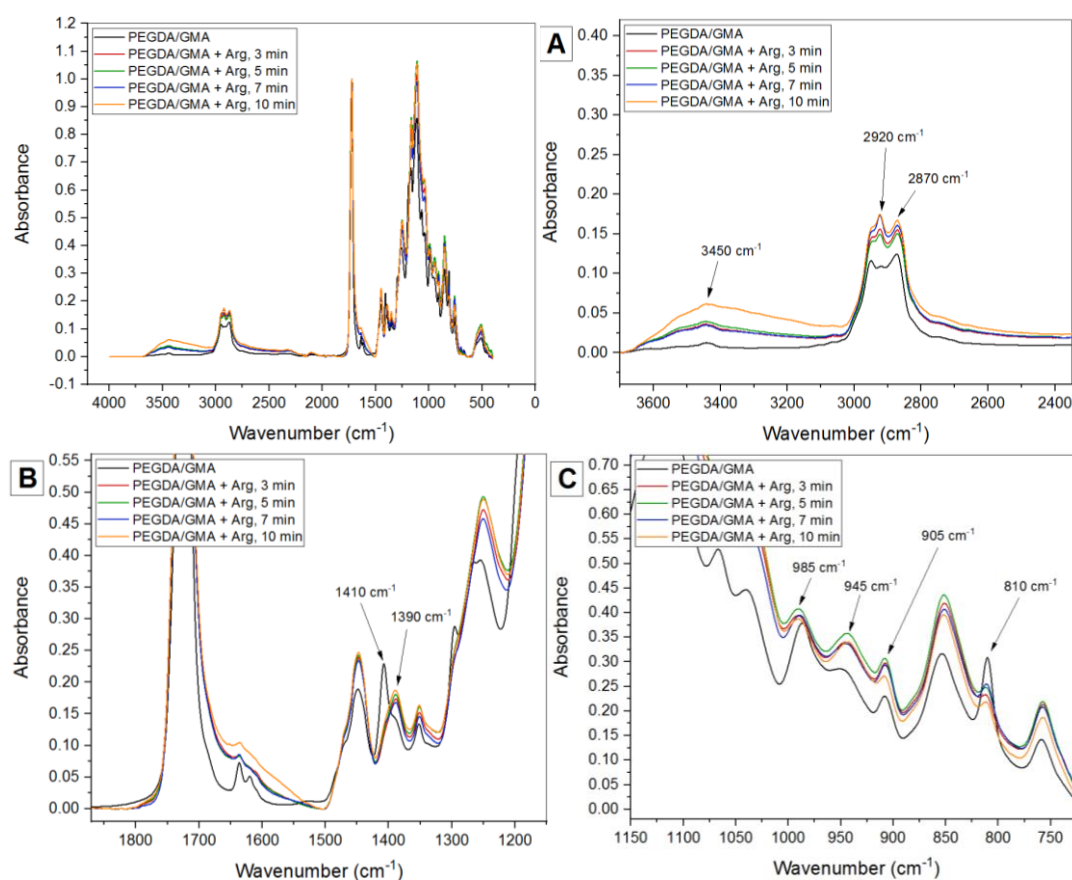


Figure 56 - IR spectrum of **PEGDA/GMA**-based matrix (8:2) modified with **arginine** by **microwave heating** at 150°C for 3, 5, 7 and 10 minutes. **(A)** Wavelengths between 3800 and 2400 cm⁻¹; **(B)** wavelengths between 1850 and 1150 cm⁻¹; **(C)** wavelengths between 1150 and 600 cm⁻¹.

We can compare the different timing of the two treatments by looking at the following graphs, which show the increase or decrease in peak intensity:

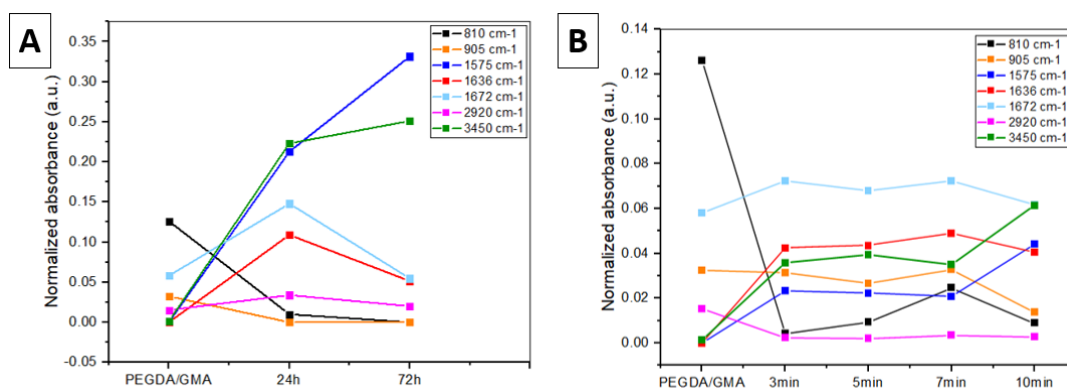


Figure 57 - Trend of peaks of interest (810, 905, 1575, 1636, 1672, 2920 and 3450 cm⁻¹) in the samples subjected to treatment of **(A)** conventional heating and **(B)** microwave heating.

5.5.2.2. PEGDA/GMA + AGMATINE

Treatment of PEGDA/GMA-based matrix samples with agmatine by conventional and microwave treatment was carried out using Tris-HCl buffer at pH of 8.6. The peaks of interest are the same as those described in the previous section.

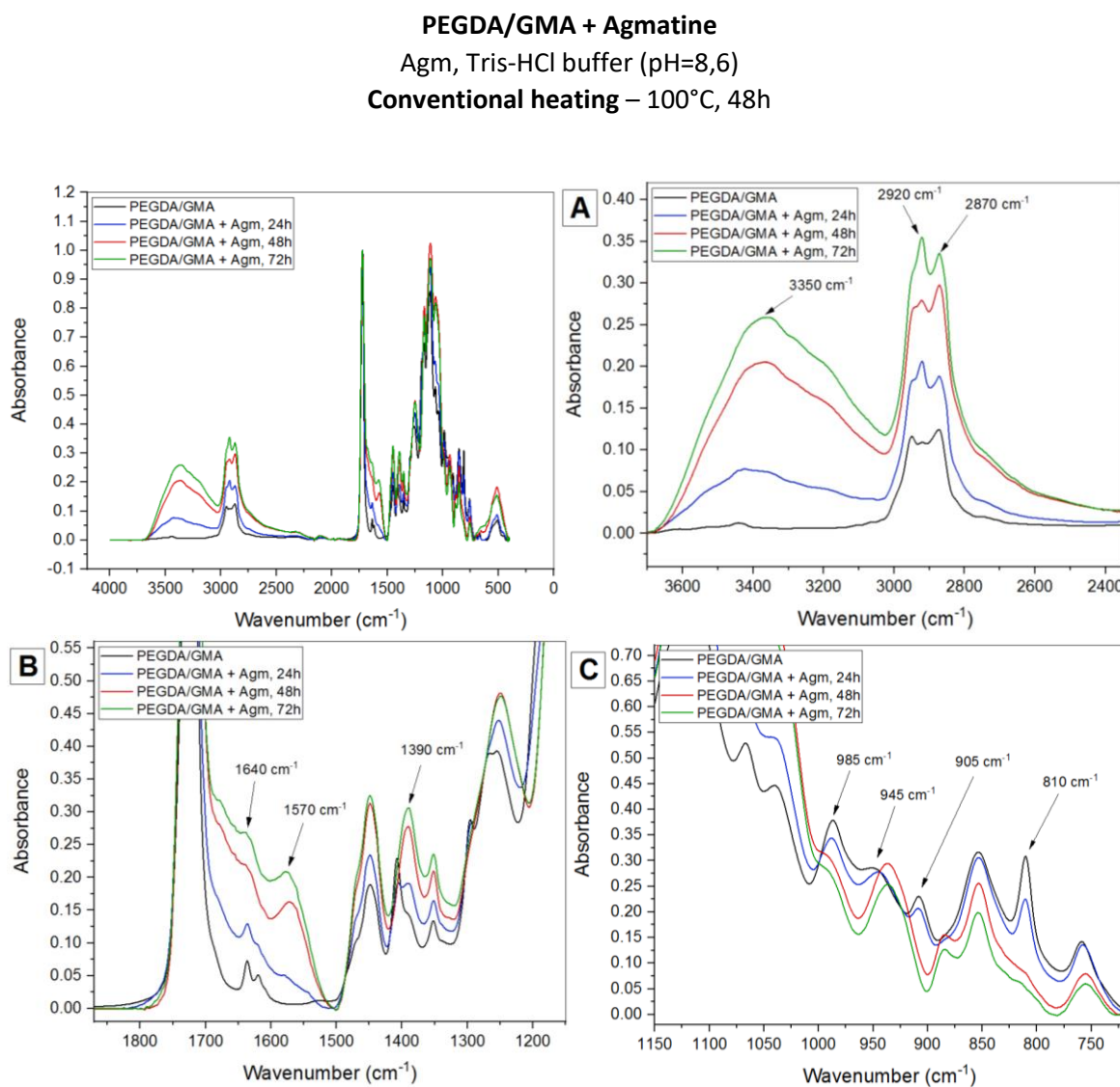


Figure 58 - IR spectrum of *PEGDA/GMA*-based matrix (8:2) modified with *agmatine* by conventional heating at 100°C for 48h. (A) Wavelengths between 3800 and 2400 cm⁻¹; (B) wavelengths between 1850 and 1150 cm⁻¹; (C) wavelengths between 1150 and 600 cm⁻¹.

PEGDA/GMA + Agmatine
 Agm, Tris-HCl buffer (pH=8,6)
 Microwave heating – 150°C, 3-5-7-10 min

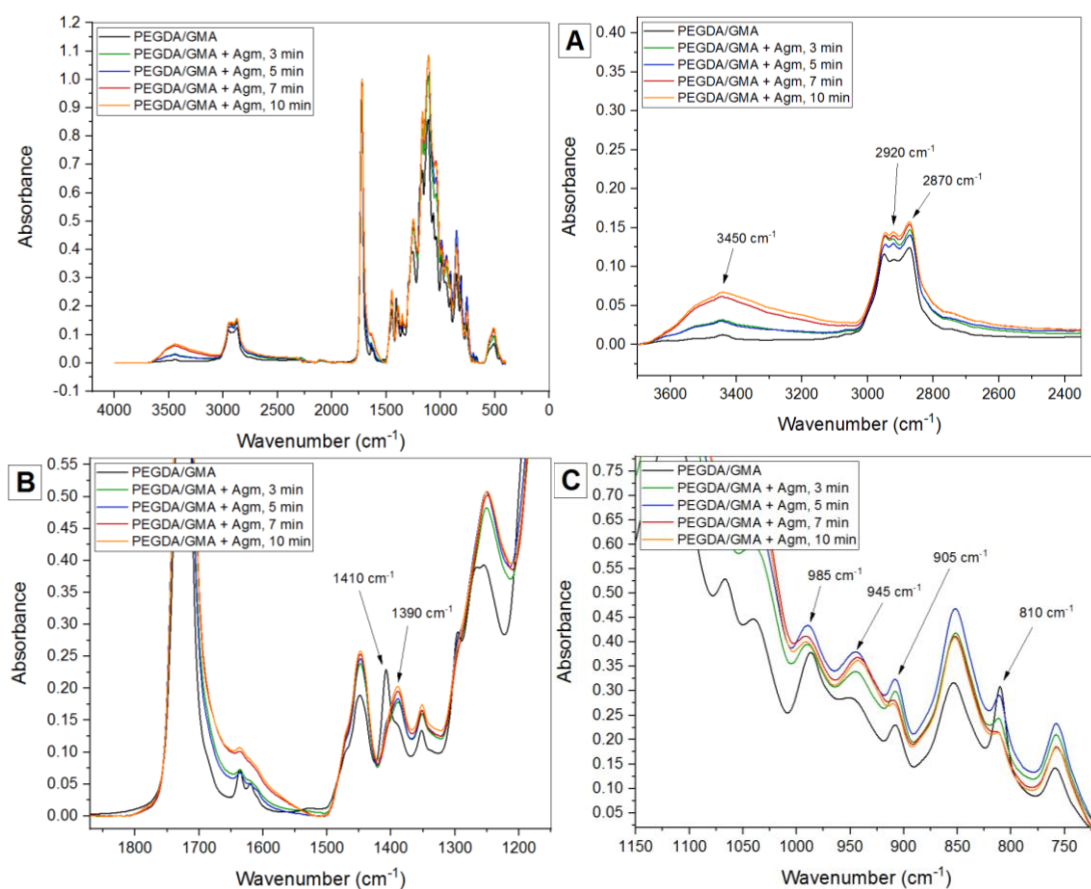


Figure 59 - IR spectrum of *PEGDA/GMA*-based matrix (8:2) modified with *agmatine* by microwave heating at 150°C for 3, 5, 7 and 10 minutes. (A) Wavelengths between 3800 and 2400 cm^{-1} ; (B) wavelengths between 1850 and 1150 cm^{-1} ; (C) wavelengths between 1150 and 600 cm^{-1} .

Again, we can visualize the trend of peak intensity as a function of reaction time.

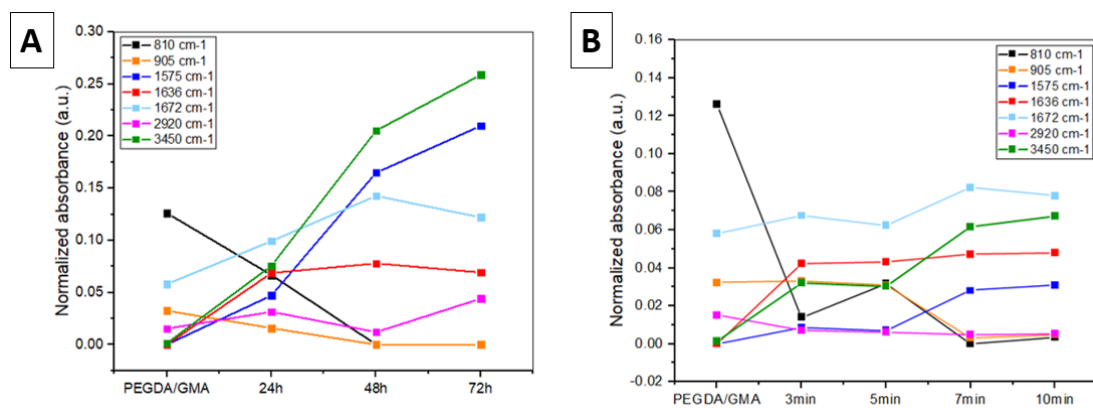


Figure 60 - Trend of peaks of interest (810, 905, 1575, 1636, 1672, 2920 and 3450 cm^{-1}) in the samples subjected to treatment of (A) conventional heating and (B) microwave heating.

5.5.2.3. PEGDA/GMA + DOPAMINE

Dopamine dip-coating treatment involves immersing the samples in a solution of dopamine and Tris-HCl at pH=8.5. The reaction proceeds in the presence of oxygen for 24 hours at room temperature.

PEGDA/GMA + Dopamine Dopamine, Tris-HCl buffer (pH=8,5) Dip coating – 24h

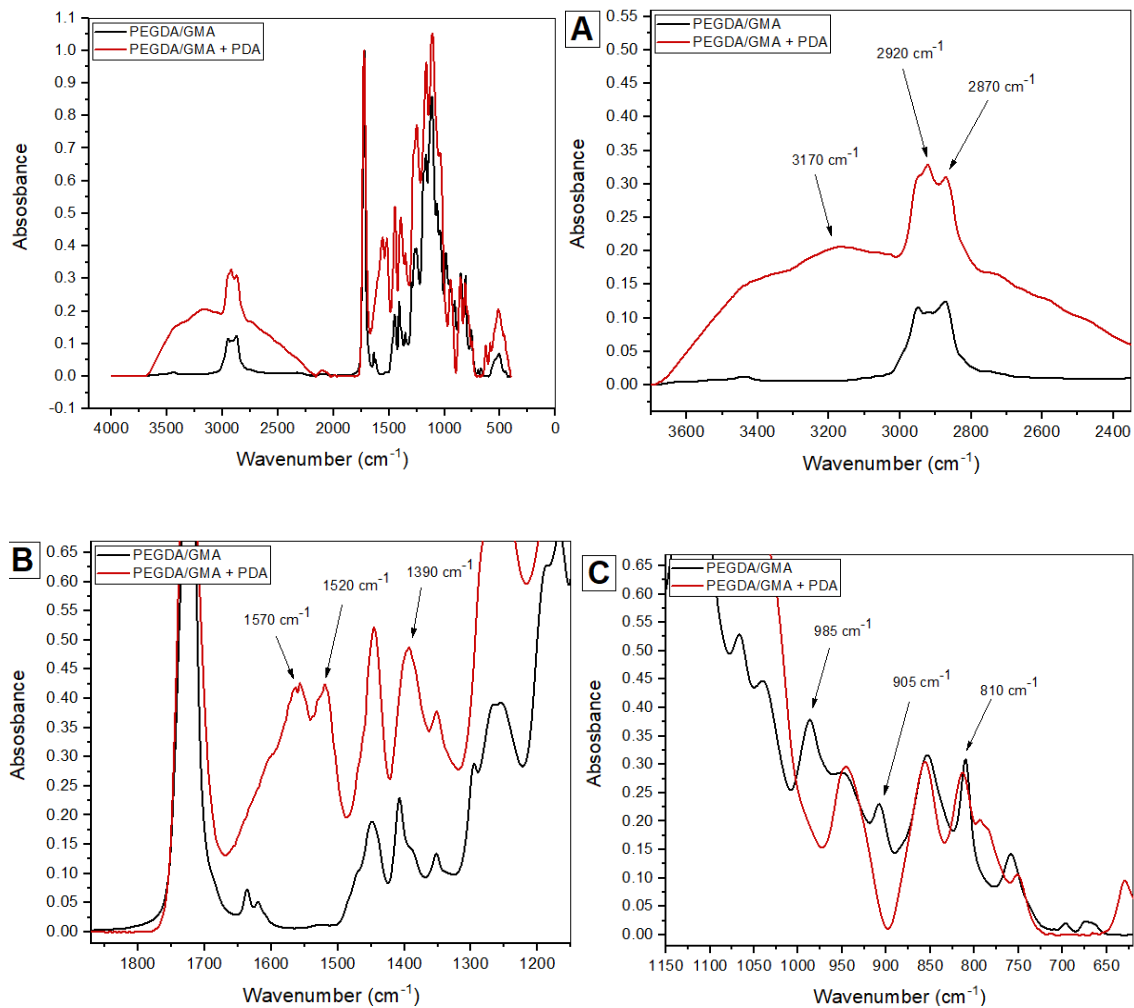


Figure 61 - IR spectrum of PEGDA/GMA-based matrix (8:2) modified with DOPAMINE by dip-coating at room temperature for 24h. (A) Wavelengths between 3800 and 2400 cm^{-1} ; (B) wavelengths between 1850 and 1150 cm^{-1} ; (C) wavelengths between 1150 and 600 cm^{-1}

5.5.2.4. PEGDA/GMA + PEI

PEI treatment is done via microwave heating in acetonitrile.

PEGDA/GMA + PEI600 PEI600, Acetonitrile Microwave heating – 150°C, 1 min

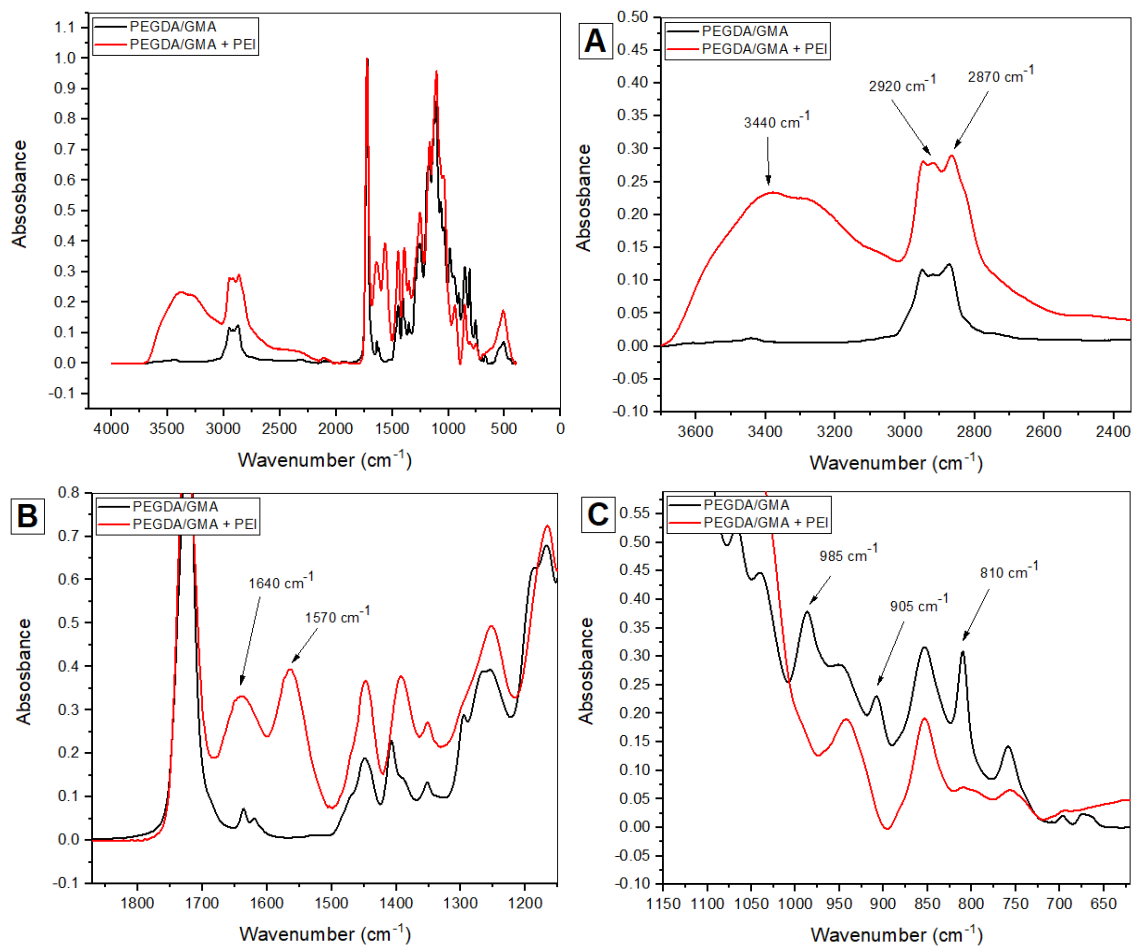


Figure 62 - IR spectrum of **PEGDA/GMA**-based matrix (8:2) modified with **PEI600** by microwave heating at **150°C** for **1 minute**. **(A)** Wavelengths between 3800 and 2400 cm⁻¹; **(B)** wavelengths between 1850 and 1150 cm⁻¹; **(C)** wavelengths between 1150 and 600 cm⁻¹.

A post-curing treatment was then performed in UV lamp at 365 nm for 7 minutes; then the samples were subjected to chlorination, following the protocol described in section 4.6.4.

PEGDA/GMA-PEI600 + Cl

1) PEI600 + Acetonitrile

Microwave heating – 150°C, 1min

1) HClO 2%

Chlorination - Room temperature, 1h, 160 rpm

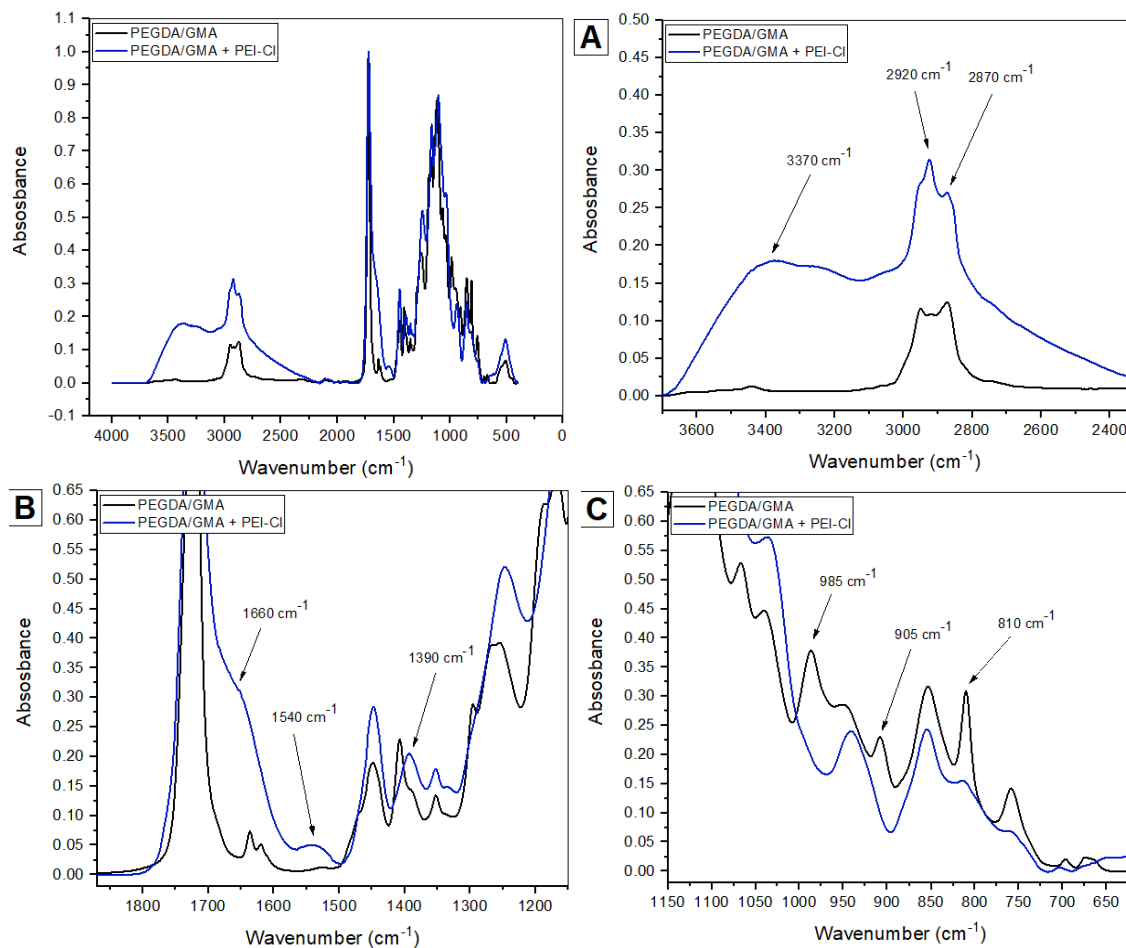


Figure 63 - IR spectrum of sample MD26: PEGDA/GMA-based matrix (8:2) modified with PEI600 by microwave heating at 150°C for 1 minute and then chlorinated in HClO solution for 1h. (A) Wavelengths between 3800 and 2400 cm⁻¹; (B) wavelengths between 1850 and 1150 cm⁻¹; (C) wavelengths between 1150 and 600 cm⁻¹

5.5.3. CONTACT ANGLE

We can use the contact angle measurement as an indicator of treatment success. Differently that in PEGDA/AA-based samples, here the contact angle trend is not always linear, and there are sometimes increases in hydrophobicity. However, these could be due to the difficulty or errors in measurement. In the case of DOPA and PEI treatments, however, the decrease in contact angle is quite marked.

5.5.3.1. PEGDA/GMA + ARGININE

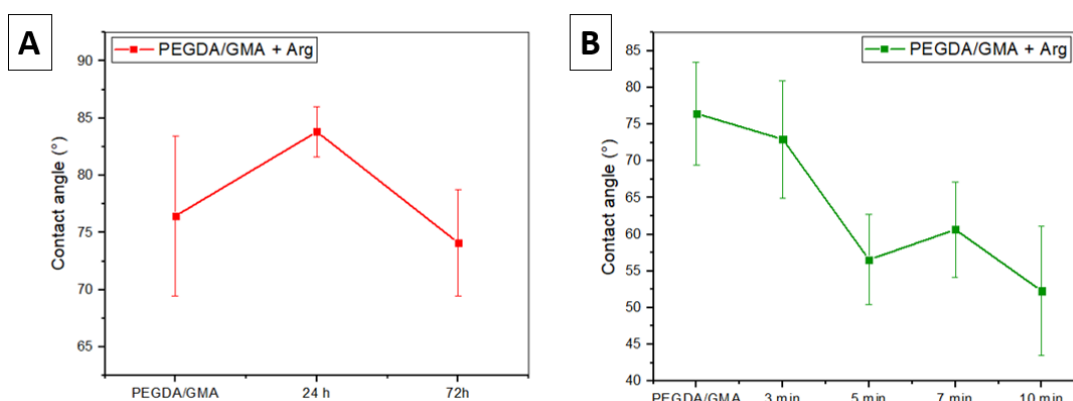


Figure 64 - Contact angle of *PEGDA/GMA*-based sample modified with *arginine* under (A) conventional heating (24h) and (B) microwave heating (3 and 5 minutes), compared to the non-treated sample

5.5.3.2. PEGDA/GMA + AGMATINE

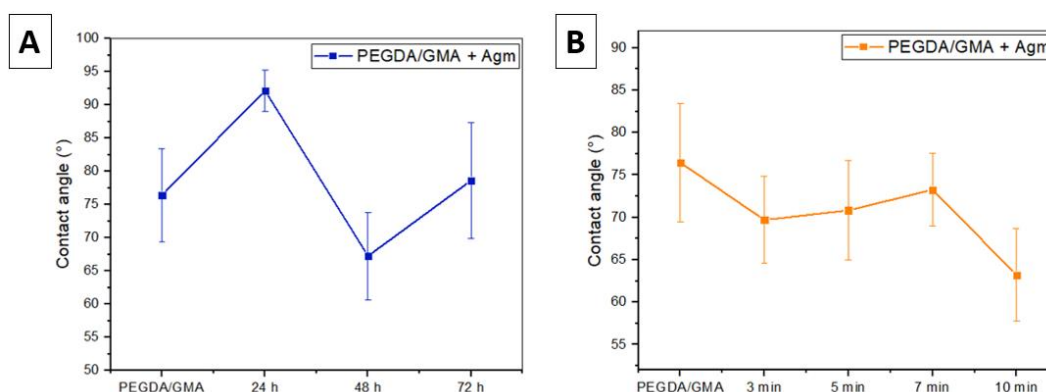


Figure 65 - Contact angle of *PEGDA/GMA*-based sample modified with *agmatine* under (A) conventional heating (24h) and (B) microwave heating (3 and 5 minutes), compared to the non-treated sample

5.5.3.3. PEGDA/GMA + DOPAMINE

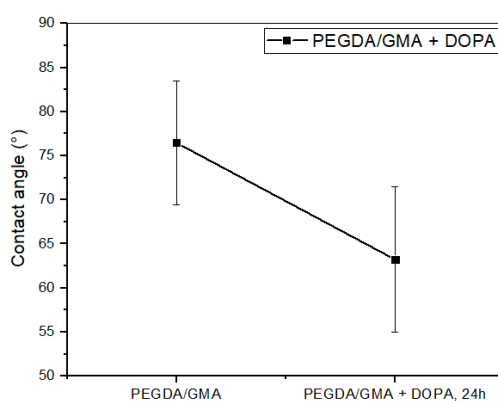


Figure 66 - Contact angle of **PEGDA/GMA**-based sample modified with **dopamine** through dip-coating (24h)

5.5.3.4. PEGDA/GMA + PEI

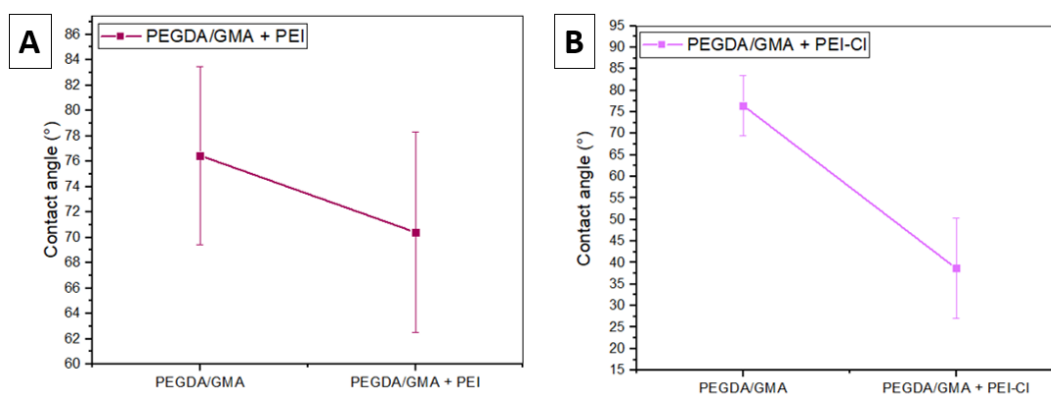


Figure 67 - Contact angle of **PEGDA/GMA**-based sample modified with **PEI600** through microwave heating (150°C, 1 min), before **(A)** and after **(B)** chlorination

5.5.4. CHOICE OF THE BEST SAMPLES

Based on the results of IR spectroscopy and contact angle analysis, we are able to choose the most appropriate modification parameters to achieve the maximum degree of functionalization, while also considering the physical damage and the least consumption of time and energy.

In samples modified with arginine by conventional heating, 72 hours of treatment gives better results than 24 hours, in terms of behavior of peaks of interest and decrease in contact angle. However, we judged that the better success of the treatment does not justify such a long duration, as already after 24 hours there are acceptable results. Concerning the microwave treatment, we can see from the intensity of the peaks that there are no degrees of difference by increasing the reaction time; therefore, we chose the shorter duration, 3 minutes.

In conventional agmatine treatment, however, 24 hours is not enough to have acceptable results, so we set a duration of 48 hours. The duration of microwave heating, on the other hand, was set at 7 minutes to have a good surface modification. Further tests will be conducted on these samples to get confirmation of the results we think we have obtained.

Finally, the samples modified with dopamine and PEI600 show satisfactory results and will be used for biological tests.

To sum up, the chosen samples are shown in the following table.

Table 11 - Chosen treatment conditions for PEGDA/GMA-based samples

Name	Functionalizing molecule	Treatment	Treatment conditions
PGMA-AR-F	Arginine	Conventional heating	100°C, 70rpm, 24h
PGMA-AR-M	Arginine	Microwave heating	150°C, 3min
PGMA-AG-F	Agmatine	Conventional heating	100°C, 70rpm, 48h
PGMA-AG-M	Agmatine	Microwave heating	150°C, 7min
PGMA-D	Dopamine	Dip-coating	80rpm, 24h
PGMA-PEI	PEI600	Microwave heating	150°C, 1min
PGMA-PEI-Cl	PEI600 + Cl	Microwave heating + chlorination	150°C, 1min + 160rpm, 1h

5.5.5. TGA

5.5.5.1. PEGDA/GMA + ARGININE

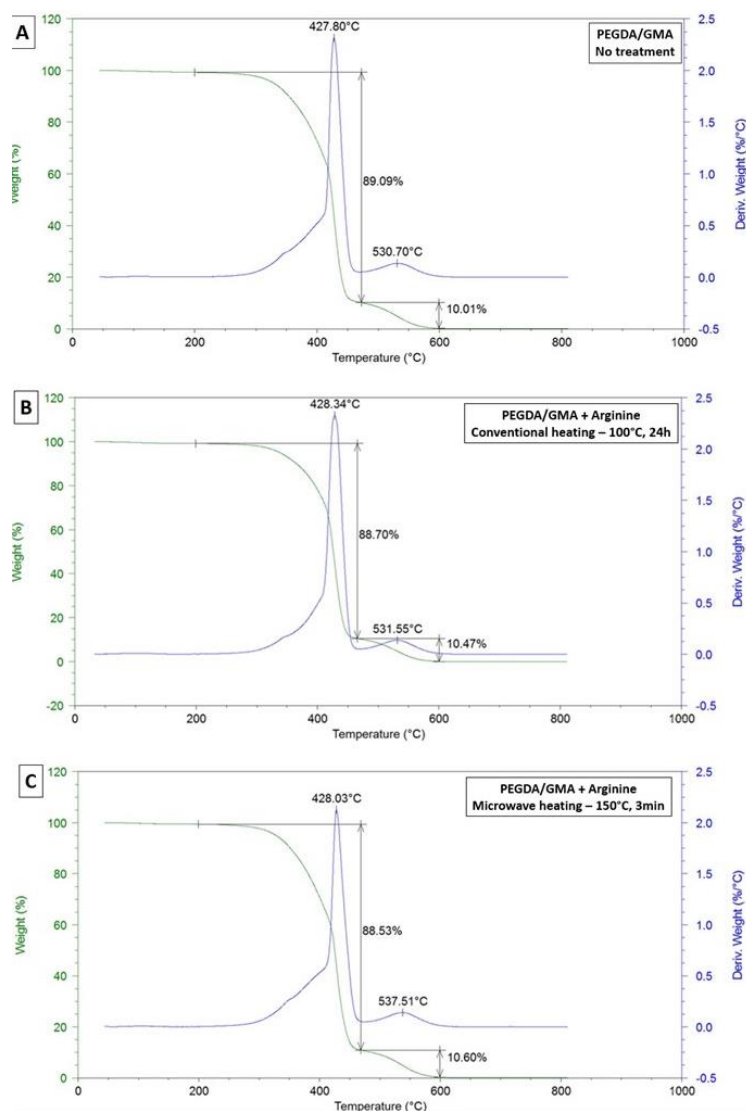


Figure 68 - Percent weight reduction as a function of temperature in samples (A) subjected to no treatment, (B) modified with *arginine* by conventional heating, and (C) modified with *arginine* by microwave heating.

For samples that were not subjected to any treatment, we note one main degradation event (89.09%), in which the maximum degradation rate is reached around 430°C. A second event occurs at higher temperatures (530°C) and contributes approximately 10% to the sample degradation. Strangely enough, the behavior of arginine-treated samples is similar in both form and extent of degradation events. So, it is quite difficult to determine, from these graphs, the degree of surface alteration.

5.5.5.2. PEGDA/GMA + AGMATINE

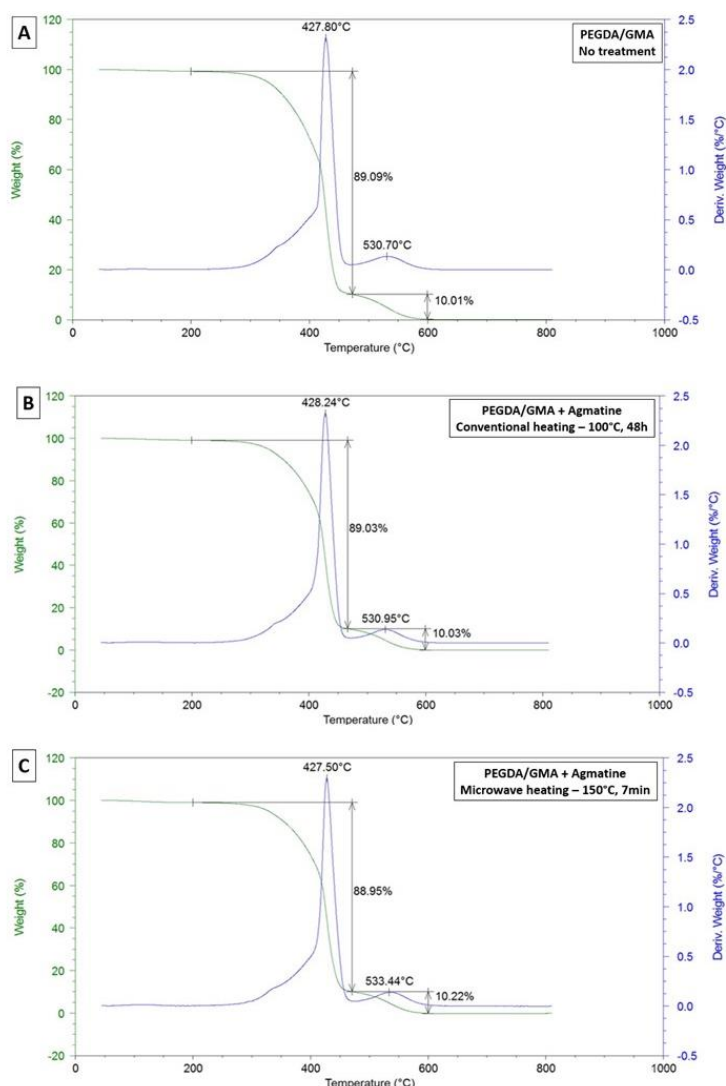


Figure 69 - Percent weight reduction as a function of temperature in samples (A) subjected to no treatment, (B) modified with **agmatine** by conventional heating, and (C) modified with arginine by microwave heating.

Even in the case of agmatine modification, the success of the surface treatment cannot be determined from these graphs. In fact, there are no particular differences in the untreated sample: the highest degradation rate occurs around 428°C, and about 89% of the weight is lost in the main degradation event.

5.5.6. EDX

The EDX technique allows us to know the percentage of nitrogen present on the surface following treatment with arginine or agmatine.

5.5.6.1. PEGDA/GMA + ARGININE

Table 12 - Results of EDX experiment for PEGDA/GMA-based sample modified with arginine

	PEGDA/GMA No treatment	PEGDA/GMA + Arg Conventional
ELEMENT	wt%	wt%
C	56.92	52.24
O	41.23	43.32
N	1.85	3.04
Na	0	0.39
Cl	0	0.55
Others	0	0.46
Total	100	100

We see that the percentage of nitrogen increases from 1.85% to 3.06% following arginine treatment by conventional heating. Nitrogen distribution is quite homogeneous on the surface.

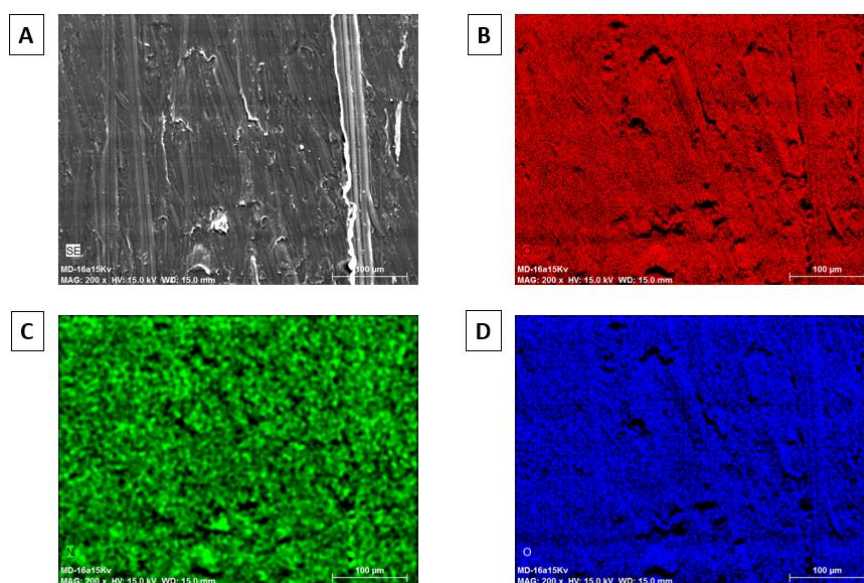


Figure 70 - Microscopic image of the surface of the arginine-modified sample (A); distribution of carbon (B), nitrogen (C) and oxygen (D) atoms on the surface.

5.5.6.2. PEGDA/GMA + AGMATINE

Table 13 - Results of EDX experiment for PEGDA/GMA-based sample modified with agmatine

	PEGDA/GMA No treatment	PEGDA/GMA + Agm Conventional	PEGDA/GMA + Agm Microwave
ELEMENT	wt%	wt%	wt%
C	56.92	52.37	54.26
O	41.23	43.09	44.25
N	1.85	2.68	0.27
Na	0	0.52	0.33
Cl	0	0.81	0.56
Others	0	0.53	0.33
Total	100	100	100

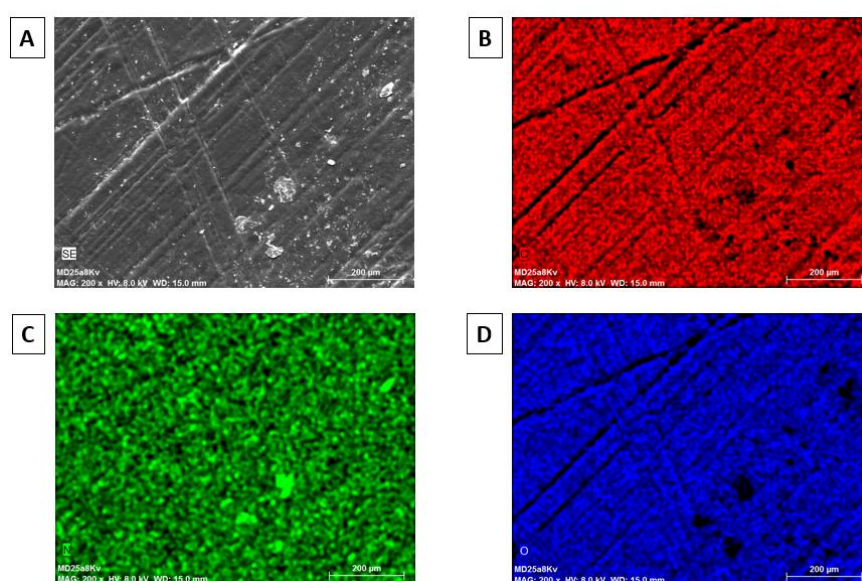


Figure 71 - Microscopic image of the surface of the agmatine-modified sample (A); distribution of carbon (B), nitrogen (C) and oxygen (D) atoms on the surface

For agmatine-treated samples, there is an increase in nitrogen content in the case of conventional heating; the distribution on the surface is also homogeneous, with a few spots. In contrast, there is no satisfactory percentage of nitrogen in the case of microwave heating treatment: nitrogen amounts to only 0.27%.

5.5.7. FINAL COMMENTS

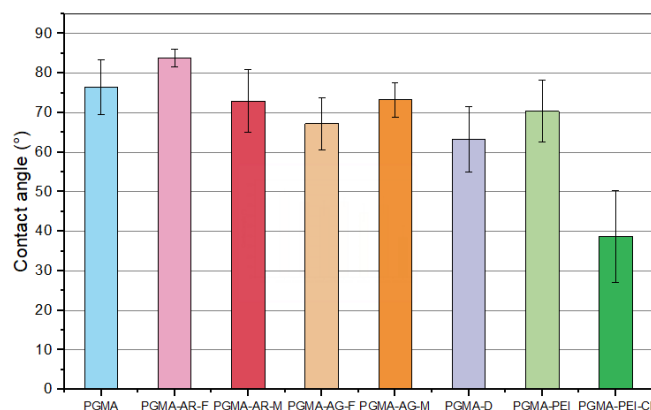


Figure 72 - Comparison of the contact angle of all the PEGDA/GMA-based samples

Again, the success of the surface treatments can be noted by observing the changes in contact angle; in particular, we highlight that the sample treated with arginine by conventional heating (PGMA-AR-F) undergoes an increase in hydrophobicity, in contrast with all the others, which instead become more hydrophilic.

These specimens also experience deterioration of mechanical properties and surface deterioration, as seen in PEGDA/AA-

based specimens. The discoloration, in this case, may be partly due to the release of the dye.

In the Figure 73 we can see the difference in color between the samples on the right (unmodified) and those on the left (samples subjected to surface modification treatment).

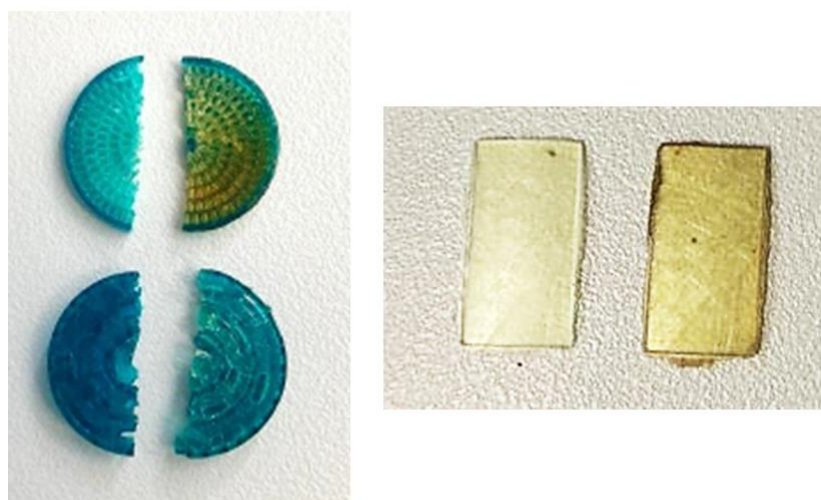


Figure 73 – Comparison between unmodified samples (on the right) and modified samples (on the left) to show the difference in color.

5.6. OTHER MATRICES: PEGDA, PEGDA/ABUT, PEGDA/AA/ABUT

5.6.1. SWELLING TEST

These are the results of swelling and recovery tests performed on the PEGDA₂₅₀, PEGDA/ABut and PEGDA/AA/ABut-based samples without any treatment:

Table 14 - Results of swelling and recovery tests on the untreated matrices

Matrix	ws%	wr%
PEGDA ₂₅₀	5.08	99.86
PEGDA/ABut	2.29	99.77
PEGDA/AA/ABut	7.47	99.80

The same tests were also performed on the samples modified with dopamine through dip-coating; the results are shown in the following table:

Table 15 - Results of swelling and recovery tests on the treated samples

Matrix	Molecule and method	ws%	wr%
PEGDA ₂₅₀	Dopamine – dip-coating	4.22	99.67
PEGDA/ABut	Dopamine – dip-coating	3.94	97.77
PEGDA/AA/ABut	Dopamine – dip-coating	5.26	99.06

5.6.2. FTIR-ATR SPECTROSCOPY

As can be seen in the following sections, FTIR spectroscopy performed on the dopamine-modified PEGDA₂₅₀ and PEGDA/ABut samples shows little difference from the untreated sample. In contrast, the dopamine-modified PEGDA/AA/ABut sample shows slightly different behavior in the area between 1500 and 1600 cm⁻¹, with two distinct peaks at 1520 and 1570 cm⁻¹.

4.6.2.1. PEGDA₂₅₀ + DOPAMINE

PEGDA₂₅₀ + Dopamine DOPA, Tris-HCl buffer (pH=8,5) Dip coating – 24h

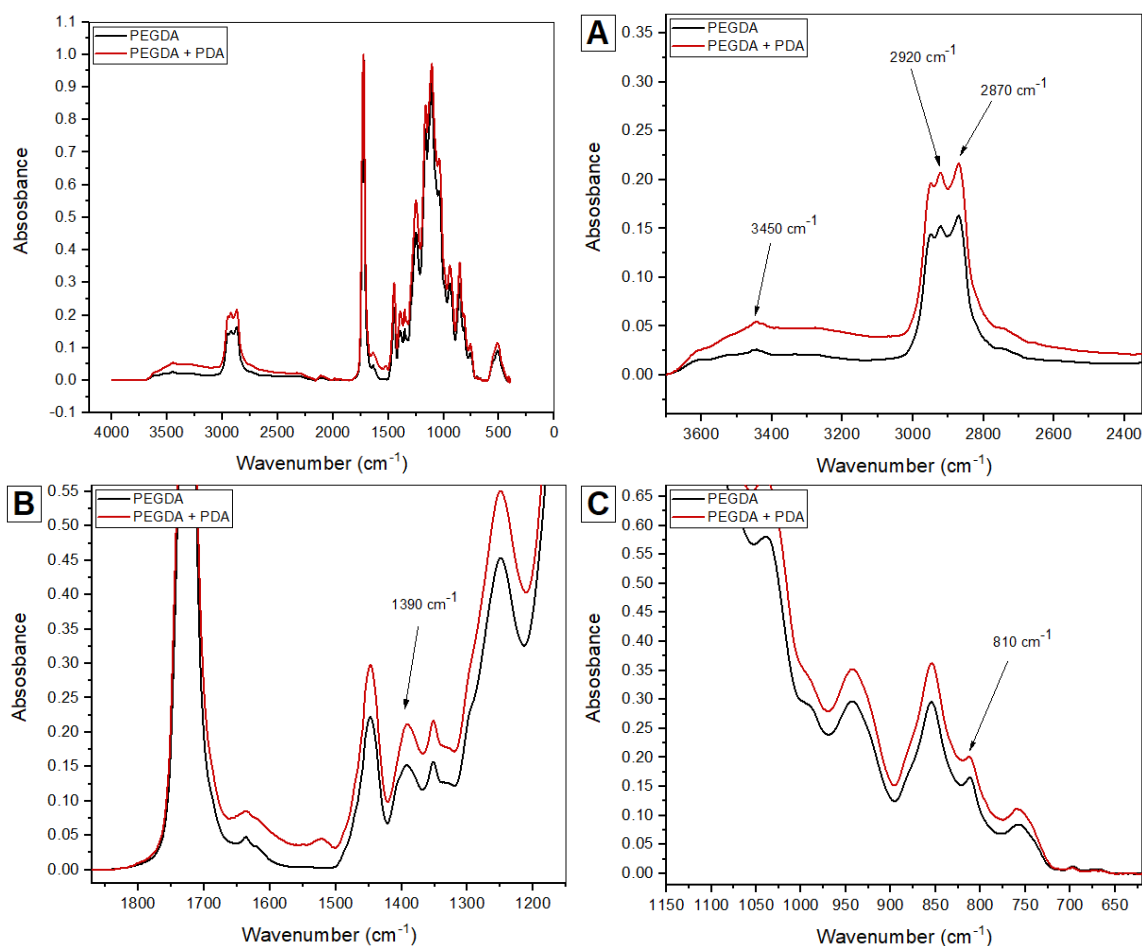


Figure 74 - IR spectrum of PEGDA₂₅₀-based matrix modified with DOPAMINE by dip-coating at room temperature for 24h. (A) Wavelengths between 3800 and 2400 cm⁻¹; (B) wavelengths between 1850 and 1150 cm⁻¹; (C) wavelengths between 1150 and 600 cm⁻¹

4.6.2.2. PEGDA/ABUT + DOPAMINE

PEGDA/ABut + Dopamine DOPA, Tris-HCl buffer (pH=8,5) Dip coating – 24h

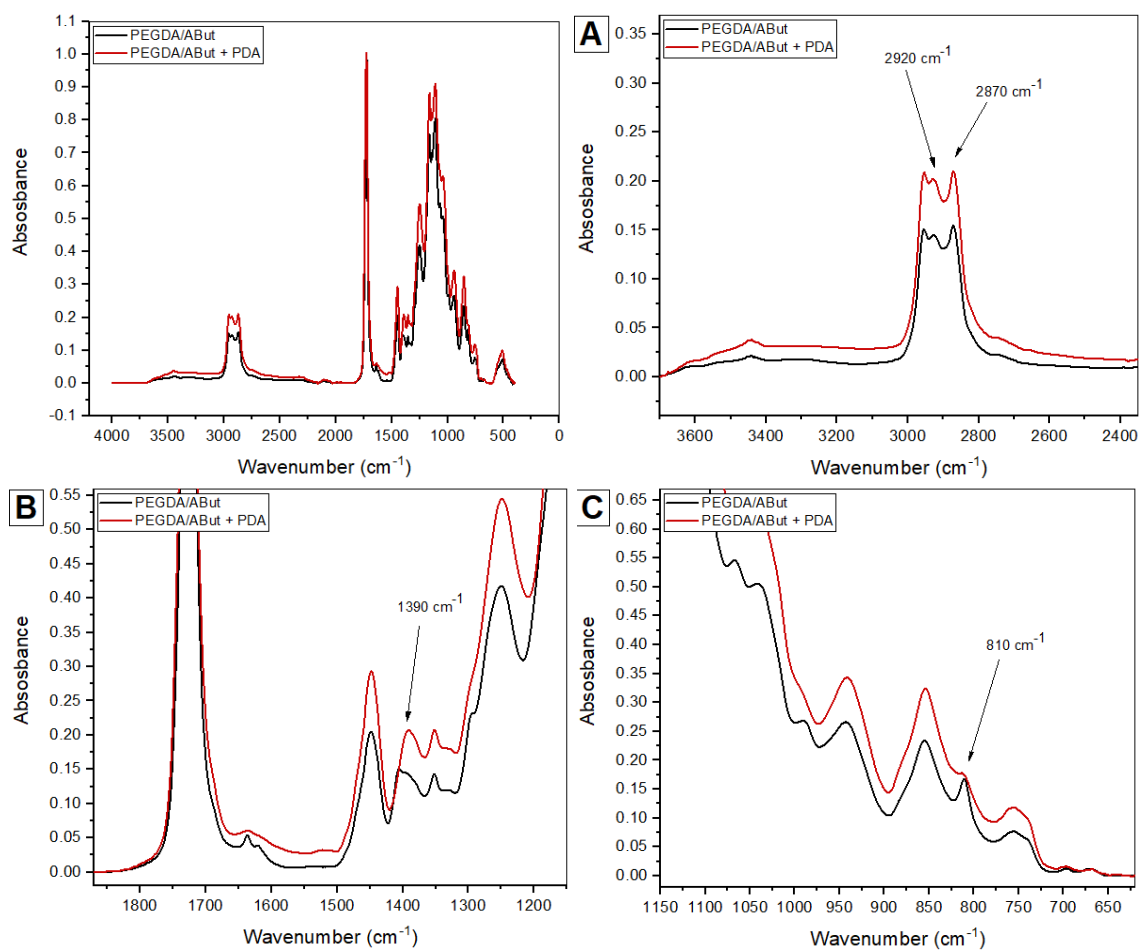


Figure 75 - IR spectrum of **PEGDA/ABut**-based matrix (8:2) modified with **DOPAMINE** by dip-coating at room temperature for **24h**. **(A)** Wavelengths between 3800 and 2400 cm^{-1} ; **(B)** wavelengths between 1850 and 1150 cm^{-1} ; **(C)** wavelengths between 1150 and 600 cm^{-1}

4.6.2.3. PEGDA/AA/ABUT + DOPAMINE

PEGDA/AA/ABut + Dopamine

DOPA, Tris-HCl buffer (pH=8,5)

Dip coating – 24h

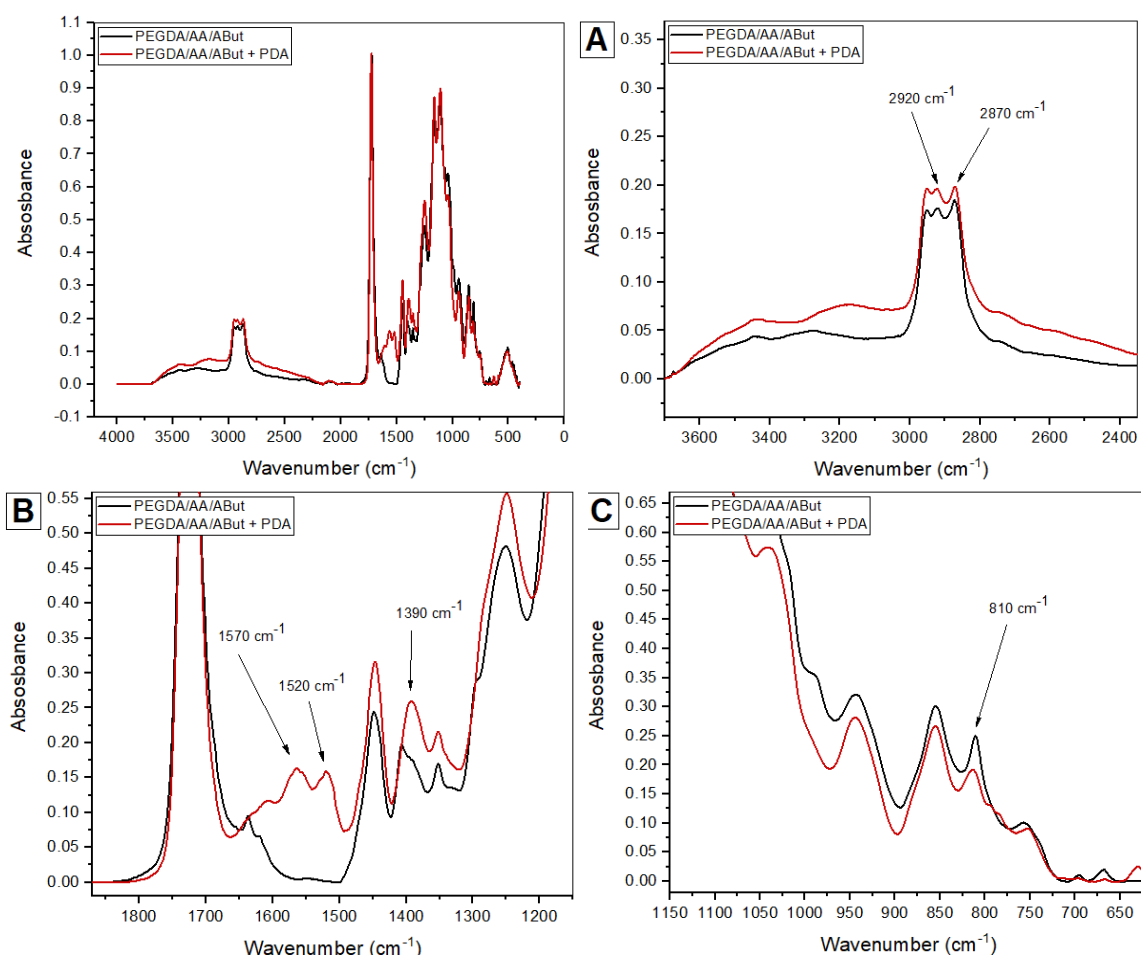


Figure 76 - IR spectrum of **PEGDA/AA/ABut**-based matrix (80:15:5) modified with **DOPAMINE** by dip-coating at room temperature for **24h**. **(A)** Wavelengths between 3800 and 2400 cm^{-1} ; **(B)** wavelengths between 1850 and 1150 cm^{-1} ; **(C)** wavelengths between 1150 and 600 cm^{-1}

5.6.3. CONTACT ANGLE

As we can see in the following figure, an increase in hydrophilicity is observed in all three dopamine-modified matrices. This indicates that a modification on the surface has nevertheless occurred, although this is not readily visible in FTIR spectroscopy.

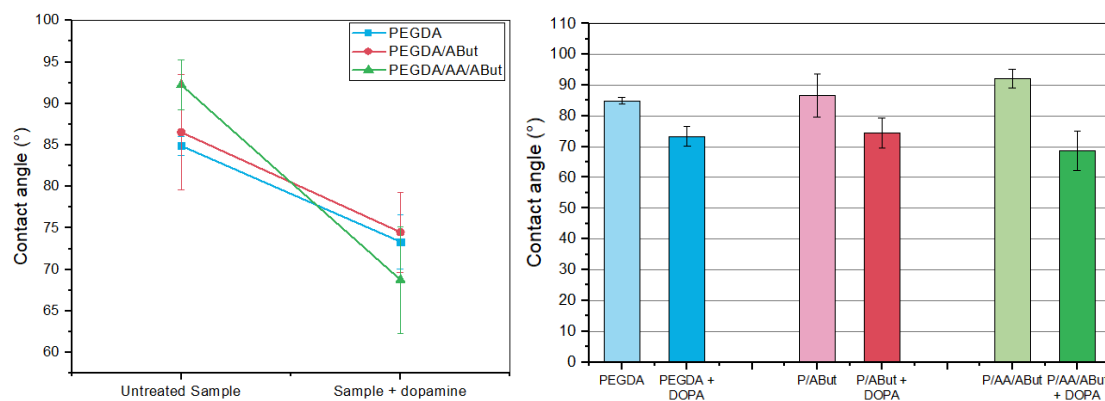


Figure 77 - Comparison of the contact angle of PEGDA250, PEGDA/ABut, PEGDA/AA/ABut- based samples, unmodified and modified with dopamine

5.6.4. FINAL COMMENTS

Samples based on these matrices have worse physical-mechanical properties than those based on PEGDA/AA and PEGDA/GMA. The samples are thinner and more fragile, even if this is mainly due to the different polymerization method used. The specimens undergo a color change, becoming darker due to oxidation of dopamine on the surface, but the physical properties are not particularly affected after treatment.

CHAPTER 6: BIOLOGICAL TESTS: RESULTS AND DISCUSSION

6.1. PEGDA/AA-BASED SAMPLES

Preliminary tests on the flat surfaces were conducted with both Gram-positive (*S. Aureus*) and Gram-negative (*E. Coli*) bacteria. Bacterial quantification was difficult on many of the samples tested, for several reasons: sometimes the samples had bent during surface treatments or other procedures, so it was impossible to focus on a single plane to detect bacteria; other times the swelling causes excessive absorption of the dyes, making it difficult to distinguish bacteria (this happens especially in dopamine-treated samples). The presence of scratches and streaks, due to the printing process and subsequent treatments, also does not help in quantifying the bacteria. All these problems seemed to be more evident with *Escherichia Coli* than with *Staphylococcus Aureus*. The biological tests conducted are summarized in the following table:

Table 16 - Summary of biological tests conducted on PEGDA/AA-based samples.

REACTANT	TREATMENT	BACTERIA	OBSERVATION
----	-----	<i>S. Aureus</i>	✓
		<i>E. Coli</i>	✗
Arginine	Conventional heating	<i>S. Aureus</i>	✓
		<i>E. Coli</i>	✗
	Microwave heating	<i>S. Aureus</i>	✓
		<i>E. Coli</i>	✗
Agmatine	Conventional heating	<i>S. Aureus</i>	✓
		<i>E. Coli</i>	✗
	Microwave heating	<i>S. Aureus</i>	✓
		<i>E. Coli</i>	✗
Dopamine	Dip-coating	<i>S. Aureus</i>	✗
		<i>E. Coli</i>	✗
PEI600	Microwave heating	<i>S. Aureus</i>	✗
		<i>E. Coli</i>	✗
PEI600 + Cl	Microwave hating + chlorination	<i>S. Aureus</i>	✗



: ANALYZED SAMPLE



: SAMPLE THAT COULD NOT BE ANALYZED

Staphylococcus Aureus

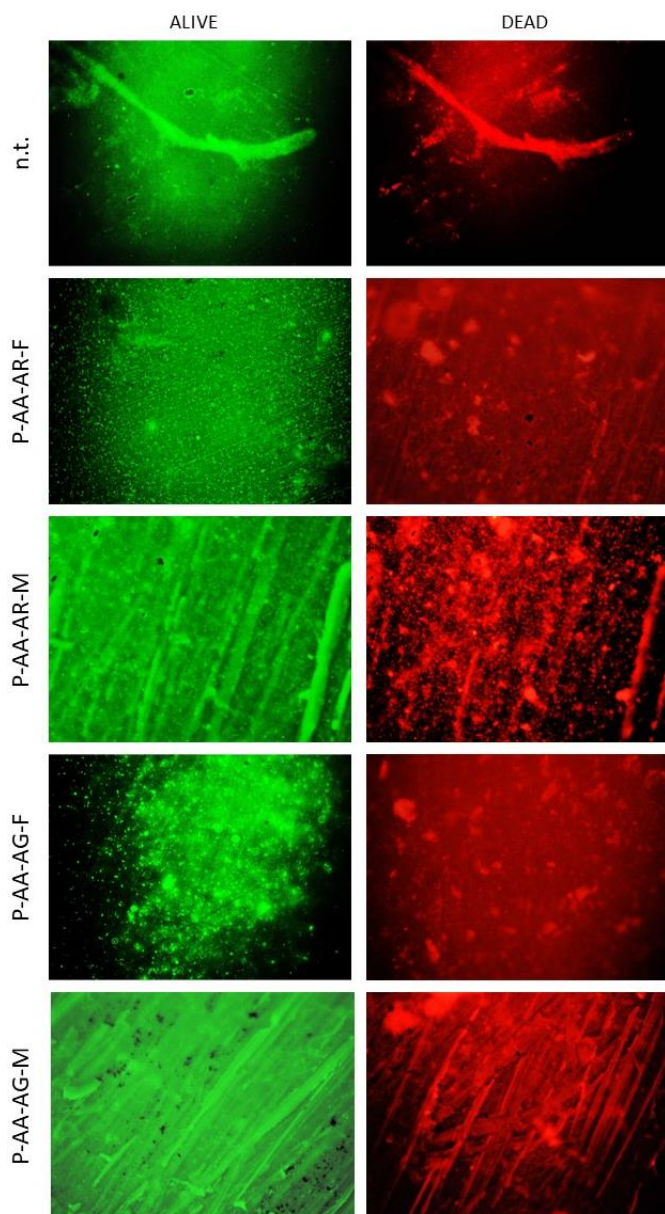


Figure 78 - Live and dead bacteria (*Staphylococcus Aureus*) on PEGDA/AA-based samples

In Figure 78 we can see the bacteria (*S. Aureus*) present on the analyzed samples. Compared to the untreated sample (in the first row), we see that the number of bacteria, both live and dead, increases in virtually all the modified samples which is a confirmation that our approach to modify the surface increases the adhesion of bacteria. In particular, the sample treated with arginine by conventional heating (P-AA-AR-F) shows the highest number of bacteria still alive on the surface, while the sample treated with the same molecule in microwave (P-AA-AR-M) is the most effective in killing bacteria.

In general, we can say from these preliminary tests that the arginine-modified samples perform better than the agmatine-modified samples, and that the conventional heating treatment is more effective than the microwave one.

This is also evident from the graph, which shows the number of bacteria present on the surface. This value was calculated with the help of ImageJ software, but it is still only an approximate number.

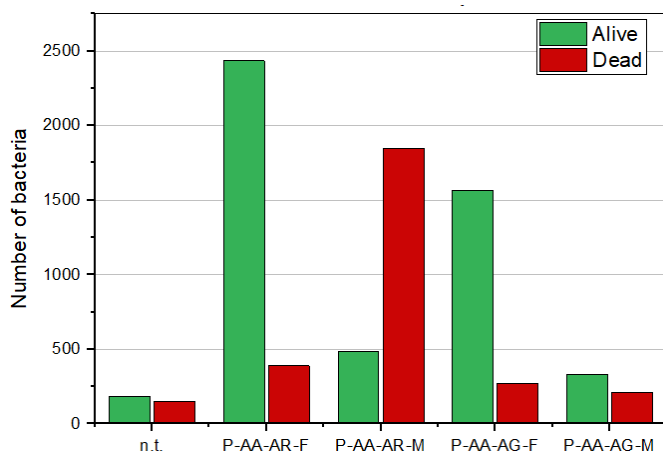


Figure 79 – Number of *Staphylococcus Aureus* bacteria (live and dead) on PEGDA/AA-based samples

6.2. PEGDA/GMA-BASED SAMPLES

Preliminary tests on the flat surfaces were conducted with both Gram-positive (*S. Aureus*) and Gram-negative (*E. Coli*) bacteria. The biological tests conducted are summarized in the following table:

Table 17 - Summary of biological tests conducted on PEGDA/GMA-based samples.

REACTANT	TREATMENT	BACTERIA	OBSERVATION
----	-----	<i>S. Aureus</i>	✓
		<i>E. Coli</i>	✗
Arginine	Conventional heating	<i>S. Aureus</i>	✓
		<i>E. Coli</i>	✗
	Microwave heating	<i>S. Aureus</i>	✓
		<i>E. Coli</i>	✗
Agmatine	Conventional heating	<i>S. Aureus</i>	✓
		<i>E. Coli</i>	✗
	Microwave heating	<i>S. Aureus</i>	✓
		<i>E. Coli</i>	✗
Dopamine	Dip-coating	<i>S. Aureus</i>	✗
		<i>E. Coli</i>	✗
PEI600	Microwave heating	<i>S. Aureus</i>	✗
		<i>E. Coli</i>	✗
PEI600 + Cl	Microwave hating + chlorination	<i>S. Aureus</i>	✗



: ANALYZED SAMPLE



: SAMPLE THAT COULD NOT BE ANALYZED

In the PEGDA-GMA-based samples, we also had the same difficulties in quantifying the bacteria, due to swelling, surface deterioration, and breaking or bending of the samples. Nevertheless, some of the samples analyzed showed promising results.

Staphylococcus Aureus

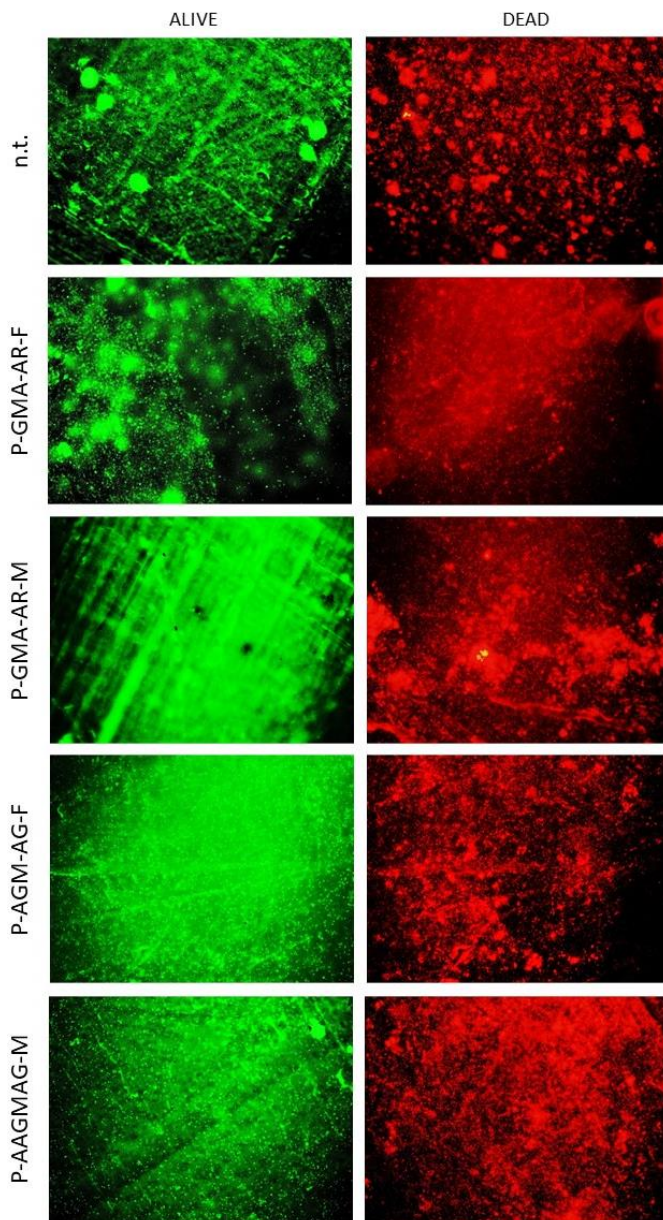


Figure 80 - Live and dead bacteria (*Staphylococcus Aureus*) on PEGDA/GMA-based samples

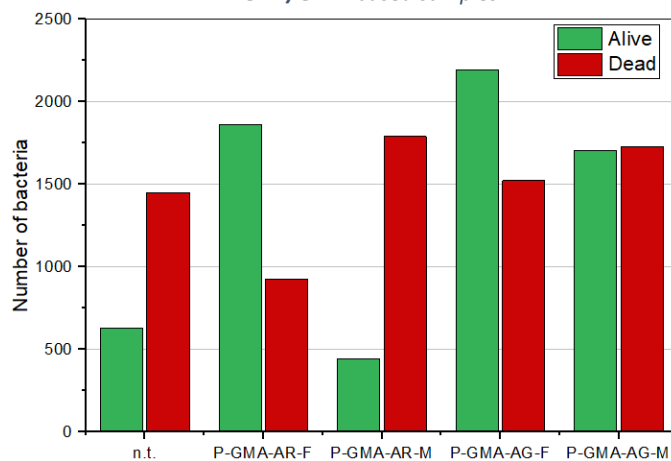


Figure 81 - Number of *Staphylococcus Aureus* bacteria (live and dead) on PEGDA/GMA-based samples

In the figures we can see the bacteria (*S. Aureus*) present in the analyzed samples. Compared with the untreated sample (in the first row), the number of bacteria adhering to the surface increases, with some exceptions: the number of live bacteria on the P-GMA-AR-M sample (microwave arginine-treated sample) decreases, as does the number of dead bacteria on the P-GMA-AR-F sample (arginine-treated by conventional heating). This is clearer if we look at the graph. These results seem unusual and further analysis will be needed to verify their reliability.

In general, however, there is good bacterial adhesion, which is better overall in arginine-treated samples.

6.3. OTHER MATRICES

Preliminary tests on the flat surfaces were conducted with both Gram-positive (*S. Aureus*) and Gram-negative (*E. Coli*) bacteria. The biological tests conducted are summarized in the following table:

Table 18 - Summary of biological tests conducted on PEGDA, PEGDA/ABut and PEGDA/AA/ABut-based samples

MATRIX	REACTANT	TREATMENT	BACTERIA	OBSERVATION
PEGDA ₂₅₀	----	-----	<i>S. Aureus</i>	✓
			<i>E. Coli</i>	✓
	Dopamine	Dip-coating	<i>S. Aureus</i>	✓
			<i>E. Coli</i>	✓
PEGDA/ABut	----	----	<i>S. Aureus</i>	✓
			<i>E. Coli</i>	✓
	Dopamine	Dip-coating	<i>S. Aureus</i>	✓
			<i>E. Coli</i>	✓
PEGDA/AA/ABut	----	----	<i>S. Aureus</i>	✓
			<i>E. Coli</i>	✓
	Dopamine	Dip-coating	<i>S. Aureus</i>	✗
			<i>E. Coli</i>	✓



: ANALYZED SAMPLE



: SAMPLE THAT COULD NOT BE ANALYZED

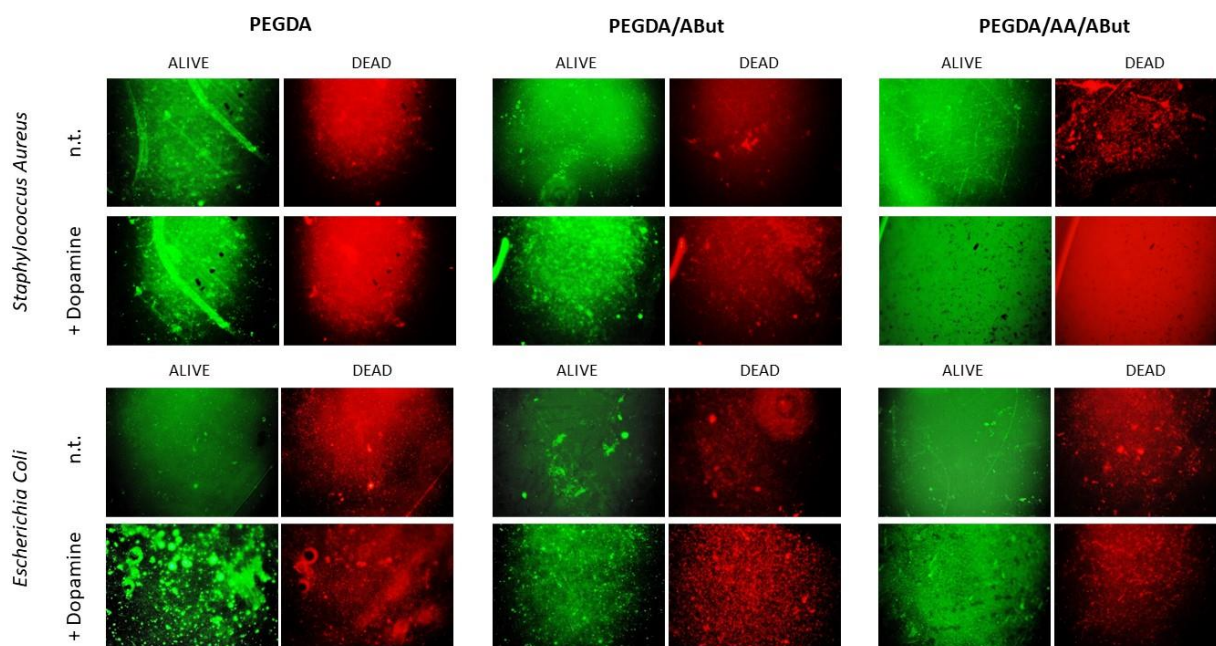


Figure 82 - Live and dead bacteria (*Staphylococcus Aureus* and *Escherichia Coli*) on PEGDA, PEGDA/ABut and PEGDA/AA/ABut-based samples, untreated and treated with dopamine

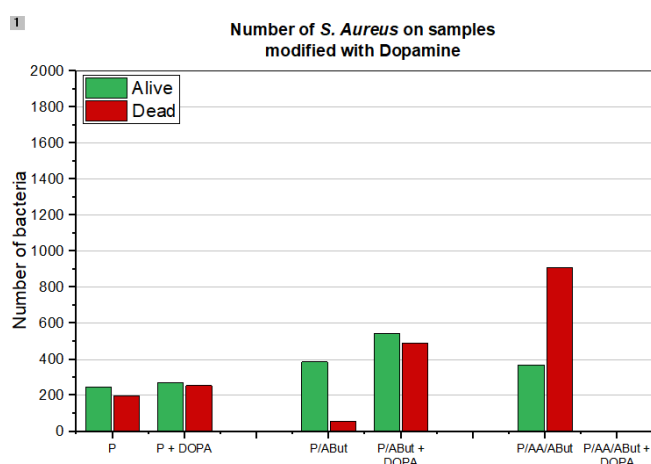


Figure 84 - Number of *Staphylococcus Aureus* on PEGDA, PEGDA/ABut and PEGDA/AA/ABut-based samples, untreated and treated with dopamine

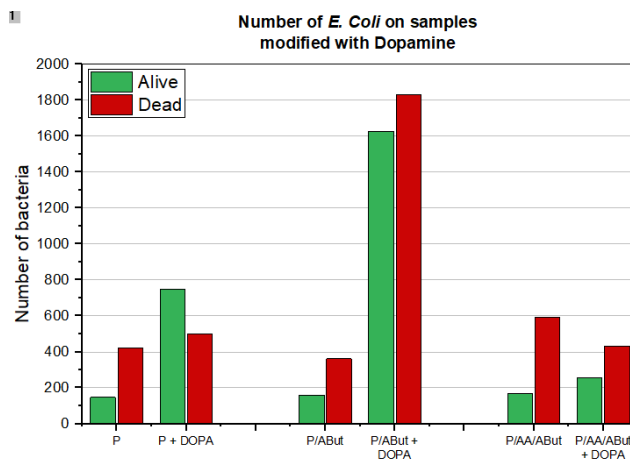


Figure 83 - Number of *Escherichia Coli* on PEGDA, PEGDA/ABut and PEGDA/AA/ABut-based samples, untreated and treated with dopamine

From these graphs we see that dopamine increases bacterial adhesion in all three matrices, although the extent is less than we expected. It is also true that the number of bacteria is generally lower than those recorded in the PEGDA/AA and PEGDA/GMA-based samples, but the ease of dopamine surface treatment makes these results very interesting. Further studies will be needed to try to increase bacterial adhesion on these matrices; in addition, it will be necessary to test the printability of these formulations to obtain air filters.

6.4. BIOLOGICAL TESTS ON FILTERS

Since some of the preliminary tests conducted on the rectangular strips went quite well, the smaller sized filters, previously processed according to the protocols described in Chapter 4, were also tested in the same way. Both geometries were tested with both *S. Aureus* and *E. coli*.

Table 19 - Summary of biological tests conducted on 3D printed filters

MATRIX	REACTANT	TREATMENT
PEGDA/AA	-----	-----
	Arginine	Conventional heating
		Microwave heating
	Agmatine	Conventional heating
		Microwave heating
	Dopamine	Dip-coating
	PEI600	Microwave heating
PEGDA/GMA	PEI600 + Cl	Microwave heating + chlorination
	-----	-----
	Arginine	Conventional heating
		Microwave heating
	Agmatine	Conventional heating
		Microwave heating
	Dopamine	Dip-coating
	PEI600	Microwave heating
	PEI600 + Cl	Microwave heating + chlorination

Unfortunately, preliminary tests on the filters did not show significant numbers of bacteria, either dead or alive. Looking at the images obtained from the fluorescence microscope, we notice that the filters undergo surface degradation and, often, the edges appear jagged and ill-defined. This can affect the bacterial adhesion properties. In addition, because the geometry is more complex, the photopolymerization process is different than for rectangular samples. Thus, it is possible for filters to release unreacted monomers and oligomers, resulting in processes that were not observed in preliminary tests with samples of simple geometry. Finally, swelling may also cause excessive adsorption of the dyes, preventing proper visualization of any bacteria. In addition, we noticed that these problems are more evident in geometry 1, which has thinner sections.

In the Figure 85 and 86 we can see the effects of surface and edge degradation.

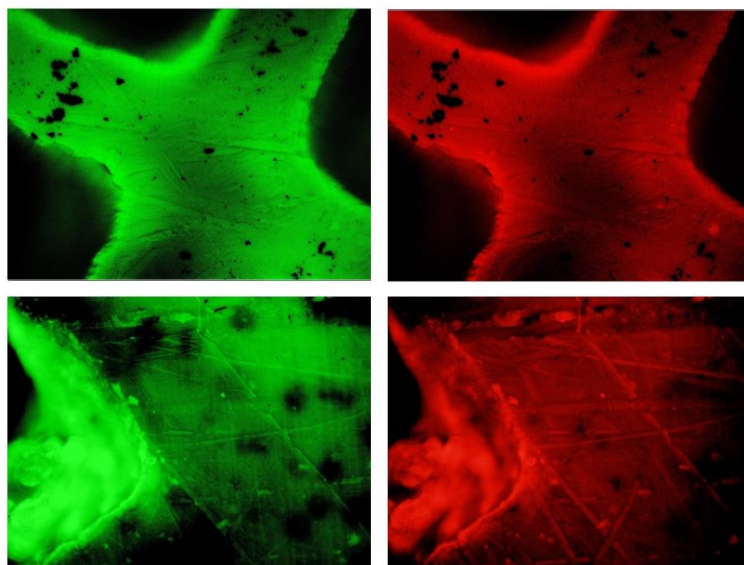


Figure 85 - Images of surface degradation on the filters (holes and scratches)

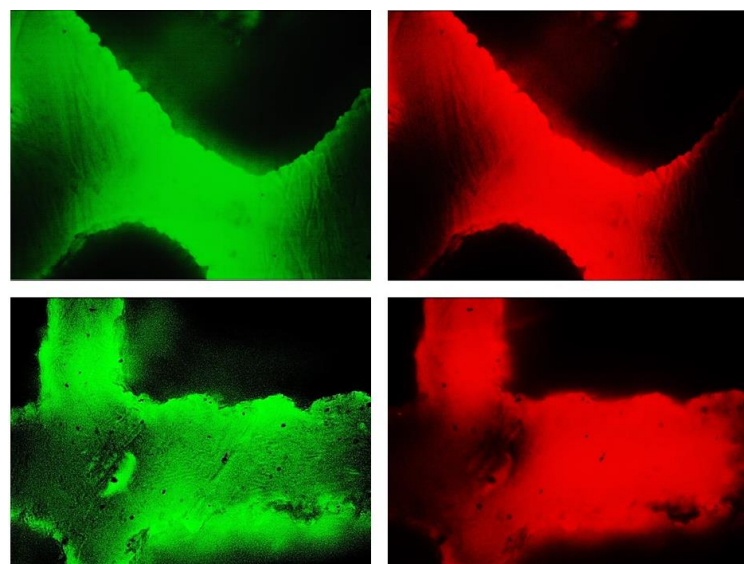


Figure 86 - Images of edge degradation on the filters

In Figure 87, instead, we see that some bacteria are concentrated on the edges, but their quantification is impossible.

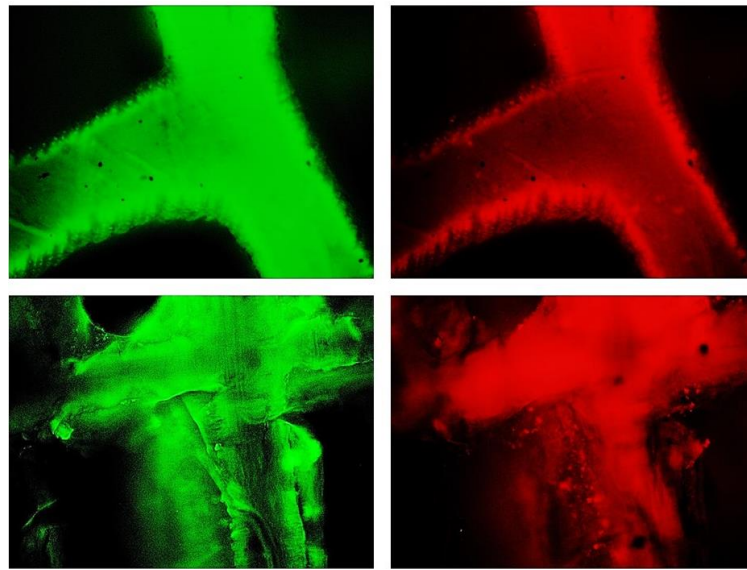


Figure 87 - Images showing the presence of bacteria on the edges

Therefore, we can say that probably the combination of swelling, surface degradation and surface un-curing cause the release of bacteria from the surface. More studies will be needed to understand how these problems affect bacterial adhesion, and how to avoid those.

However, despite the problems they had, some samples showed the presence of bacteria on the surface (Figure 88). Further testing will be needed to validate these results and avoid the problems encountered.

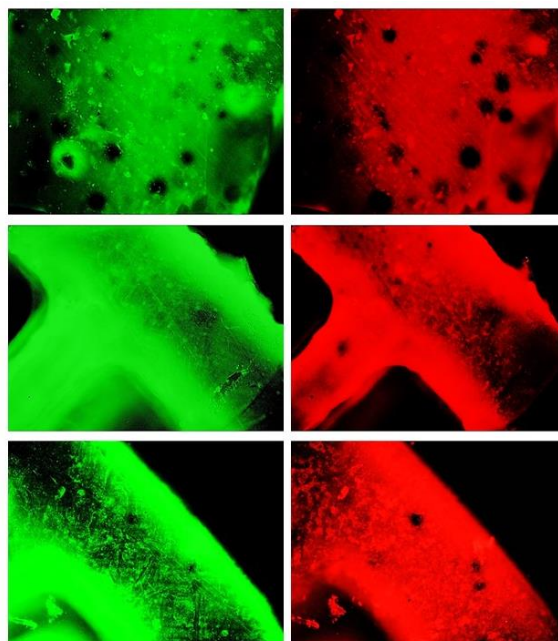


Figure 88 - Images showing the presence of bacteria on the filters' surface

CHAPTER 7: CONCLUSION

In this thesis work, air filters with antibacterial properties were fabricated by 3D printing.

In the first part of the thesis, the design of the filters was studied and several CAD geometries were designed, with the goal of maximizing the air/filter contact time and surface area. The two geometries chosen for printing have different characteristics: the first has greater mechanical stability, but allows only axial flow, while the second is also effective for radial air flows.

The objects were printed by the DLP method, a vat printing technique that uses UV light to photopolymerize a liquid resin in desired points. Photocurable polymer resins based on acrylic monomers were used. The printing parameters for each formulation were optimized to achieve an object with good mechanical properties in the shortest possible time.

3D printing by DLP resulted in objects of high geometric complexity with high resolution of approximately 40 μm , good mechanical properties and good fidelity to the original CAD model.

The second part of this work was carried out at the “*Instituto de Ciencia y Tecnología de Polímeros (ICTP – CSIC)*” in Madrid. The aim was the modification of the surface of the printed samples to give them bacterial adhesion characteristics.

Different functionalization techniques and different molecules were used, all containing amine groups for binding to the filter. This choice was based on literature report, which witnesses the antibactericity of these chemical groups.

With the aim to modify surface and thus efficiently anchoring molecules, five different matrices (PEGDA/AA, PEGDA/GMA, PEGDA₂₅₀, PEGDA/ABut and PEGDA/AA/ABut) were modified, using 4 different molecules (arginine, agmatine, dopamine and polyethylenimine) and 4 functionalization techniques (grafting by conventional heating and by microwave heating, dip-coating and chlorination).

The grafting with arginine and agmatine was done only on the PEGDA/AA and PEGDA/GMA-based samples, both by conventional and microwave heating. Grafting with PEI, on the other hand, was performed on these matrices by microwave only. In addition, some of the PEI-modified samples were subjected to subsequent chlorination treatment to obtain N-halamines on the surface.

On all matrices, dopamine coating by dip-coating was also tried.

The conditions of each treatment (reaction time and temperature, pH of the solution, presence and concentration of coupling agents) were optimized. In general, microwave treatment is faster, but conventional heating allows for a greater degree of functionalization by using a lower temperature.

The success of the treatments was evaluated by analyzing the samples with different techniques: FTIR-ATR spectroscopy, contact angle measurement, swelling test, EDX and TGA.

Despite the similarity between arginine and agmatine, in general the treatment with the former was easier and more effective, resulting in better results in less time. Treatment with PEI is also very effective, mainly due to the high number of amine groups in this molecule, thanks to which substrate binding occurs very quickly. Finally, dopamine treatment was chosen for its simplicity and effectiveness on all kinds of substrates.

Bacterial adhesion on the modified samples was tested at the “*Institute for Biofunctional Studies of the Universidad Complutense (UCM)*” of Madrid.

Samples were tested with Gram-positive and Gram-negative bacteria. After bacterial seeding, a live/dead test was performed to evaluate bacterial adhesion on the surface. The tests were performed on both simple geometry samples (flat surfaces) and filters.

Preliminary tests on the simple geometry samples yielded conflicted results: some of the samples were difficult to analyze due to swelling or degradation of the sample itself. However, some tests showed promising results. In particular, among the PEGDA/AA-based samples, those modified with arginine by conventional heating were the best in terms of the number of live bacteria on the surface; the fact that conventional heating is generally better than microwave treatment may be due to a different type of binding between the functionalization molecule and the surface. Among the PEGDA/GMA-based samples, on the other hand, the total number of bacteria (both live and dead) remaining attached to the surface was higher in agmatine-modified samples. Probably, agmatine binding is more effective on this matrix than on the PEGDA/AA matrix, for which the results with this molecule were worse.

PEGDA/ABut-based samples modified with DOPA were also effective against Gram-negative bacteria.

The tests conducted on filters, however, presented some difficulties, probably due to a combination of surface degradation, un-curing and swelling, so bacterial analysis and quantification was impossible.

In conclusion, we can say that the printing and functionalization of the filters were successful, demonstrating the versatility of 3D printing and the effectiveness of different surface treatments.

Further tests will be needed to assess the surface degradation of filters during biological testing, and to figure out how to avoid it. In addition, strategies will need to be developed to prevent the release of unreacted monomers, which inhibit bacterial adhesion.

Nevertheless, preliminary tests on samples of simpler geometry have demonstrated the effectiveness of surface treatments, and they can be further developed to achieve filters with bacterial adhesion properties.

REFERENCES

- [1] Laura M. Henning et al., «Review on Polymeric, Inorganic, and Composite Materials for Air Filters: From Processing to Properties,» *Advanced Research Energy and Sustainability*, vol. 2, n. 5, 2021.
- [2] Haijun He et al., «3D Printed and Electrospun, Transparent, Hierarchical Polylactic Acid Mask Nanoporous Filter,» *International Journal of Bioprinting*, vol. 6, n. 4, p. 309, 2020.
- [3] Ainur Sabirova et al., «Flexible isoporous air filters for high-efficiency particle capture,» *Polymer*, vol. 213, 2021.
- [4] Muhammad Alia et al., «Advances in air filters based on electrospun fibers,» *Environmental Contaminants Reviews*, vol. 3, n. 1, pp. 32-36, 2020.
- [5] Shadpour Mallakpour et al., «Fabrication of air filters with advanced filtration performance for removal of viral aerosols and control the spread of COVID-19,» *Advances in Colloid and Interface Science*, vol. 303, 2022.
- [6] Xi Xu et al., «3D-Printed Grids with Polymeric Photocatalytic System as Flexible Air Filter,» *Applied Catalysis B: Environmental*, vol. 262, 2019.
- [7] Gianluca Palmara et al., «Functional 3D printing: Approaches and bioapplications,» *Biosensors and Bioelectronics*, vol. 175, p. 112849, 2020.
- [8] Michael Layani et al., «Novel Materials for 3D Printing by Photopolymerization,» *Advanced materials*, vol. 30, n. 41, 2018.
- [9] Hong-Bo Sun, «Two-Photon Photopolymerization and 3D Lithographic Microfabrication,» *Advances in Polymer Science, NMR, 3D Analysis, Photopolymerization*, vol. 170, pp. 169-273, 2004.
- [10] Manmeet Kaur et al., «Photopolymerization: a review,» *Journal of Macromolecular science*, vol. 42, n. 4, pp. 481-512, 2002.
- [11] Christina Schmidleithner et al., 3D printing, IntechOpen, 2018.
- [12] Gustavo Gonzalez et al., «Fabrication and Functionalization of 3D Printed Polydimethylsiloxane-Based Microfluidic Devices Obtained through Digital Light Processing,» *Advanced materials technologies*, vol. 5, n. 9, 2020.
- [13] Zhi Zhao et al., «Engineering materials with light: recent progresses in digital light processind based 3D printing,» *Journal of Materials Chemistry*, vol. 8, pp. 13896-13917, 2020.

- [14] Ali Bagheri et al., «Photopolymerization in 3D Printing,» *ACS Applied Polymer Materials*, vol. 1, n. 4, pp. 593-611, 2019.
- [15] «Royal Society of Chemistry,» [Online]. Available: <https://www.rsc.org/>.
- [16] Hossam Kadrya et al., «Digital light processing (DLP) 3D-printing technology and photoreactive polymers in fabrication of modified-release tablets,» *European journal of pharmaceutical sciences*, vol. 135, pp. 60-67, 2019.
- [17] Y. Zhang, «Post-printing surface modification and functionalization of 3D-printed biomedical device,» *International journal of bioprinting*, vol. 3, n. 2, 2017.
- [18] Pan Jiang et al., «Surface functionalization - a new functional dimension added to 3D printing,» *Journal of Materials chemistry*, vol. 8, pp. 12380-12411, 2020.
- [19] Y. Liu et al., «Influence of surface energy of modified surfaces on bacterial adhesion,» *Biophysical Chemistry*, vol. 117, n. 1, pp. 39-45, 2005.
- [20] Ki Dong Park et al., «Bacterial adhesion on PEG modified polyurethane surfaces,» *Biomaterials*, vol. 19, n. 7-9, pp. 851-859, 1998.
- [21] Yue Yuan et al., «Surface characteristics influencing bacterial adhesion on polymeric substrates,» *RSC Advances*, vol. 7, n. 23, pp. 14254-14261, 2017.
- [22] Yuehuei H. An et al., «Laboratory methods for studies of bacterial adhesion,» *Journal of Microbiological Methods*, vol. 30, n. 2, pp. 141-152, 1997.
- [23] X. Zhang et al., «Superhydrophobic Surfaces for the Reduction of Bacterial Adhesion,» 2013.
- [24] Shehla Mushtaq et al., «Antibacterial Amphiphilic Copolymers of Dimethylamino Ethyl Methacrylate and Methyl Methacrylate to Control Biofilm Adhesion for Antifouling Applications,» *Polymers*, vol. 13, n. 2, pp. 216-229, 2021.
- [25] J. P. Dardan Hetemi, «Surface functionalisation of polymers,» *Reactive and functional polymers*, vol. 4, pp. 5-34, 2017.
- [26] Zhiqiang Cao et al., «Reversibly Switching the Function of a Surface between Attacking and Defending against Bacteria,» *Angewandte Chemie International Edition*, vol. 51, n. 11, pp. 2602-2605, 2012.
- [27] Srinivasa Kartik Nemani et al., «Surface Modification of Polymers: Methods and Applications,» *Advanced Materials Interfaces*, vol. 5, n. 14, 2018.
- [28] Jafar Hasan et al., «Antibacterial surfaces: the quest for a new generation of biomaterials,» *Trends in biotechnology*, vol. 31, n. 5, pp. 295-304, 2013.

- [29] Yumei Wanga et al., «Antibacterial material surfaces/interfaces for biomedical applications,» *Applied Materials Today*, vol. 25, p. 101192, 2021.
- [30] Nazihah Nasri et al., «Past and Current Progress in the Development of Antiviral/Antimicrobial Polymer Coating towards COVID-19 Prevention: A Review,» *Polymers*, vol. 13, n. 4234, 2021.
- [31] Ankita Arora et al., «Antibacterial Polymers – A Mini Review,» *Materials today: proceedings*, vol. 5, n. 9, pp. 17156-17161, 2018.
- [32] Leonard T. Nguyen et al., «The expanding scope of antimicrobial peptide structures and their modes of action,» *Trends in Biotechnology*, vol. 29, n. 9, pp. 464-472, 2011.
- [33] Wei Jiang et al., «Elucidation of Functional Groups on Gram-Positive and Gram-Negative Bacterial Surfaces Using Infrared Spectroscopy,» *Langmuir*, vol. 20, n. 26, pp. 11433-11442, 2004.
- [34] Ilaria Armentano et al., «The Interaction of Bacteria with Engineered Nanostructured Polymeric Materials: a Review,» *Scientific world journal*, pp. 410-423, 2014.
- [35] D. B. W. Hannah H. Tusona, «Bacteria–surface interactions,» *Soft matter*, vol. 9, pp. 4368-4380, 2013.
- [36] Ievgen S. Donskyi et al., «Functionalized nanographene sheets with high antiviral activity through synergistic electrostatic and hydrophobic interactions,» *Nanoscale*, vol. 11, pp. 15804-15809, 2019.
- [37] S. Das et al., «Prospects of microwave processing: An overview,» *Bulletin of Materials Science*, vol. 32, n. 1, pp. 1-13, 2009.
- [38] Oliver Kappe et al., *Practical Microwave Synthesis for Organic Chemists*, WILEY-VHC, 2009.
- [39] Ai Qin Hou et al., «Effect of microwave irradiation on the physical properties and morphological structures of cotton cellulose,» *Carbohydrate Polymers*, vol. 7, n. 4, pp. 934-937, 2008.
- [40] G. González, «Vat 3D printable materials and post-3D printing procedures for the development of engineered devices for the biomedical field,» Zenodo, 2020.
- [41] Sanghun Lee, Semin Kim, «Universal surface modification using dopamine-hyaluronic acid conjugates for anti-biofouling,» *International Journal of Biological Macromolecules*, vol. 151, pp. 1314-1321, 2020.
- [42] Changjiang Fan et al., «A mussel-inspired double-crosslinked tissue adhesive intended,» *Acta Biomaterialia*, vol. 33, pp. 15-63, 2016.

- [43] Ji Hyun Ryu et al., «Polydopamine Surface Chemistry: A Decade of Discovery,» *ACS Applied Materials & Interfaces*, vol. 10, n. 9, pp. 7523-7540, 2018.
- [44] Chunyan Cui et al., «Recent advances in wet adhesives: Adhesion mechanism, design principle and applications,» *Progress in Polymer Science*, vol. 116, p. 101388, 2021.
- [45] Alideertu Dong et al., «Chemical Insights into Antibacterial N-Halamines,» *Chemical Reviews*, vol. 117, n. 6, p. 4806–4862, 2017.
- [46] Y. S. Zhaobin Chen, «N-Halamine-Based Antimicrobial Additives for Polymers: Preparation, Characterization and Antimicrobial Activity,» *Industrial & engineering chemistry research*, vol. 45, n. 8, pp. 2634-2640, 2006.
- [47] Natalia Rekowska et al., «Thermal, Mechanical and Biocompatibility Analyses of Photochemically Polymerized PEGDA250 for Photopolymerization-Based Manufacturing Processes,» *Pharmaceutics*, vol. 14, n. 628, 2022.
- [48] S. R. L. Khatiya Chelidze, «Brilliant Green Staining of the fingernails,» *Cutis*, vol. 105, n. 6, pp. 317-318, 2020.
- [49] «sigmaaldrich.com,» [Online].
- [50] Kalina Hristova et al., «A look at arginine in membranes,» *The Journal of Membrane Biology*, vol. 239, n. 1-2, p. 49.56, 2011.
- [51] W. Raasch et al., «Agmatine, the bacterial amine, is widely distributed in mammalian tissues,» *Life Sciences*, vol. 56, n. 26, pp. 2319-2330, 1995.
- [52] T. I. Omprakash Yemul, «Synthesis and characterization of poly(ethyleneimine) dendrimers,» *Biomacromolecules*, vol. 3, pp. 1030-1037, 2008.
- [53] «www.anton-paar.com,» [Online].
- [54] Haeshin Lee et al., «Mussel-Inspired Surface Chemistry for Multifunctional Coatings,» *Science*, vol. 318, n. 5849, pp. 426-430, 2007.
- [55] D. P. Subedi, «Contact Angle Measurement for The Surface Characterization of Solids,» *Hymalayan Physics*, vol. 2, 2011.
- [56] D. K. Supranee Kaewpirom, «Curing behavior and cured film performance of easy-to-clean UV-curable coatings based on hybrid urethane acrylate oligomers,» *Journal of Polymer Research*, vol. 19, n. 11, pp. 1-12, 2012.
- [57] E. van Dijk-Wolthuis et al., «Synthesis, Characterization, and Polymerization of Glycidyl Methacrylate Derivatized Dextran,» *Macromolecules*, vol. 28, n. 18, pp. 6317-6322, 1995.
- [58] A. Barth, «The infrared absorption of amino acid side chains,» *Progress in Biophysics and*

Molecular Biology, vol. 74, n. 3-5, pp. 141-173, 2000.

- [59] A. Bosch et al., «Characterization of *Bordetella pertussis* growing as biofilm by chemical analysis and FT-IR spectroscopy,» *Applied microbiology and biotechnology*, vol. 71, n. 5, pp. 736-747, 2006.
- [60] S. P. Meenambal Murugesan, «Corresponding Fourier transform infrared (FT-IR) spectroscopic analysis of *Spirulina*,» *International Journal of Pharmaceutical & Biological Archives*, vol. 3, n. 4, pp. 969-972, 2012.
- [61] Hui-Lin Guo et al., «A green approach to the synthesis of graphene nanosheets,» 2009.
- [62] Nelly Flores-Ramirez et al., «Characterization and degradation of functionalized chitosan with glycidyl methacrylate,» *Journal of Biomaterials Science, Polymer edition*, vol. 16, n. 4, p. 473–488, 2012.